AD-A021 344

AN ANALYTIC AND EXPERIMENTAL INVESTIGATION OF
THE WAKES BEHIND FLAPPED AND UNFLAPPED WINGS

Alan J. Bilanin, et al

Aeronautical Research Associates of
Princeton, Incorporated

Prepared for:

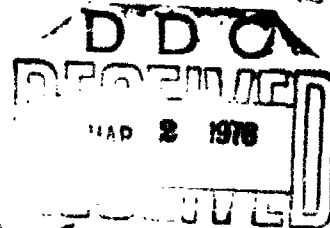Air Force Flight Dynamics Laboratory

September 1974

AFFDL-TR-74-90

069140

AN ANALYTIC AND EXPERIMENTAL INVESTIGATION OF THE WAKES BEHIND FLAPPED AND UNFLAPPED WINGS

AERONAUTICAL RESEARCH ASSOCIATES OF PRINCETON, INC.
PRINCETON, NEW JERSEY 08540

SEPTEMBER 1974

DDC

MAR 2 1976

A

AIR FORCE FLIGHT DYNAMICS LABORATORY
AIR FORCE SYSTEMS COMMAND
WRIGHT-PATTERSON AIR FORCE BASE, OHIO 45433

NOTICE

When government drawings, specifications, or other data are used for any purpose other than in connection with a definitely related Government procurement operation, the United States Government thereby incurs no responsibility nor any obligation whatsoever; and the fact that the government may have formulated, furnished, or in any way supplied the said drawings, specifications, or other data is not to be regarded by implication or otherwise as in any manner licensing the holder or any other person or corporation, or conveying any rights or permission to manufacture, use, or sell any patented invention that may in any way be related thereto.

"This report has been reviewed and cleared for open publication and/or public release by the appropriate Office of Information (OI) in accordance with AFR 190-17 and DODD 5230.9. There is no objection to unlimited distribution of this report to the public at large or by DDC to the National Technical Information Service (NTIS)."

This technical report has been reviewed and is approved.

Evard H. Flinn, Acting Chief
Control Criteria Branch
Flight Control Division
AF Flight Dynamics Laboratory

Copies of this report should not be returned unless return is required by security considerations, contractual obligations, or notice on a specific document.

REPORT DOCUMENTATION PAGE		READ INSTRUCTIONS BEFORE COMPLETING FORM
1. REPORT NUMBER AFFDL-TR-74-90	2. GOVT ACCESSION NO.	3. RECIPIENT'S CATALOG NUMBER
4. TITLE (and Subtitle) An Analytic and Experimental Investigation of the Wakes Behind Flapped and Unflapped Wings		5. TYPE OF REPORT & PERIOD COVERED Final
		6. PERFORMING ORG. REPORT NUMBER
7. AUTHOR(s) Alan J. Bilanin, Coleman duP. Donaldson, and Richard S. Snedeker		8. CONTRACT OR GRANT NUMBER(s) F-33615-73-C-3138
9. PERFORMING ORGANIZATION NAME AND ADDRESS Aeronautical Research Associates of Princeton 50 Washington Road, Princeton N.J. 08540		10. PROGRAM ELEMENT, PROJECT, TASK AREA & WORK UNIT NUMBERS Proj/Task: 1929-0310
11. CONTROLLING OFFICE NAME AND ADDRESS Air Force Flight Dynamics Laboratory Wright-Patterson Air Force Base Ohio 45433		12. REPORT DATE September 1974
		13. NUMBER OF PAGES 142
14. MONITORING AGENCY NAME & ADDRESS(if different from Controlling Office)		15. SECURITY CLASS. (of this report)
		15a. DECLASSIFICATION/DOWNGRADING SCHEDULE

16. DISTRIBUTION STATEMENT (of this Report)

Approved for public release; distribution unlimited

17. DISTRIBUTION STATEMENT (of the abstract entered in Block 20, if different from Report)

18. SUPPLEMENTARY NOTES

19. KEY WORDS (Continue on reverse side if necessary and identify by block number)

Trailing Vortices
Aircraft Wake Turbulence

20. ABSTRACT (Continue on reverse side if necessary and identify by block number)

An analytic and experimental, program was undertaken to define the near wake structure behind flapped and unflapped wings. The vortex wake structure is determined, given the wing lift and drag distributions with models developed in the spirit of Betz. A procedure to estimate the turbulent kinetic energy distribution in the vortex is also given, as well as a method to determine discrete vortex positions in the downstream wake.

DD FORM 1473 1 JAN 73   EDITION OF 1 NOV 65 IS OBSOLETE

i

FOREWORD

ABSTRACT

An analytic and experimental program was undertaken to define the near wake structure behind flapped and unflapped wings. The vortex wake structure is determined, given the wing lift and drag distributions with models developed in the spirit of Betz. A procedure to estimate the turbulent kinetic energy distribution in the vortex is also given, as well as a method to determine discrete vortex positions in the downstream wake. Theoretical models are compared with detailed three-component velocity measurements in the wake of a flapped model wing. Predicted wake velocities are in very good agreement with measurements made in the wake at distances downstream where roll-up is essentially complete. Computed discrete vortex positions in the downstream wake compare most favorably with results of flow visualization studies. Estimates of the downstream turbulent structure of the wake vortices are made using an invariant turbulent model developed at A.R.A.P.

TABLE OF CONTENTS

LIST OF ILLUSTRATIONS

List of Illustrations (cont'd)

List of Illustrations (cont'd)

List of Illustrations (cont'd)

List of Illustrations (cont'd)

LIST OF SYMBOLS

a	constant (see Eq. (27))
AR	wing aspect ratio
b	wing span and constant (see Eq. (27))
b'	trailer separation
b_1	wing span of trailing model
B	constant (see Eq. (42))
B(t)	see Eq. (A.12)
c	wing chord
c_d	sectional drag coefficient
c_{d_i}	sectional induced drag coefficient
c_{d_p}	sectional profile drag coefficient
C_L	wing lift coefficient
C_{L_α}	wing lift curve slope
d(y)	sectional drag
e	one-half the vertical separation between two vortex pairs
$f(\delta)$	see Eq. (A.8)
g(t)	see Eq. (A.6)
h(y)	see Eq. (34)
$h_1(y)$	see Eq. (34)
J	constant (see Eq. 38))
$\ell(y)$	sectional lift exerted on the fluid
n	integer
p	pressure
q	dynamic pressure and $\sqrt{\overline{u'^2} + \overline{v'^2} + \overline{w'^2}}$
q'(r)	radial distribution of $\sqrt{\overline{u'^2} + \overline{v'^2} + \overline{w'^2}}$ in the vortex
q'_{max}	maximum value of q'
q'_{cl}	value of q' at r = 0
r_t	radius of the Betz vortex
R	characteristic radius of curvature of a vortex sheet
Re	Reynolds number
s	wing semi-span
t	time
T	torque

List of Symbols (cont'd)

u, v, w	mean velocity components in the x,y,z directions, respectively
u', v', w'	fluctuating velocity components in the x,y,z directions, respectively
U, V, W	velocity components in the x,r,θ directions, respectively
U_∞	freestream speed
x, r, θ	circular cylindrical coordinates
x, y, z	Cartesian coordinates
$\bar{y}$	spanwise location of the centroid of shed vorticity
$\bar{y}_v(+)$	position of the developing tip vortex
α	wing geometric angle of attack
γ	vortex sheet strength
Γ	spanwise circulation distribution
Γ'	radial distribution of circulation in the vortex
Γ_o	wing root circulation
Γ_f	circulation in the flap vortex
Γ_s	circulation in the vortex sheet
Γ_t	circulation in the tip vortex
δ	see Eq. (A.9)
δ_f	flap deflection angle
ζ	dummy variable for r
η	dummy variable for y
ν	kinematic viscosity
ρ	fluid density
ω	x (downstream) component of vorticity
$(\overline{\quad})$	time average of ( )

SECTION I

INTRODUCTION

The hazard associated with aircraft wake turbulence is now well known, and there is currently underway an extensive effort by the FAA and NASA to respond to this problem. This effort, however, is not concerned directly with vortex wake problems which are unique to the Air Force; namely, hazards associated with short interval take-offs, mid-air refueling, and formation flight. Since wake intensity can be so severe that encountering aircraft have been known to lose control, it is of grave importance to be able to determine for which aircraft and under what operating conditions hazards to other aircraft exist. In regard to the specific operating conditions which are unique to the Air Force, this hazard can only be assessed from a detailed description of the aircraft wake. This description must answer three basic questions:

1) What is the pattern of vorticity shed in the immediate vicinity of an aircraft, and how does this vorticity pattern tend to concentrate (roll up) behind the aircraft?

2) What are the effects of diffusion, turbulent and laminar, on the vortex patterns that develop? We call these effects aging.

3) Are these initial patterns of concentration stable, or will the patterns undergo Crow instability and vortex breakdown?

The answers to all of these questions are relevant to the Air Force.

The research described in this report attempts to provide a logical answer to the first two questions. In Section II, we review the Betz roll-up model and its extension to include the roll-up of "interior" vortices. While these techniques are now well documented in the literature, we include them here and show how a new physical interpretation of the model allows further generalization. The result is a model which can predict the vortex axial and swirl velocity distribution for either tip or "interior" roll-ups given the wing lift and drag distribution. The structure of each individual vortex in the wake is not complete, however, without specifying how the turbulent kinetic energy in the boundary layer on the wing might be distributed in the rolled-up vortices. A procedure for doing this, in the spirit of the Betz model, is also presented. The local turbulent structure of the individual vortices may then be calculated using a three-dimensional turbulent vortex program which has been developed by A.R.A.P. for ARL under Contract F33615-72-C-2116. The structure of the wake is completed by developing a model by which the motion of the vortices which comprise the wake may be determined. In short, Section II develops theoretical models

from which a complete description of the near-field rolled-up aircraft vortex wake is possible.

Section III describes the design and implementation of a test program to check, where possible, the above-described models. The test program was carried out in the V/STOL tunnel at NASA's Langley Research Center. Detailed measurements were made by Langley personnel of the wake structure and the model wing lift distributions.

In Section IV, the results from this test program are analyzed and compared with calculations from theoretical models.

Finally, in Section V, conclusions and recommendations are offered.

SECTION II

REVIEW AND DEVELOPMENT OF THEORETICAL MODELS

It is well known that a finite aspect ratio wing which develops circulation lift, sheds vorticity as a consequence of this lift. This vorticity, which forms the wake, is shed from the trailing edge and is commonly referred to as a shed vortex sheet (the fluid containing vorticity is very thin in a direction normal and aft relative to the planform of the wing). At the trailing edge, the sheet is more or less planar, but does not remain so. A short distance downstream, the sheet, as a result of a convective instability, tends to roll up into discrete vortices, as shown schematically in Figure 1. These vortices can be quite persistent and, when of sufficient intensity, are a hazard to other aircraft.

Calculation of the details of the roll-up is quite difficult, and investigators have resorted to simplified models to describe the phenomenon. One such model popularized by Westwater in 1935 (Ref. 1) calculates the roll-up of a two-dimensional sheet by replacing the sheet with discrete vortex elements. This approach has formed the basis of several recent investigations (Refs. 2-5). One difficulty is that the similarity solution of Kaden (Ref. 6) shows that the center of the rolled-up spiral contains an infinite number of turns and, as Westwater points out, can never be modeled by a finite number of vortices. Recently, Moore (Ref. 5) has used a scheme whereby the difficulties associated with modeling the spiral structure with discrete vortices are circumvented. He replaces the exact spiral structure with an irrotational tip vortex, thereby eliminating the need to keep track of the many discrete vortices which model the spiral. While the results of these calculations are encouraging, it is unfortunate that the detailed structure is lost. Calculations based on this method are valuable in that they are able to estimate time to roll-up.

When the details of the roll-up are not needed, two models have been suggested to obtain the vortex wake structure. The first model, proposed by Spreiter and Sacks (Ref. 7), equates the swirl kinetic energy per unit length of wake to the induced drag of the aircraft. The calculation requires an assumption as to the nature of the swirling velocity distribution, with sufficient free parameters that circulation about each vortex and the impulse of the system are conserved. In Reference 7, the vorticity was assumed to be distributed uniformly in the vortex. For an elliptically loaded wing, vortex radius was obtained to be 0.155 the semi-span of the wing. While calculations of this nature are straightforward, they do not give a unique relationship between wing load distribution and vortex velocity distribution.

The second model was proposed by Betz and, while available for some time, received little attention until Donaldson (Ref. 8) showed that the swirl velocity distribution calculated in this way

3
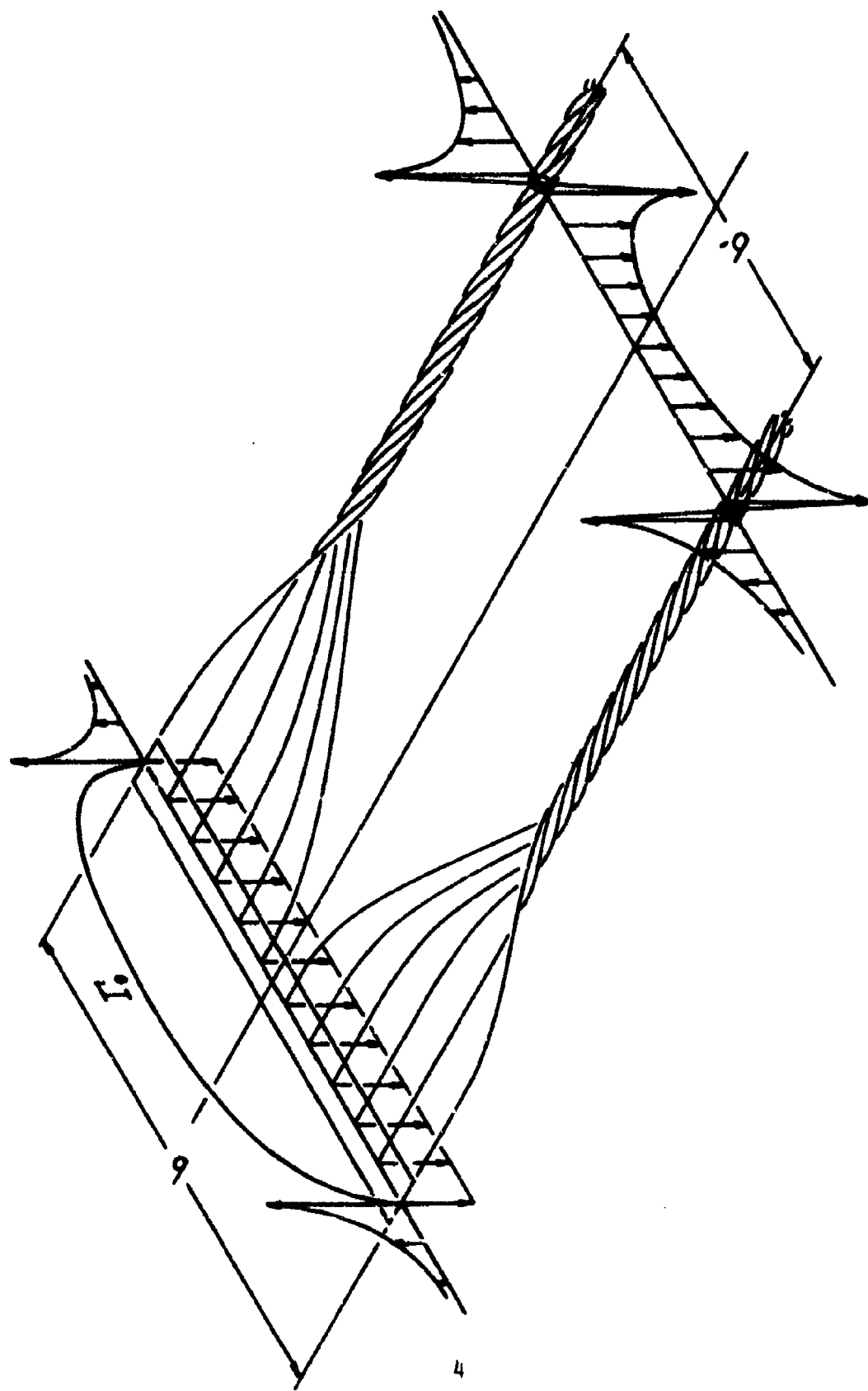
Figure 1.   Illustration of the roll-up of shed vorticity from a simply loaded wing (from Ref. 8)

compared most favorably with measurements. Recently, several studies in the spirit of Betz have been undertaken (Refs. 9-12), and Donaldson, et al. (Ref. 13) has shown how the roll-up of flap vortices may be calculated according to the Betz assumption. Since the comparison of the Betz model and the extensions proposed in Ref. 13 with experimental measurements forms a significant portion of the effort reported herein, it is appropriate to review this model.

1. THE BETZ ROLL-UP MODEL AND EXTENSIONS TO INCLUDE INTERIOR VORTICES

The method described by Betz for calculating roll-up relates the circulation Γ at wing station y to the circulation Γ' calculated at radius r in an axisymmetric line vortex. The method is based upon the assumption that global invariants applicable to an unbounded, two-dimensional, incompressible, inviscid fluid medium may be applied locally behind a wing to obtain an approximate description of the vortical wake. The fundamental assumption is that vortical motions are such as to preserve the inertial moment about the centroid of vorticity; that is,

$$- \int_y^s \frac{d\Gamma(\eta)}{d\eta}[\eta - \bar{y}(y)]^2 d\eta = \int_0^r \zeta^2 \frac{d\Gamma'}{d\zeta} d\zeta \tag{1}$$

and

$$\bar{y}(y) = \frac{1}{\Gamma(y)} \int_y^s \eta \frac{d\Gamma(\eta)}{d\eta} d\eta \tag{2}$$

where $\bar{y}(y)$ is the centroid of the vorticity shed between stations y and s.

Equation (1) is approximate and, as will be shown in Section II.2, can be manipulated so as to allow physical interpretation. With Eq. (1) and a statement of Kelvin's theorem

$$\Gamma(y) = - \int_y^s \frac{d\Gamma(\eta)}{d\eta} d\eta = \int_0^r \frac{d\Gamma'}{d\zeta} (\zeta)d\zeta = \Gamma'(r) \tag{3}$$

which is exact for an inviscid flow, Betz was able to give a rather complicated expression for the swirling velocity in the rolled-up wake of an elliptically loaded wing. By manipulating Eqs. (1) - (3), Donaldson, et al., Rossow, and Jordan have independently shown the surprisingly simple result: the relationship

5

between r and y is

$$r = \bar{y}(y) - y \qquad (4)$$

This result, along with Eq. (3), states that the value of the circulation at wing station y is the value of the circulation at radial distance r in an axisymmetric vortex. The radial distance r is equal to the distance from y to the centroid $\bar{y}$ of all the shed vorticity outboard of y . When all the vorticity can be considered rolled up, the vortex center is located at $y = \bar{y}(0)$ in order to preserve the vertical momentum of the flow. Since r also equals $\bar{y}(0)$, the circular regions conta_ning vorticity just touch along the aircraft centerline. Figure 2 depicts the Betz roll-up model.

When an aircraft has flaps and/or spoilers deployed, the wing load distribution may be such that a single roll-up proceeding from the tip is no longer possible. In such cases, Ref. 13 has given a criterion which specifies how the vorticity distribution will divide itself and roll up into multiple discrete vortices. The criterion is best presented by considering the example given in Figure 3. The function $d\Gamma/dy$ is the strength of the vortex sheet shed from the wing. Consider the distribution of the absolute value of the shed vorticity $|d\Gamma/dy|$. This function has three minima which are denoted by points A, B, and C. It was assumed that the vorticity shed between B and C would roll up into what was generally called a fuselage vortex. The vorticity shed between stations A and B would form a flap vortex, and all the vorticity outboard of A would roll up as a tip vortex. The strengths of these vortices are $\Gamma_C - \Gamma_B$,

$\Gamma_B - \Gamma_A$, and Γ_A , respectively. Furthermore, it was assumed that the roll-up of the flap and fuselage or "interior" vortices would proceed from the points where $|d\Gamma/dy|$ is maximum, namely, y_{mB} and y_{mC} . This is physically motivated and compatible with observation. Recently, Yates (Ref. 14) has checked these assumptions by the direct calculation of the initial in-plane acceleration of the vortex sheet. He was able to show that these assumptions are quite accurate and give a simple method to determine the number and strength of the vortices to be expected in a wake.

The circulation distribution in "interior" vortices was calculated in Ref. 13 by extending the Betz model. To see how this was done, consider the vorticity shed between stations A and B in Figures 3 and 4. First, the assumption regarding the relationship between the inertia moment of the vorticity distribution (Eq. (1)) is modified to read

$$- \int_{y_1}^{y_2} \frac{d\Gamma}{d\eta} (\eta - \bar{y}_{12})^2 d\eta = \int_0^r \zeta^2 \frac{d\Gamma'}{d\zeta} d\zeta \qquad (5)$$

6
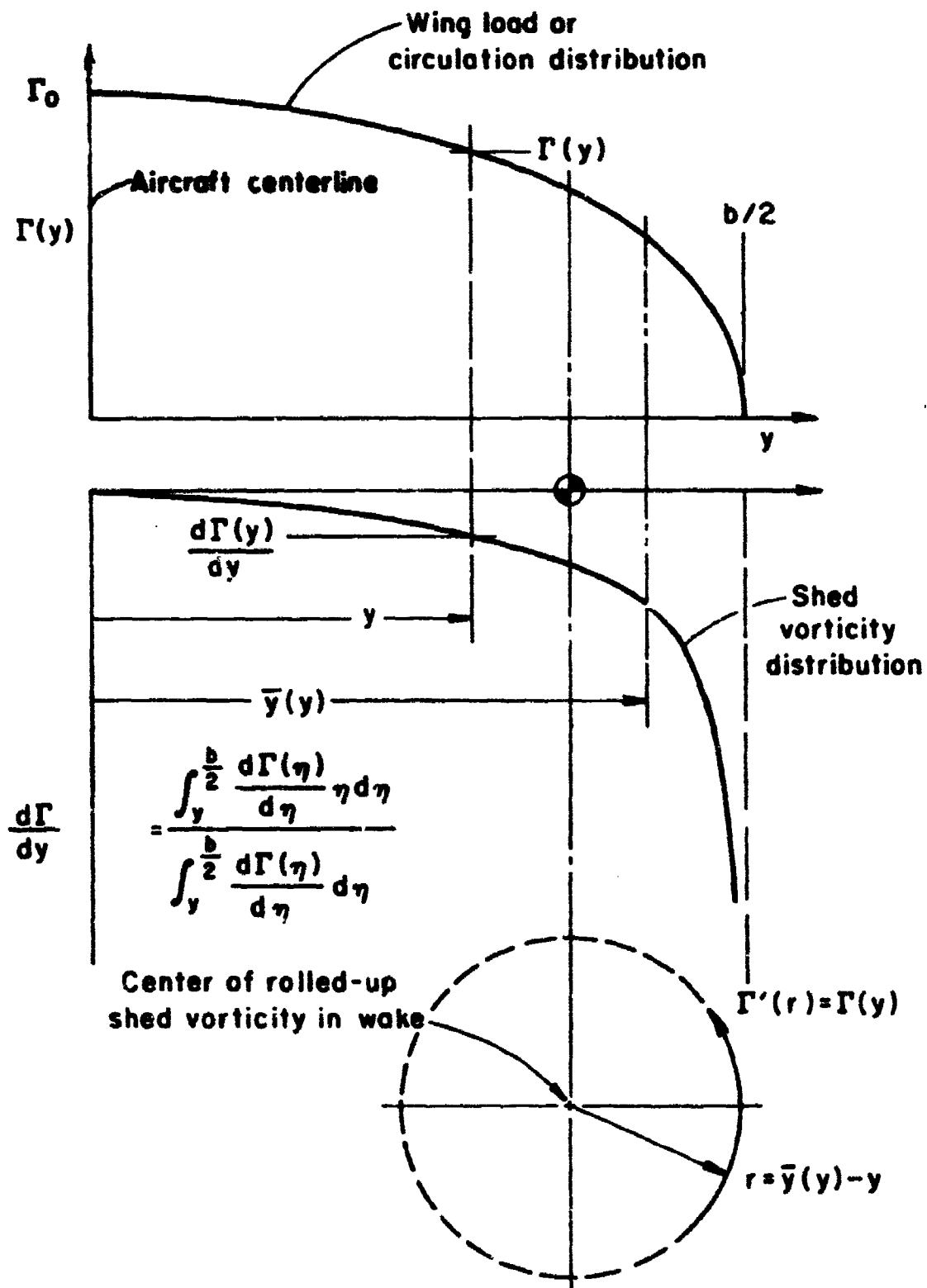
Figure 2. Illustration of the Betz roll-up model for a simply loaded wing (from Ref. 13)
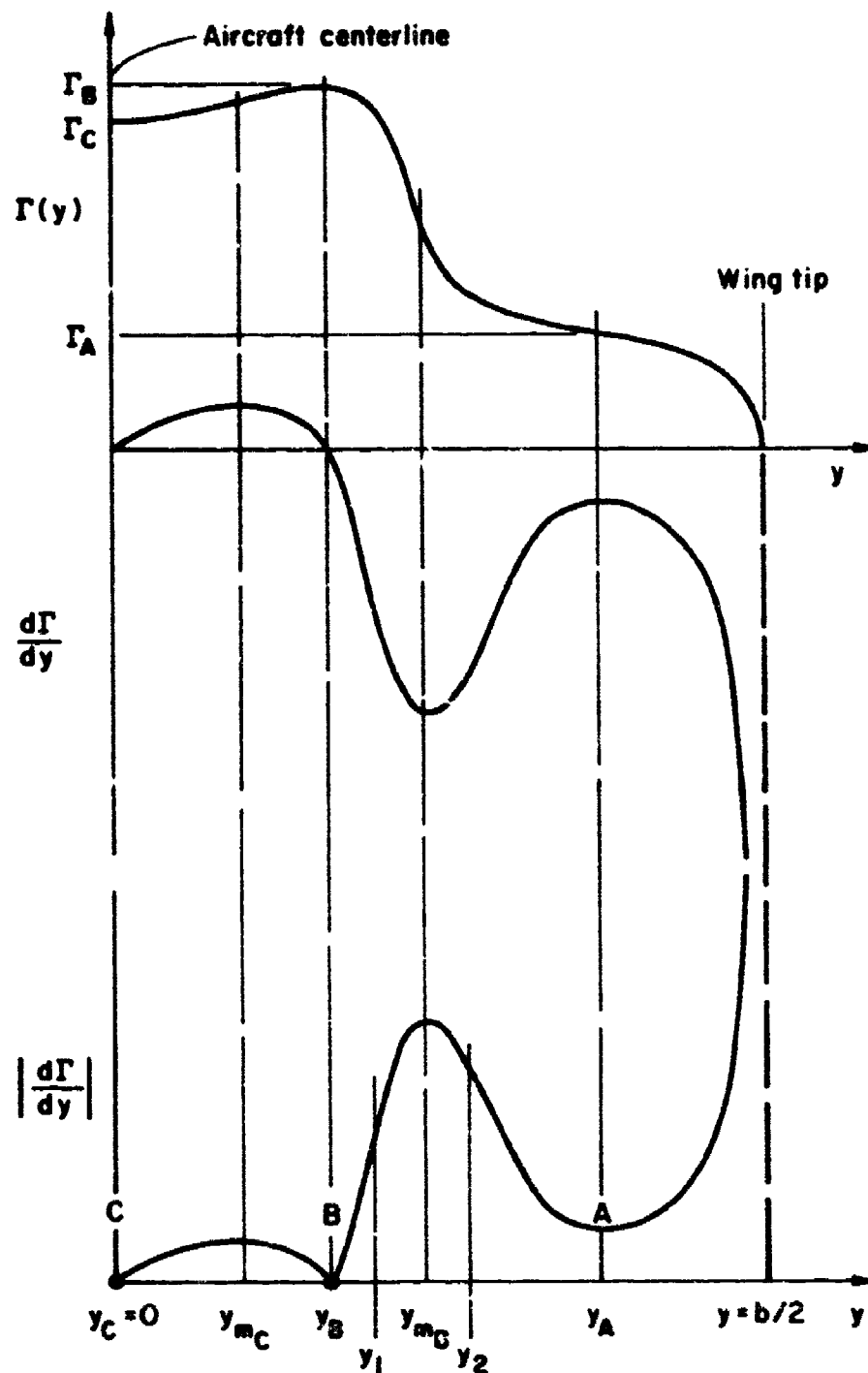
Figure 3.   Load distribution which will produce three vortices
            (from Ref. 13)
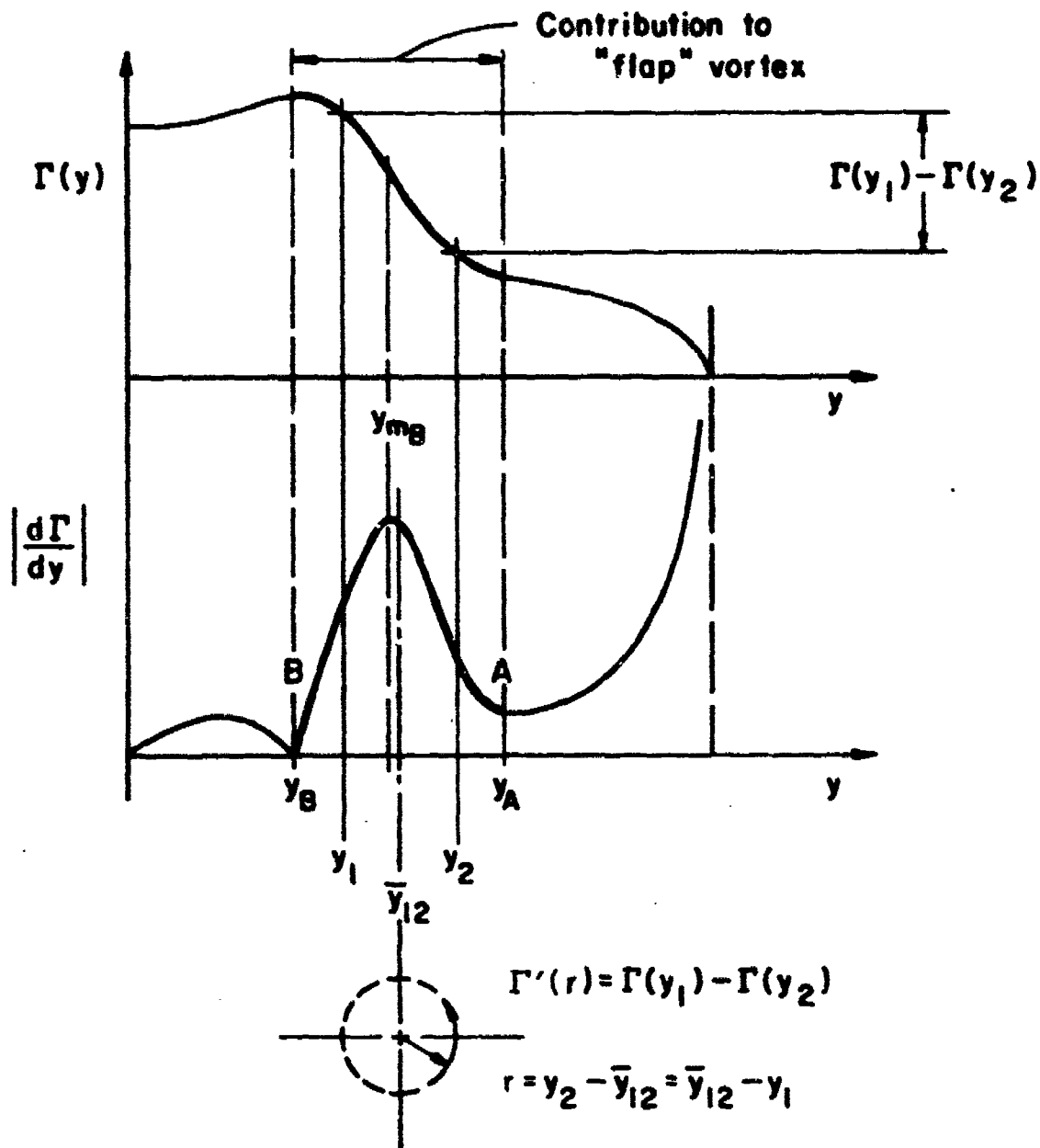
Figure 4. Illustration of the Betz roll-up model for the flap vortex (from Ref. 13)

where y_1 and y_2 are arbitrary points inboard and outboard of y_{mB}. $\bar{y}_{12}$ is defined by

$$\bar{y}_{12} = \frac{1}{\Gamma_2 - \Gamma_1} \int_{y_1}^{y_2} \eta \frac{d\Gamma}{d\eta}\, d\eta \qquad \cdot \qquad (6)$$

and is the centroid of the shed vorticity between y_1 and y_2. Kelvin's theorem rewritten for an interior vortex is

$$\Gamma(y_1) - \Gamma(y_2) = -\int_{y_1}^{y_2} \frac{d\Gamma}{d\eta}\, d\eta = \int_0^r \frac{d\Gamma'}{d\zeta}\, d\zeta = \Gamma(r) \qquad (7)$$

Equations (5) - (7) are not sufficient to describe an "interior" vortex until a relationship between y_1 and y_2 is prescribed. This relationship was taken to be

$$(y_2 - \bar{y}_{12})^2 = (y_1 - \bar{y}_{12})^2 \qquad (8)$$

and is equivalent to the expression found by Betz for a tip roll-up. By manipulating Eqs. (5) - (8), it may now be shown that

$$r = y_2 - \bar{y}_{12} = \bar{y}_{12} - y_1 \qquad (9)$$

The similarity with the result obtained for tip roll-up (4) is obvious. Equation (9) taken with (7) determines the circulation distribution in an "interior" vortex, providing y_1 remains greater than y_B and y_2 remains less than y_A. If y_2 reaches y_A before y_1 reaches y_B, the roll-up is to be continued by holding y_2 and, hence, Γ_2 fixed and proceeding with the roll-up, letting $r = \bar{y}_{12} - y_1$ until y_1 reaches y_B. If y_1 reaches y_B before y_2 reaches y_A, then roll-up is continued, holding y_1 and, hence, Γ_1 fixed, letting $r = y_2 - \bar{y}_{12}$.

Before proceeding to the next section and showing how axial velocity in the vortex might be included in the Betz model, we will present the results obtained in Ref. 13 regarding the magnitude of the swirling velocity at the center of the vortex. It was shown that

$$V(0) = -\frac{1}{\pi} \frac{d\Gamma}{dy} \qquad (10)$$

where $d\Gamma/dy$ is to be evaluated at $y = b/2$ for a tip vortex and at y_m (the point of maximum sheet strength) for an "interior" vortex. This result is significant in that the maximum inviscid swirling velocity to be expected is simply a function of the maximum rate of change of the load distribution. Of course, these velocities are never achieved in a real vortex since viscous effects require that $V(0) = 0$.

2. THE EFFECTS OF WING DRAG ON INVISCID VORTEX STRUCTURE

While the Betz model and extensions to include "interior" vortices provide much information regarding the mean discrete vortex structure, it is not complete until we determine how the wing drag distribution influences this structure. The further extension of the Betz model to include this effect is straight-forward and can be physically motivated. The development can be shortened by considering only the roll-up of an "interior" vortex. The result for a tip vortex is obtained by setting the upper limit of integration y_2 equal to $b/2$ in the integrals which follow.

Equation (5) is multiplied by $-\rho U_\infty/2$ and integrated by parts to yield

$$\frac{\rho U_\infty}{2} \left[\Gamma_2 (y_2 - \bar{y}_{12})^2 - \Gamma_1 (y_1 - \bar{y}_{12})^2 + r_B^2 \Gamma_B' \right]$$

$$+ \int_{y_1}^{y_2} \ell(\eta)(\eta - \bar{y}_{12}) d\eta$$

$$= \int_0^r \rho \zeta V(\zeta) U_\infty 2\pi\zeta \, d\zeta \tag{11}$$

where $\ell(y) = -\rho U_\infty \Gamma(y)$ is the sectional wing loading exerted on the fluid. The first term in Eq. (11) vanishes when (7) and (3) are substituted. The remaining terms prescribe the distribution of angular momentum in the vortex. The Betz model therefore distributes the angular momentum such that the torque exerted by the wing (calculated about $\bar{y}_{12}$) between y_1 and y_2 equals the flux of angular momentum through a circle of radius r. In light of this physical interpretation, nonuniform axial velocity in the vortex may be included by modifying Eq. (11) to read

$$\int_{y_1}^{y_2} \ell(\eta)(\eta - \bar{y}_{12}) d\eta = \int_0^r \rho \zeta V(\zeta) U(\zeta) 2\pi\zeta \, d\zeta \tag{12}$$

The geometry of the flow model for a tip roll-up might be thought to be that illustrated in Figure 5. By differentiating (12) with respect to r and using Eq. (6), we obtain

$$\Gamma_1 d(y_1 - \bar{y}_{12})^2 - \Gamma_2 d(y_2 - \bar{y}_{12})^2 = \frac{U(r)}{U_\infty} \Gamma' \, dr^2 \tag{13}$$

Substituting (7) and (8) yields the simple result

$$U_\infty d(y_1 - \bar{y}_{12})^2 = U(r) dr^2 \tag{14}$$

11
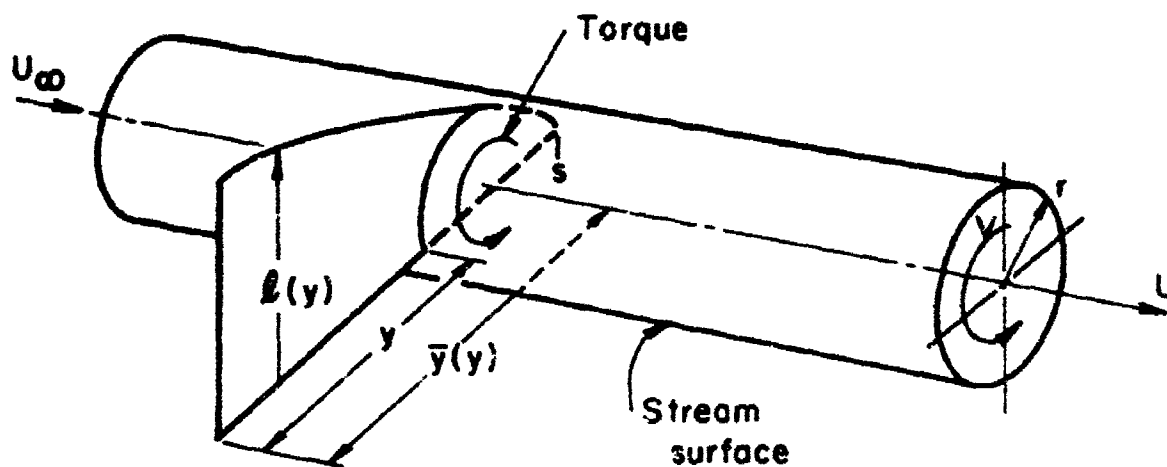
Figure 5. Illustration of the Betz flow model to include axial velocity

12

When y_2 is set equal to $b/2$, Eq. (14) is valid for a tip roll-up. When $U(r) = U_\alpha$, the results given in Eqs. (4) and (9) are readily obtained.

Before coupling the wing drag distribution to the axial velocity in the vortex, it is possible to show how the axial velocity modifies the velocity $V(0)$ at the center of the vortex. Assuming that $U(0)$ is finite, Eq. (14) may be integrated for small r to yield

$$r = \left[\frac{U_\infty}{U(0)}\right]^{1/2} (\bar{y}_{12} - y_1) \tag{15}$$

as $r \to 0$. Following Ref. 13, the tangential velocity for the "interior" vortex is

$$V(r) = \frac{\Gamma'(r)}{2\pi r} = \frac{\Gamma(y_1) - \Gamma(v_2)}{2\pi r} \tag{16}$$

As $r \to 0$, we may write

$$V(0) = \frac{1}{2\pi} \left.\frac{d\Gamma}{dy}\right|_{y=y_m} \left.\left(\frac{dy_1}{dr} - \frac{dy_2}{dr}\right)\right|_{y_1=y_2=y_m} \tag{17}$$

Calculating dv_1/dr and dy_2/dr from Eqs. (15) and (8) and substituting these values into Eq. (17) yields

$$V(0) = -\frac{1}{\pi} \left[\frac{U(0)}{U_\infty}\right]^{1/2} \left.\frac{d\Gamma}{dy}\right|_{y=y_m} \tag{18}$$

For a tip vortex, Eq. (15) becomes

$$r = \left[\frac{U_\infty}{U(0)}\right]^{1/2} (\bar{y}(y) - y) \tag{19}$$

and (16) is written

$$V(0) = \frac{1}{2\pi} \left.\frac{d\Gamma}{dy}\right|_{b/2} \left.\frac{dy}{dr}\right|_{b/2} \tag{20}$$

as $r \to 0$. Differentiating (19), taking the limit using (2) and substituting this result for $\left.\frac{dy}{dr}\right|_{b/2}$ yields

$$V(0) = -\frac{1}{\pi} \left[\frac{U(0)}{U_\infty}\right]^{1/2} \left.\frac{d\Gamma}{dy}\right|_{b/2} \tag{21}$$

13

For both "interior" and tip vortices, deficits in axial velocity $(U(0)/U_\infty < 1)$ result in a reduction of the inviscid centerline swirl velocity.

We may now turn our attention to coupling the axial velocity in the vortex to the wing drag distribution. Making an axial momentum balance across a "cylindrical" control volume of radius r containing the portion of the wing between y_1 and y_2 yields

$$\int_{y_1}^{y_2} d(\eta)d\eta + 2\pi \int_0^r [p + \rho U(U - U_\infty)]\zeta d\zeta = 0 \tag{22}$$

where the axial velocity of the fluid fluxing through the "cylindrical" surface is approximated by U_∞ . The pressure far upstream has been taken to be zero and d is the wing sectional drag. When the U^2 term is linearized, Eq. (22) is that given by Brown (Ref. 10). Equation (22) is written in the same spirit as Eqs. (1) - (5) since it assumes that the wing drag distributes itself in the rolled-up vortex in the same manner as the shed axial vorticity. As discussed by Brown, the assumption is a natural one since the axial vortex lines and the viscous wake are one and the same.

Differentiating Eq. (22) and substituting (14) yields

$$d(y_1) - d(y_2) \frac{dy_2}{dy_1} = \pi U_\infty \left[\frac{p}{U} + \rho(U - U_\infty) \right] \frac{d(y_1 - \bar{y}_{12})^2}{dy_1} \tag{23}$$

For a tip roll-up, $dy_2/dy_1 = 0$. The nonuniform pressure in the vortex is primarily a result of the swirl and may, therefore, be calculated from

$$p = - \frac{\rho}{4\pi^2} \int_r^\infty \frac{\Gamma'^2}{\zeta^3} d\zeta \tag{24}$$

Equations (14), (23), and (24) form the nonlinear system to be solved. The boundary conditions are

$$\left. \begin{array}{l} p \Big|_{y_1=y_A} = - \frac{\rho}{2} V^2 \Big|_{y_1=y_A} \\[3mm] r \Big|_{y_1=y_m} = 0 \end{array} \right\} \tag{25}$$

Together, Eqs. (14), (23), (24) and (25) determine the inviscid axial and swirl velocities in either an "interior" or tip vortex given the lift and drag distribution over the appropriate region of the wing from which the vortex develops. Nonlinearity and the nature of the boundary conditions dictate that, in general, solutions will have to be obtained numerically.

14

At this point, it is appropriate to find a simple analytical solution which will illustrate the effect of wing drag distribution on inviscid vortex structure. Unfortunately, the direct problem of specifying the lift and drag distribution does not appear to yield analytic solutions. However, the indirect problem of specifying the axial velocity and lift distribution and determining the drag distribution and swirling velocity is straightforward for a simple distribution.

Equation (14) can be integrated if the wing loading is linear (a tip roll-up) and therefore of the form

$$\Gamma = \Gamma_o\left(1 - \frac{y}{s}\right) \tag{26}$$

and the axial velocity is given by

$$U = U_\infty\left[a + b\left(\frac{r}{r_t}\right)^2\right] \tag{27}$$

The constants a and b may be chosen such that U is positive; therefore, $a \geq 0$. Negative axial velocities imply a flux of angular momentum from downstream and violate the assumptions implied in Eq. (12). The radius of the region containing all the vorticity shed between the wing root and tip r_t is to be determined. Integrating Eq. (14) yields

$$(s - y)^2 = 4ar^2 + \frac{2br^4}{r_t^2} \tag{28}$$

When $r = r_t$, $y = 0$ and, therefore,

$$\frac{2r_t}{b} = \frac{1}{2}\left(a + \frac{b}{2}\right)^{-1/2} \tag{29}$$

The Betz result is obtained with $a = 1$, $b = 0$; all the vorticity is contained within a circle having radius $b/4$. Referring to Eq. (27), sufficient conditions for an axial velocity excess in the wake occur when $a > 1$ and $b \geq 0$; r_t decreases and the vortex is intensified in that the swirl velocities are increased. Axial velocity defects are associated with increases in r_t and, therefore, more diffuse vortices. It is important to remember, however, that since the lift distribution is unchanged the total axial flux of angular momentum from the region containing axial vorticity is not changed. Therefore, the intensity of the vortex, as measured by the flux of angular momentum, is unchanged by drag. The deintensification which does, in fact, occur is brought about by redistributing the angular momentum outward so that small encountering aircraft could interact with less of the vortex. Since drag is likely to result in higher turbulence levels in the vortex (at least initially), it is likely that the outward

15

redistribution of angular momentum, as calculated here, is further aided by turbulent processes.

The circulation and swirl velocity distributions in the vortex are given by

$$\frac{\Gamma'}{\Gamma_o} = \left[a + \frac{b}{2} \left(\frac{r}{r_t} \right)^2 \right]^{1/2} \frac{4r}{b} \tag{30}$$

$$\frac{V \pi b}{\Gamma_o} = 2 \left[a + \frac{b}{2} \left(\frac{r}{r_t} \right)^2 \right]^{1/2} \tag{31}$$

Referring to Figure 6, the drag on the wing is calculated from Eq. (23) for five cases. At an average drag coefficient of about 0.012 (a typical value), the axial velocity in the vortex is uniform and equal to the free stream value (case 3). The vortex radius is 0.55 b/2 and is taken to define a reference circular area so that we may illustrate the deintensification which results as a consequence of wing drag. By increasing the average drag coefficient by nearly an order of magnitude to 0.11, the vortex radius is increased 16% to 0.585 b/2 (case 2). The flux of angular momentum through the reference area when compared with case 3 is one measure of the deintensification which can be achieved by increased drag. The calculation shows that the flux in case 2 is reduced a highly desirable 43%. However, the model suggests that vortex deintensification brought about solely by this technique will have prohibitively large drag penalties. The problem of the least intense vortex for a given lift and drag coefficient is surely worthy of additional study.

It is now apparent that axial velocities in the vortex may be either an excess or defect depending on the wing lift and drag distribution. In addition, it is quite possible that axial velocity distributions can result which have an excess over certain radial intervals and defects over others. Figure 7 illustrates such a situation. Tailoring the drag distribution so that strong axial velocity gradients develop may prove to be an effective means of enhancing turbulent decay.

To summarize the results of this section, it has been shown that the Betz model and extensions to calculate the roll-up of aircraft vortices may be further modified to include the effect of wing drag distribution on vortex structure. Simple sample calculations show that increased drag reduces the intensity of the vortex by redistributing the flux of angular momentum over a greater area in the wake. Large restructuring of the wake by increased drag, however, appears to require large drag penalties.

3. ROLL-UP OF THE TURBULENT BOUNDARY LAYER

Having developed a model to predict the mean swirl and axial velocity distributions in wake vortices, there remains the problem
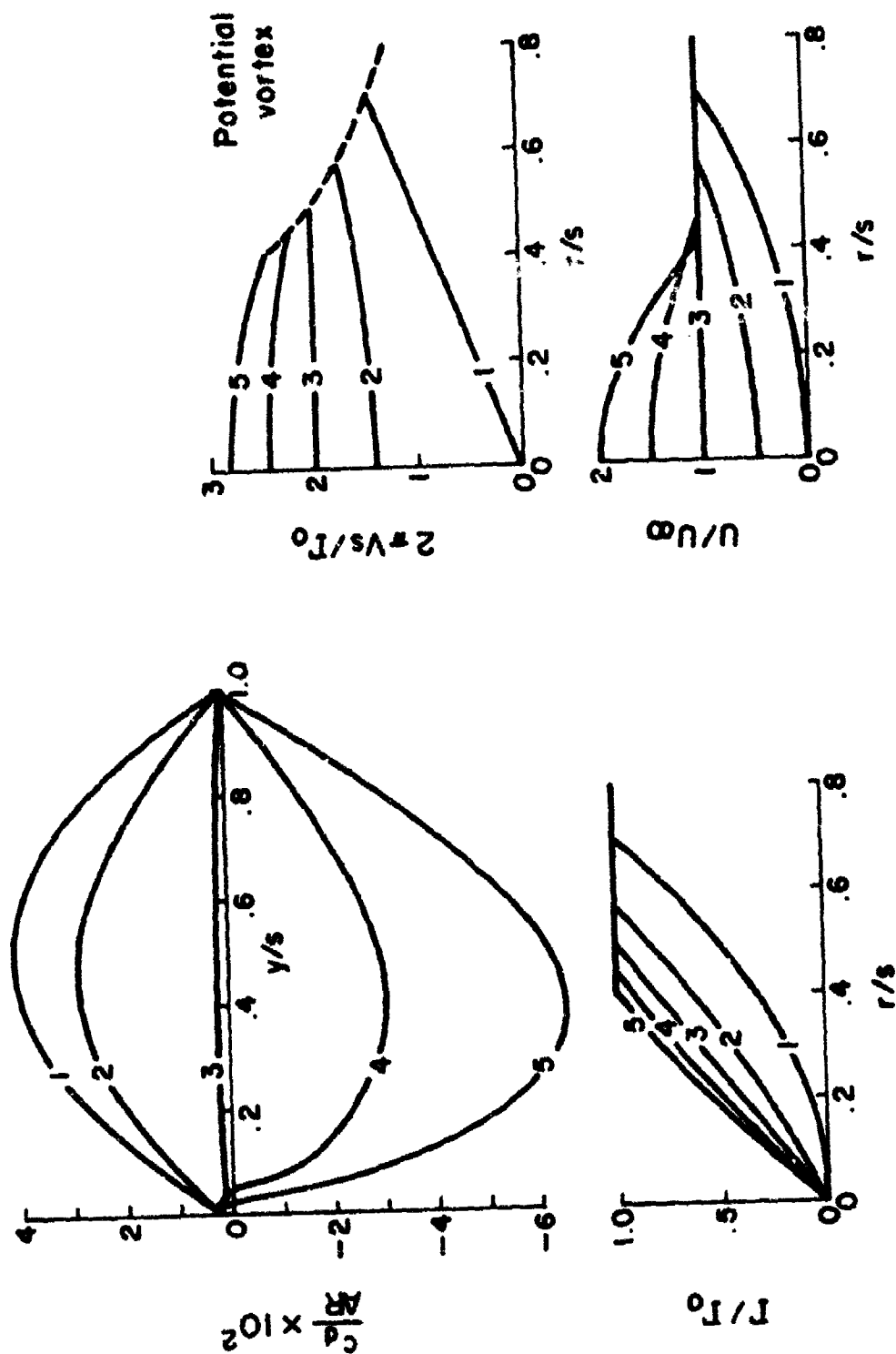
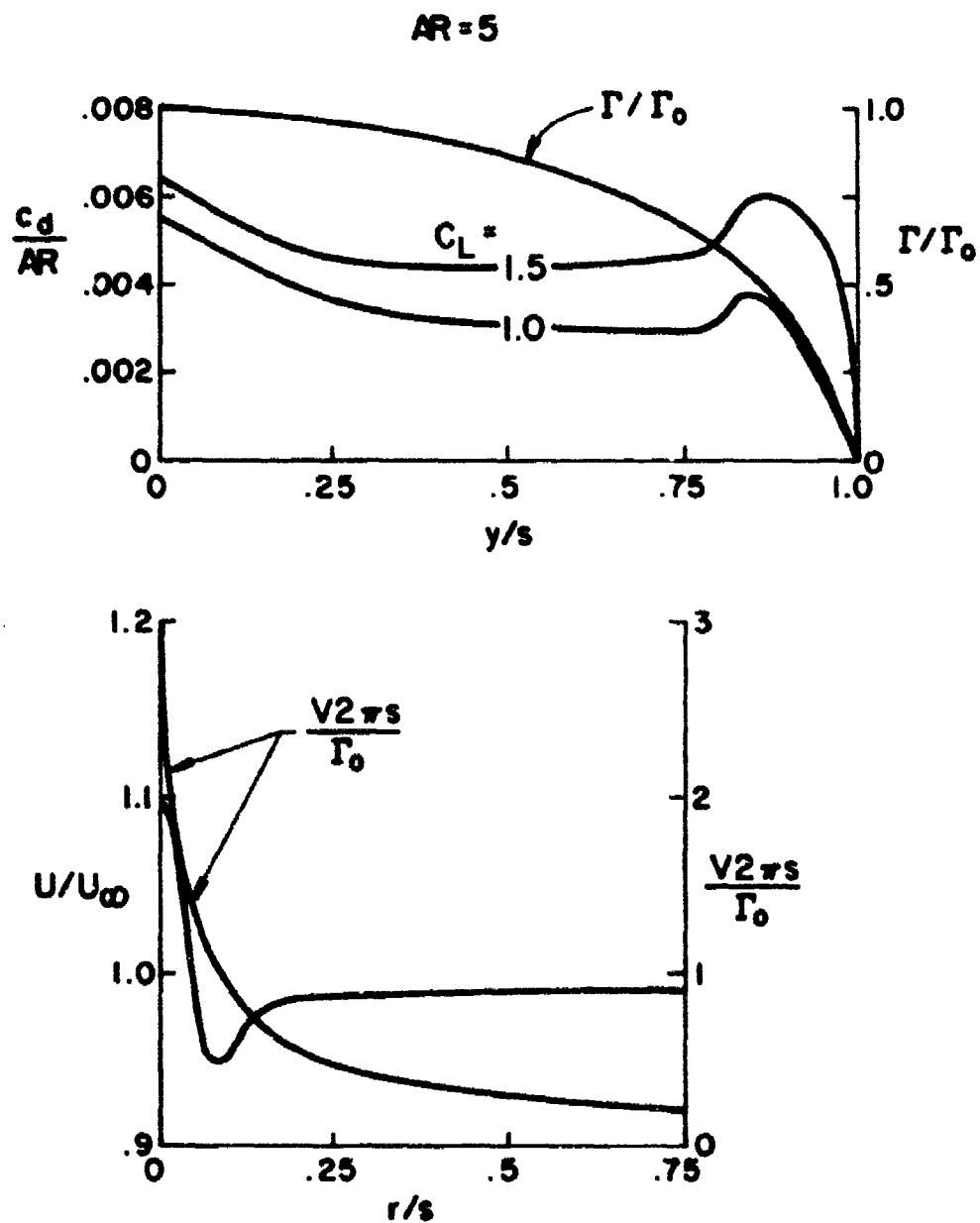Figure 6. Vortex wake structure for a linearly loaded wing

Figure 7. Examples of drag distributions which result in regions of axial velocity excess and defect in the vortex

of estimating how the turbulent kinetic energy from the wing distributes itself in the rolled-up vortex. Once this is known, it is possible to make detailed calculations of the local turbulent decay of these vortices using a computer program which was developed by A.R.A.P. (Ref. 15) for ARL. One might then ask the questions as to how much turbulence is required and where on the wing would we introduce it to bring about the most rapid aging of the vortex. The answers to these questions have obvious applications. We will only treat the roll-up of a tip vortex here, although extending the analysis to interior vortices is straight-forward.

In order to derive a simple expression which gives the distribution of turbulent kinetic energy $q'^2(r)$ in the rolled-up vortex, it is necessary to make a somewhat tenuous assumption; namely, the production, dissipation, and diffusion of turbulence are negligible during the roll-up process. We might refer to the turbulence as being in a "frozen" state so that we may write

$$\int_{-h(y)/2}^{+h(y)/2} q^2(y,z)U(y,z)dz\, dy = -q'^2(r)2\pi r U(r)dr \qquad (32)$$

Equation (32) states that the flux of turbulent kinetic energy immediately behind the wing through the area $h(y)dy$ equals the flux in the annular area $2\pi r\, dr$. $h(y)$ must be calculated from mass conservation. Substituting Eq. (14) into (32) yields

$$q'^2(r) = \frac{-\displaystyle\int_{-h(y)/2}^{+h(y)/2} q^2(y,z)\,\frac{U(y,z)}{U_\infty}\,dz}{-h_1(y)} \qquad (33)$$

$h_1(y) = \pi d(y - \bar{y})^2/dy$ and is the height of a rectangular area of width dy through which the volume flux equals that in the annular area $2\pi r\, dr$. The relationship between h_1 and h is simply

$$h_1(y) = \int_{-h(y)/2}^{+h(y)/2} \frac{U(y,z)}{U_\infty}\,dz \qquad (34)$$

and h accounts for the mass defect in the turbulent boundary layer. Since h is, in general, much greater than the turbulent boundary layer thickness (except at the wing tip), the integral in (33) is independent of $h(y)$ and, as the vortex rolls up, the turbulent kinetic energy in the vortex will diminish as $h_1(y)^{-1}$. The drop-off outward from the vortex center is a consequence of the fluid containing turbulent kinetic energy near the wing root being distributed over a larger area in the vortex than that fluid near the wing tip.

19

4. INTERACTIVE MOTION OF SHED VORTICITY

To complete the description of an aircraft wake, there remains the problem of determining how the discrete vortices, whose structure has been determined with the models developed in the previous sections, move under each other's influence. We are not concerned here, however, with self-induced motions such as those which in the presence of other vortices give rise to the Crow instability (Ref. 16). Our aim here is only to explore wake geometry by determining the approximate locations of the discrete vortices which form the wake.

We start with what is now the commonplace practice of modeling discrete vortices with infinite two-dimensional irrotational vortices. This assumption is correct as long as gradients in the flight direction of the wake are small. When this condition is met, the radii of curvature of the vortex filaments are large and the self-induced motion may be neglected. The motion of the vortices then does not depend crucially on the vortex structure (see Ref. 17). The condition for small axial gradients is one which requires that C_L/AR be small, since the motions perpendicular to the flight direction proceed with velocity of order Γ/b and axial gradients are, therefore, of order Γ/bU_∞. Obviously this condition is met under most circumstances since $C_L \sim \mathcal{O}(1)$ and AR is typically $\mathcal{O}(10)$. We may then make the equivalence between time and downstream distance through $d/dt = U_\infty(d/dx)$.

We consider the motion of n irrotational vortices of strength $\kappa_i = \Gamma_i/2\pi$ at instantaneous locations (y_i, z_i). The velocity of motion of the jth vortex is equal to the fluid motion at the point (y_j, z_j) in the absence of the jth vortex. Mathematically, the instantaneous velocity is calculated from

$$\frac{dy_j}{dt} = -\sum_{i(\neq j)}^{n} \frac{\kappa_i(z_j - z_i)}{r_{ij}^2} \tag{35}$$

$$\frac{dz_j}{dt} = \sum_{i(\neq j)}^{n} \frac{\kappa_i(y_j - y_i)}{r_{ij}^2} \tag{36}$$

and the summation is to exclude the jth vortex. r_{ij} is the distance between the jth and ith vortex and is given by

$$r_{ij}^2 = (y_i - y_j)^2 + (z_i - z_j)^2 \tag{37}$$

Figure 8 illustrates the configuration to be studied. Some simplification now results since the vortices occur in pairs, and it is not difficult to show from the calculation of the vertical momentum of the flow that
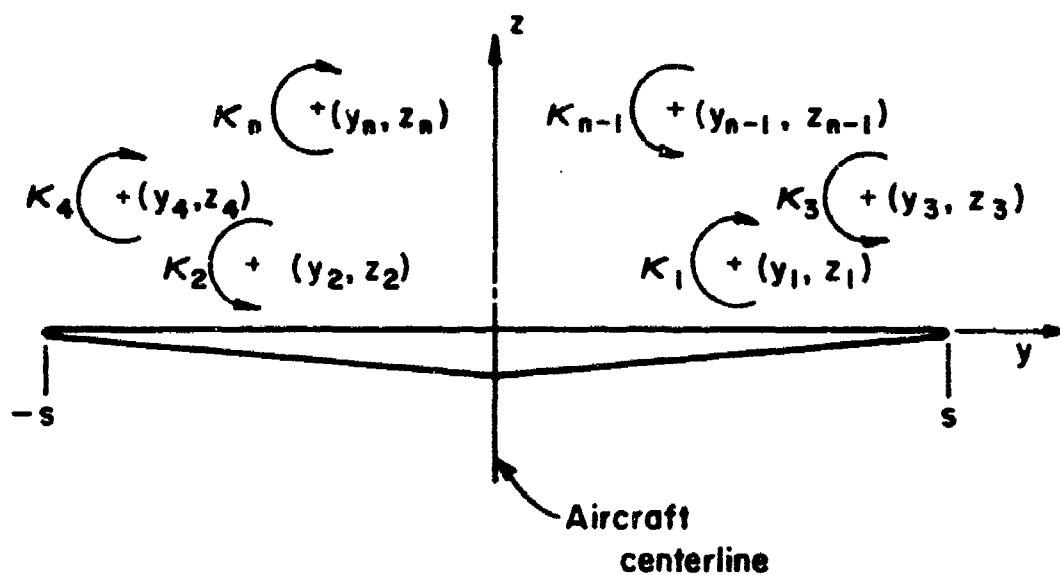
20

Figure 8. Geometry for the calculation of the downstream location of vortex centroids

$$\sum_{i=1}^{n} y_1 \kappa_1 = J \tag{38}$$

where J is a constant. In general, however, except for a few special cases, the solution to Eqs. (35) and (36) must be obtained by numerical integration.

If, for the time being, we do not concern outselves with the time history of the motion, we may then obtain information regarding the relative trajectories of the vortices. Dividing Eq. (35) by (36), it is quite remarkable that the expression can be integrated to yield

$$W = -\sum_{i}^{n} \sum_{j}^{n} \kappa_1 \kappa_j \log r_{ij} \tag{39}$$
$$(i \neq j)$$

It is readily recognized that W is the integral by noting that (35) and (36) may be written in the form

$$\kappa_j \frac{dy_j}{dt} = \frac{\partial W}{\partial z_j} \tag{40}$$

$$\kappa_j \frac{dz_j}{dt} = -\frac{\partial W}{\partial y_j} \tag{41}$$

It may be shown that W is related to that portion of the kinetic energy of the flow that depends on only the relative distance between vortices.

While the aircraft wake may be made up of any number of pairs of vortices, it is likely that most aircraft wakes can be described by three or fewer pairs. When two pairs are adequate, a great deal can be said regarding the geometry of the wake without resorting to numerical calculation. For two-pair wakes having a common axis of symmetry (the aircraft centerline), Eq. (39) can be written in the form

$$B = \left[\frac{e^2 + (y_1 + y_3)^2}{e^2 + (y_1 - y_3)^2} \right] (y_3)^{\kappa_3/\kappa_1} (y_1)^{\kappa_1/\kappa_3} \tag{42}$$

where e is 1/2 the vertical separation distance between pairs. y_1 or y_3 may be eliminated from (42) by substituting (38). The constant B is to be evaluated with $e = 0$ (the trailing vortex pairs lie in the same plane at the wing). Equation (42) then describes all possible relative vortex trajectories with a rather simple expression. The obvious question is, "For what values of J and B are trajectories which have $e \to \infty$ possible?" The investigation of the relative trajectories, while

22

very interesting, is tedious and we only present the results here. It is possible to construct what might be called a wake classification chart for four vortex wakes, as shown in Figure 9. From this chart, knowing the relative vortex strengths and initial locations, it is possible to determine if the wake geometry will be such that the vortex pairs will remain contiguous or separate downstream.

We have carried out four sample calculations, shown in Figures 10-13. The trajectories are viewed from downstream behind the aircraft. The quite diverse behavior of the vortices is predicted by Figure 9 where we have shown where these cases lie on the wake classification chart. The ability to predict wake behavior should prove to be of great use to the aircraft designer as well as to the aerodynamicist concerned with wake alleviation.

When the aircraft vortex wake must be modeled by three or more pairs of vortices, trajectories can only be obtained by direct numerical calculation. To check our numerical scheme for three-pair wakes, we chose to model the wake of an aircraft where flow visualization was available. Farlett and Shivers (Ref. 18) describe such a test of an E.B.F.V/STOL model. The aircraft was one which had a blown inboard flap and was consequently highly loaded there. From data presented, we crudely estimated the lift distribution due to circulation lift to be that shown in Figure 14. In Figures 15-17, the results of the numerical solution of Eqs. (35) and (36) are presented. The aircraft is at 10° angle of attack and is a scale representation of the test model. The results are shown in perspective to help resolve the complicated wake geometry that results. As can be seen, a strong outboard flap vortex-tail interaction is predicted by the calculation. Figure 18 has been reproduced from Figure 17b in Reference 18 and clearly shows the interaction just described. It is reported in Reference 18 that the aircraft tested became longitudinally unstable at angles of attack in excess of 7° due to the strong downwash field induced at the tail. Simple calculations of this type should prove to be extremely useful in that they are able to predict the observed unfavorable vortex tail interference. With an estimate of the rate at which vortex sheets roll up (a simple model is developed to do this in Appendix A) and with the models previously described, the ability to accurately predict the downwash field in the near wake will be possible.
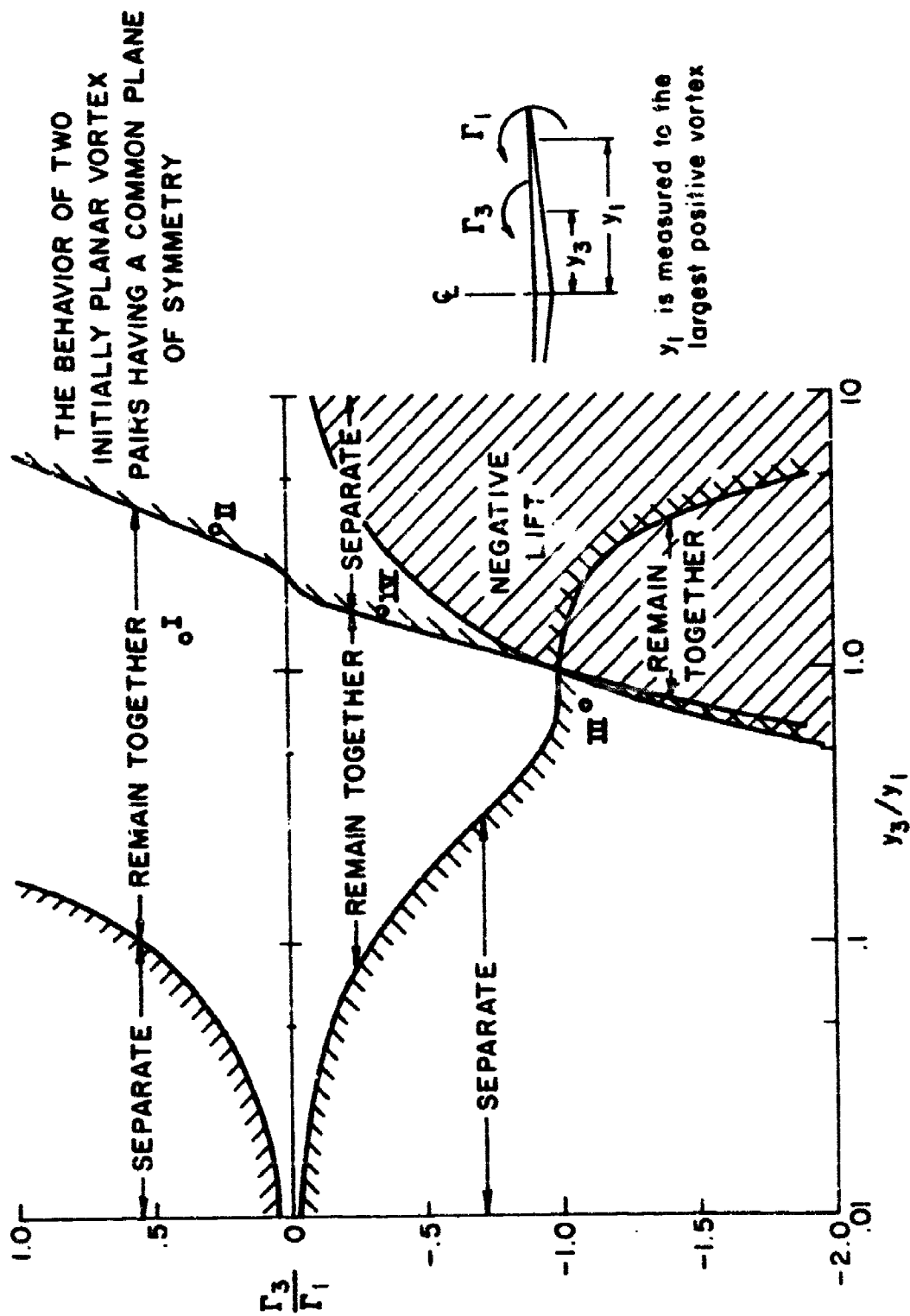
Figure 9. Wake classification chart for two-vortex-pair wakes

TRAILER TRAJECTORIES
INBOARD FLAP
$s_f/s = .8 \quad \delta_f = 20° \quad C_L = 1.0 \quad \Gamma_t/\Gamma_f = .37$
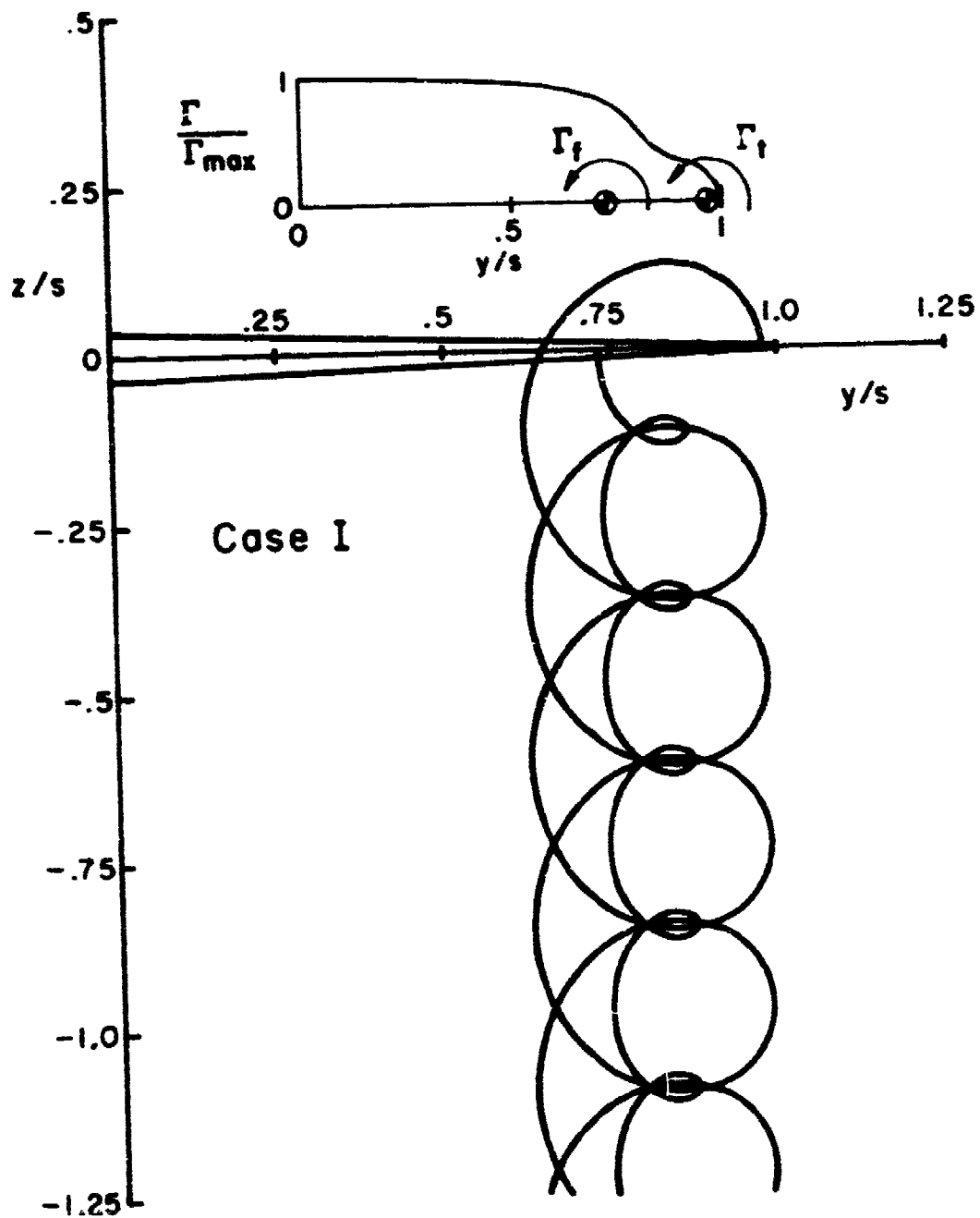

Figure 13. Vortex centroid locations as seen from downstream with strong interaction between neighboring locations

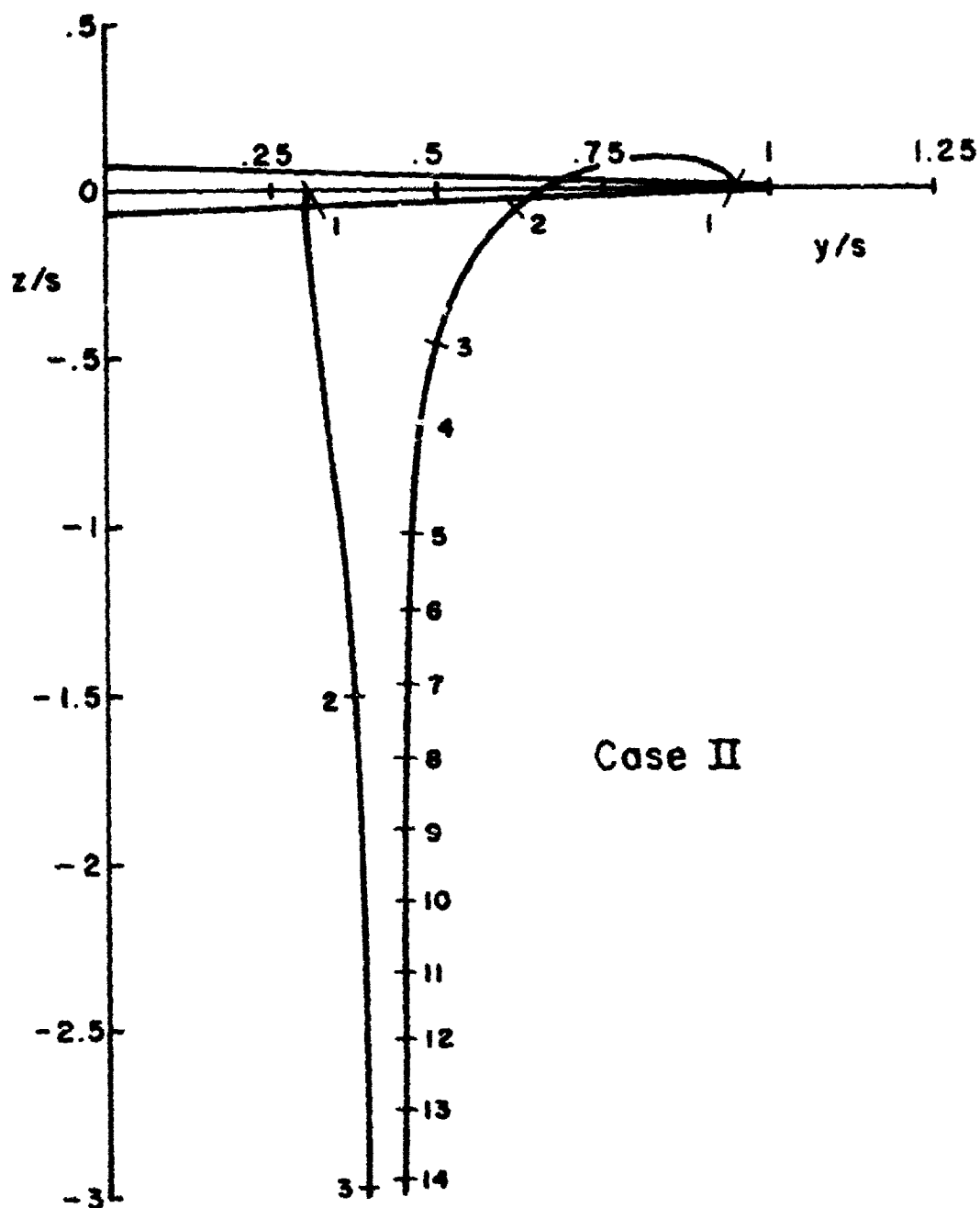# TRAILER TRAJECTORIES

$$\Gamma_t / \Gamma_f = .2$$

Figure 11. Vortex centroid locations as seen from downstream with weak interaction between vortex pairs; pairs diverge

TRAILER TRAJECTORIES
OUTBOARD FLAP

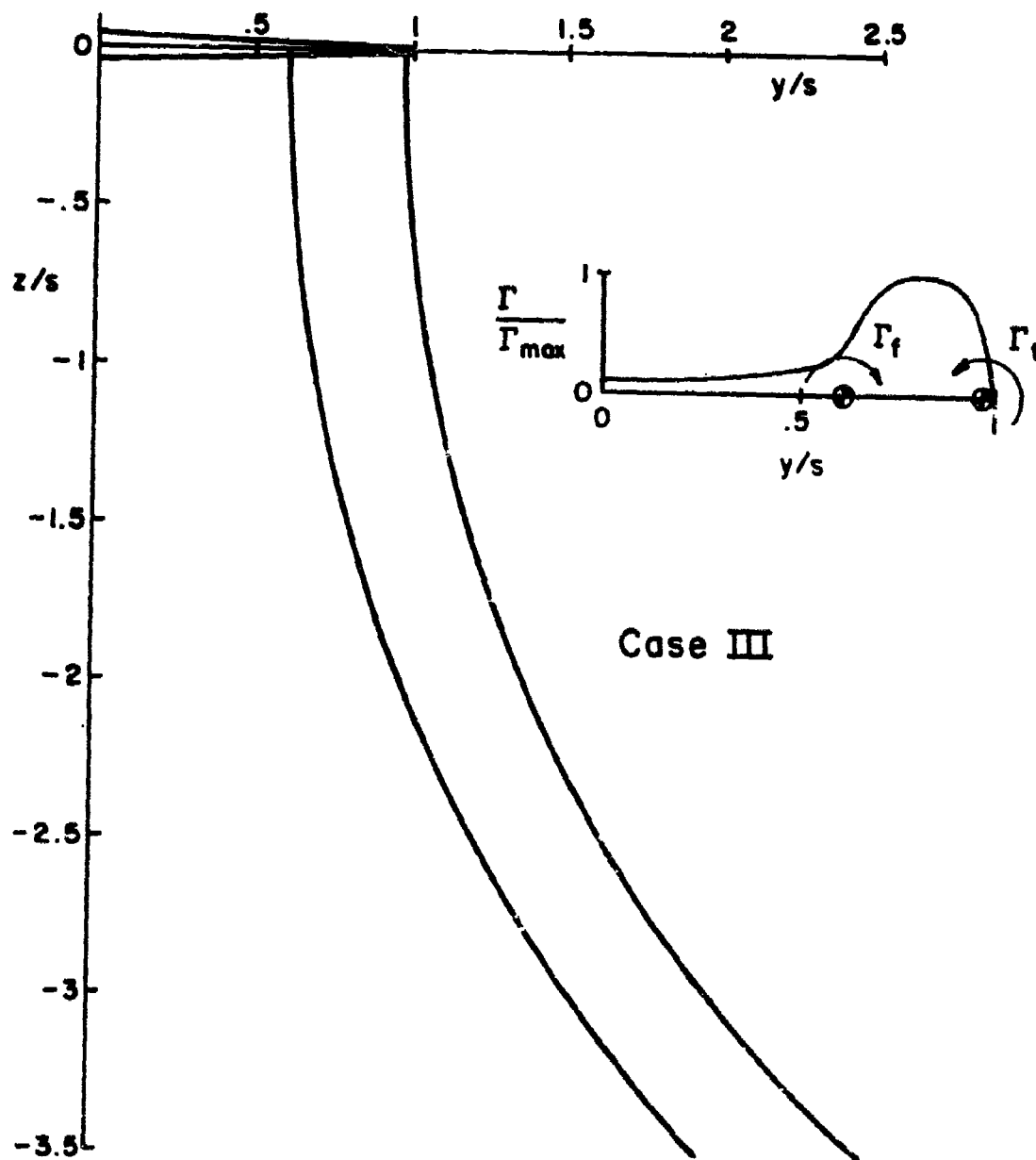$s_f/s = .33$ $\delta_f = 40°$ $\Gamma_t/\Gamma_f = -1.1$
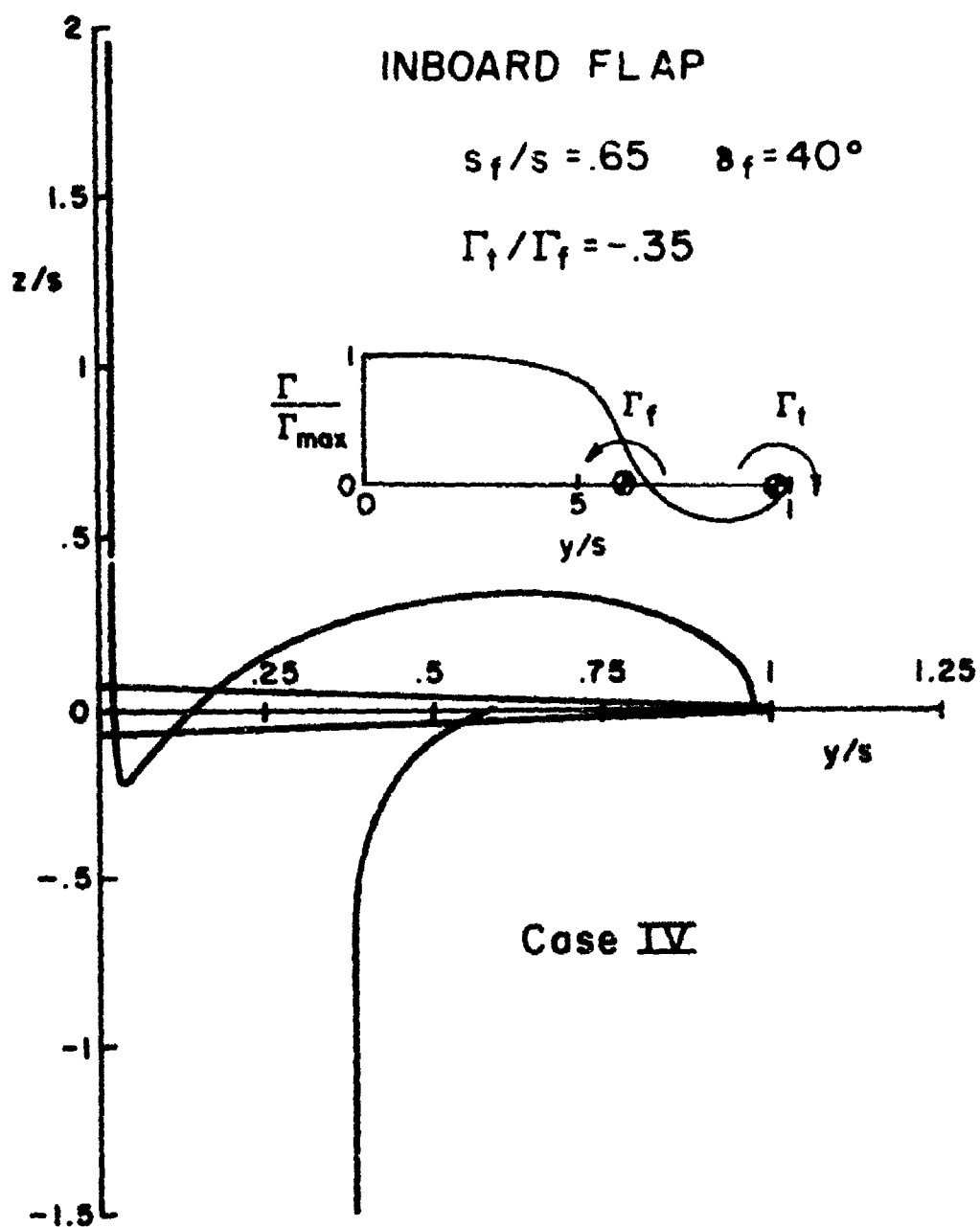

Case III

Figure 12.   Vortex centroid locations as seen from downstream;
pairs of opposite sign. Pairs remain together.

TRAILER TRAJECTORIES

INBOARD FLAP

$$s_f/s = .65 \qquad \delta_f = 40°$$

$$\Gamma_t/\Gamma_f = -.35$$

Case IV

Figure 13.   Vortex centroid locations as seen from downstream;
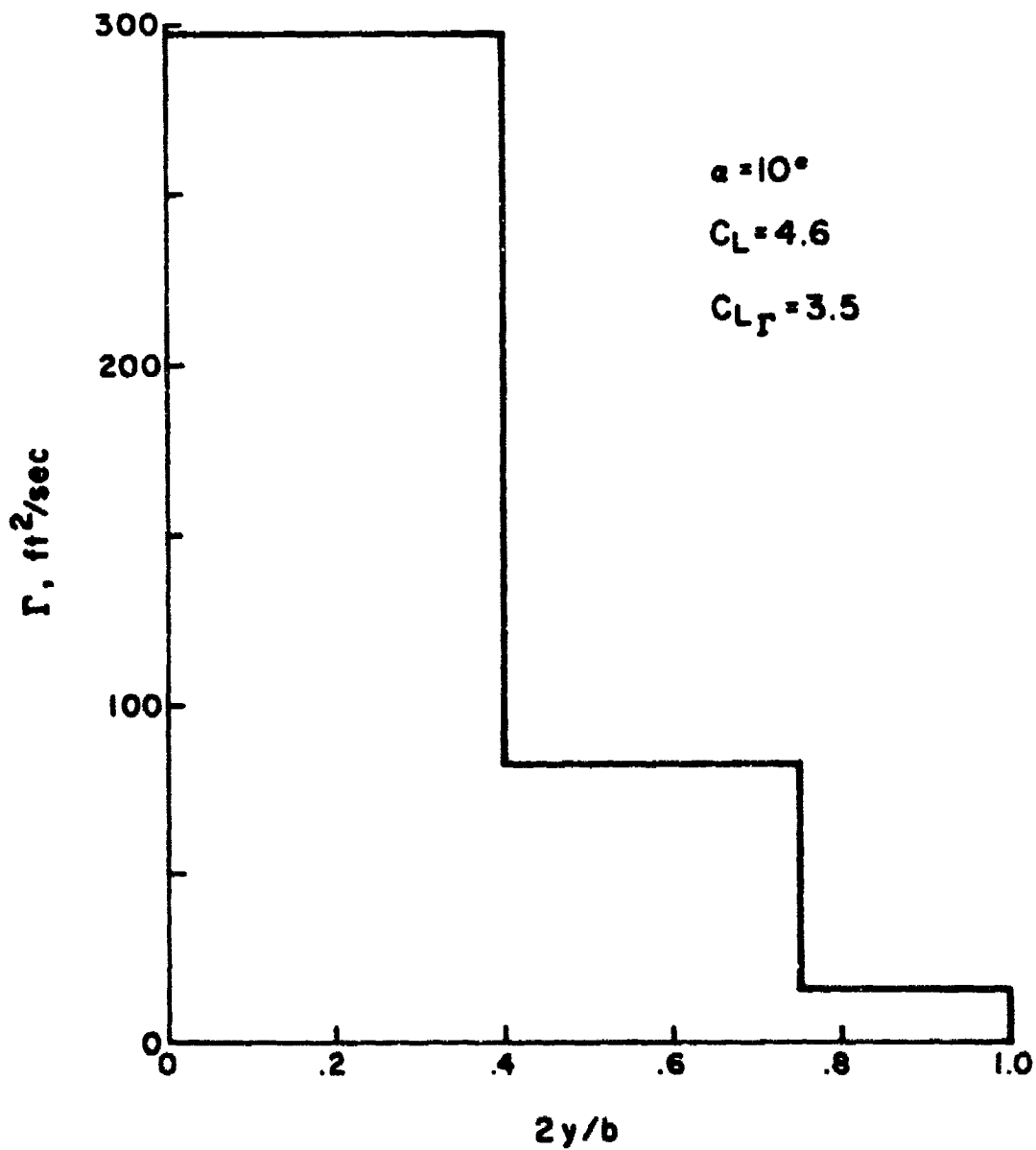pairs of opposite sign.   Weak interaction between
pairs; pairs diverge.

Figure 14. Estimated circulation lift distribution on a NASA prototype E.B.F. STOL model
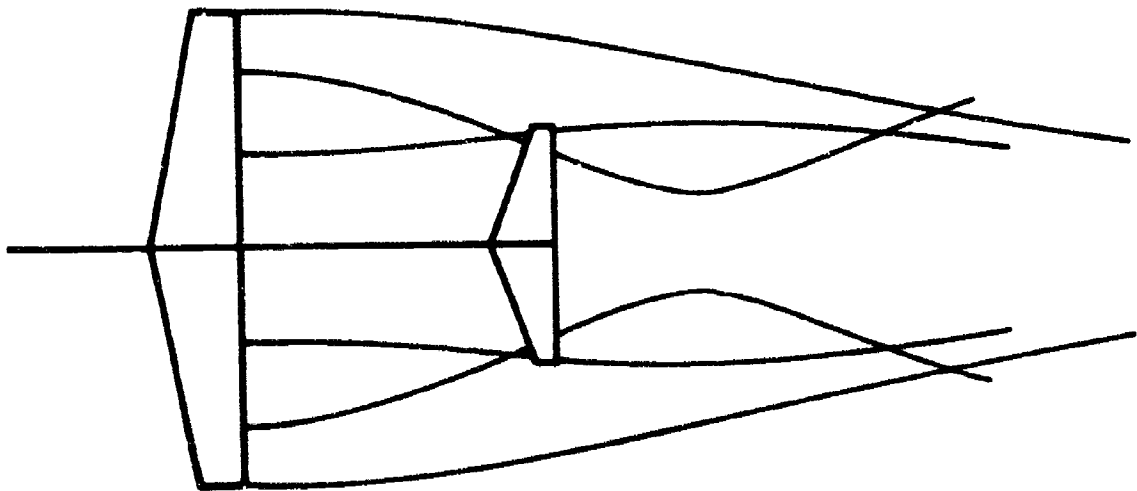
TOP VIEW

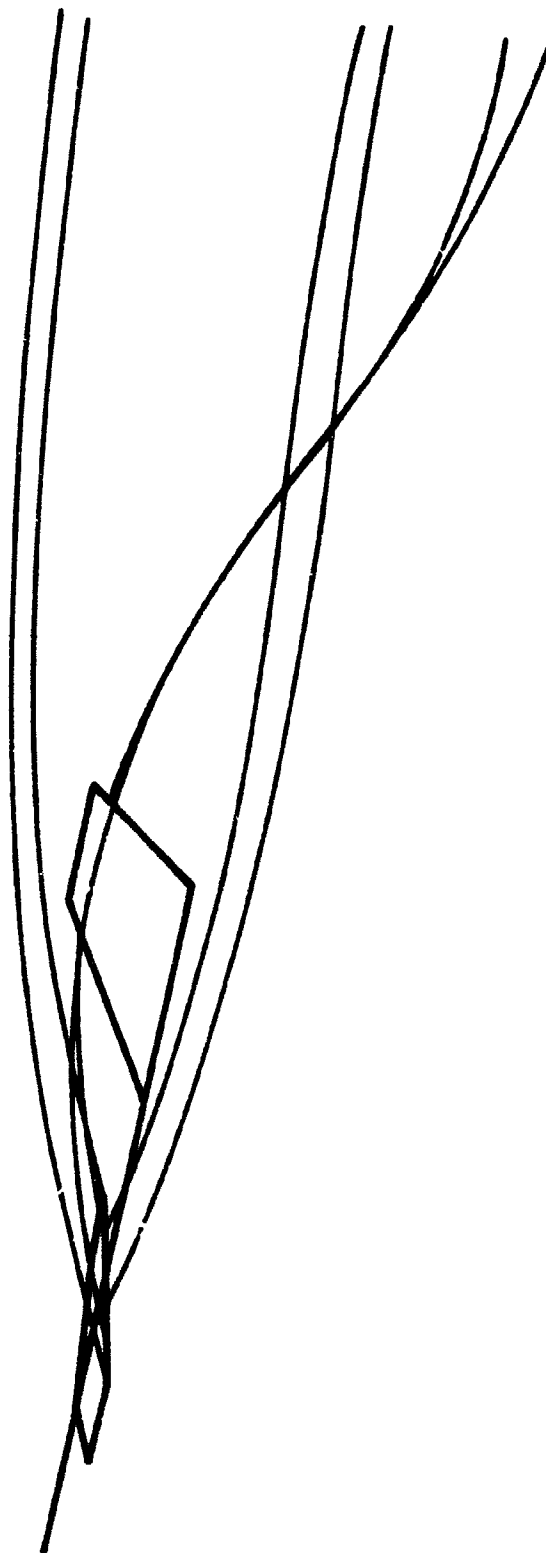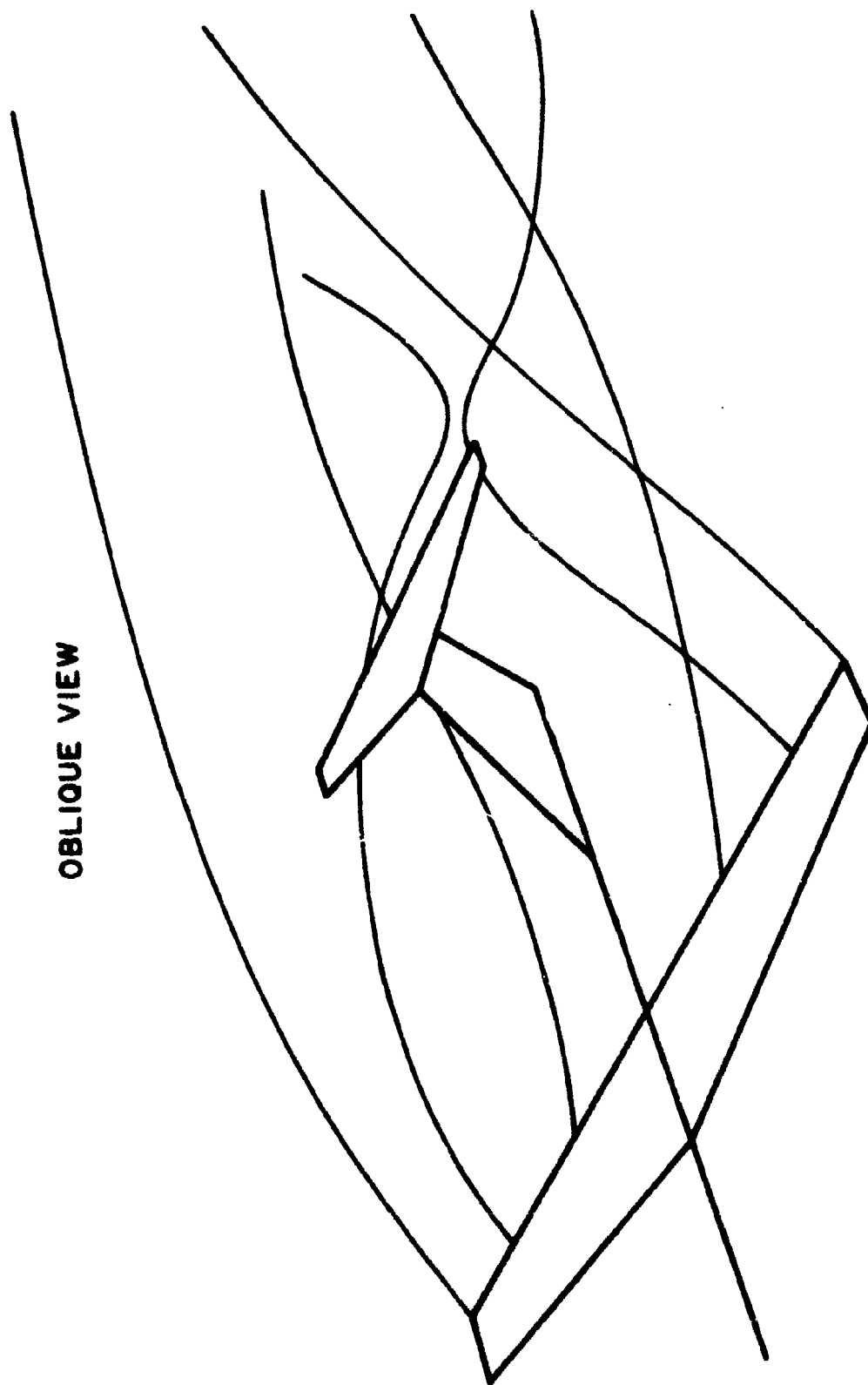Figure 15. Calculated wake geometry; top view

SIDE ELEVATION

Figure 16. Calculated wake geometry; side elevation

OBLIQUE VIEW
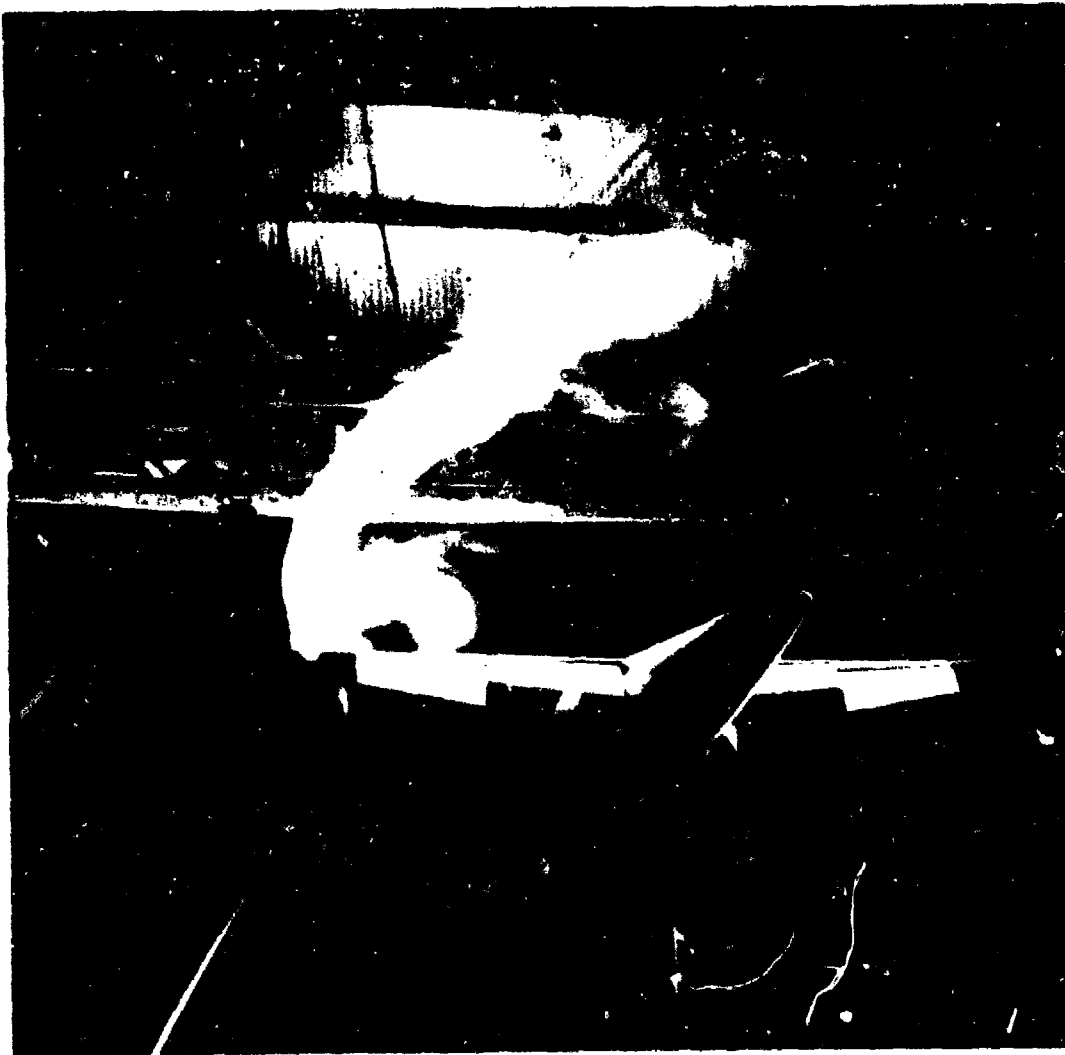
Figure 17. Calculated wake geometry; oblique view

32

Figure 18. Smoke visualization showing the outboard flap vortex in proximity to the stabilizer

SECTION III

THE EXPERIMENTAL EFFORT

The validity of the Betz models and those extensions developed in this report were checked, where possible, with experimental measurements made in the V/STOL tunnel at NASA Langley Research Center. This section describes the design and implementation of the test program which was carried out.

1. WAKE CLASSIFICATION AND EXPERIMENT DESIGN

In order to check the models which describe the mean wake structure (the turbulent structure was not to be measured here), it was necessary to obtain wing lift and drag distributions and the velocity distributions in the downstream wake. The test model and tunnel facility were supplied by the government.

It was decided that the test would concern itself with two-vortex-pair wakes. One pair would result from an "interior" roll-up and the second, obviously, as a result of a tip roll-up. The results of the two-vortex-pair trajectory model suggest that the geometry of two-vortex-pair wakes may be classified such that they fall into one of four categories:

1) Both pairs are of the same sign and the pairs remain together (e.g., see Fig. 10).

2) Both pairs are of the same sign and the pairs separate (e.g., see Fig. 11).

3) The pairs are of opposite sign and remain together (e.g., see Fig. 12).

4) The pairs are of opposite sign and separate (e.g., see Fig 13).

Categories (3) and (4) were judged unlikely to occur under current aircraft operating conditions and, therefore, only one configuration which produced two vortex pairs of opposite sign was tested.

The model supplied by the government is shown with relevant dimensions in Figure 19. Six, roughly equal plain flaps span the entire trailing edge of the wing. Flap deflection angles were fixed by brackets but covered a wide range so that the number of configurations possible was very large. With one configuration being the clean wing, the four test configurations are shown schematically in Figure 20.

The tunnel facility was the V/STOL tunnel at NASA Langley. The tunnel test section measures 14.5 ft high, 21.75 ft wide, and 50 ft long. The tunnel speed range is 0-200 knots. The model was sting-mounted as shown in Figure 21. During testing, the model was positioned as near to the tunnel centerline as possible.
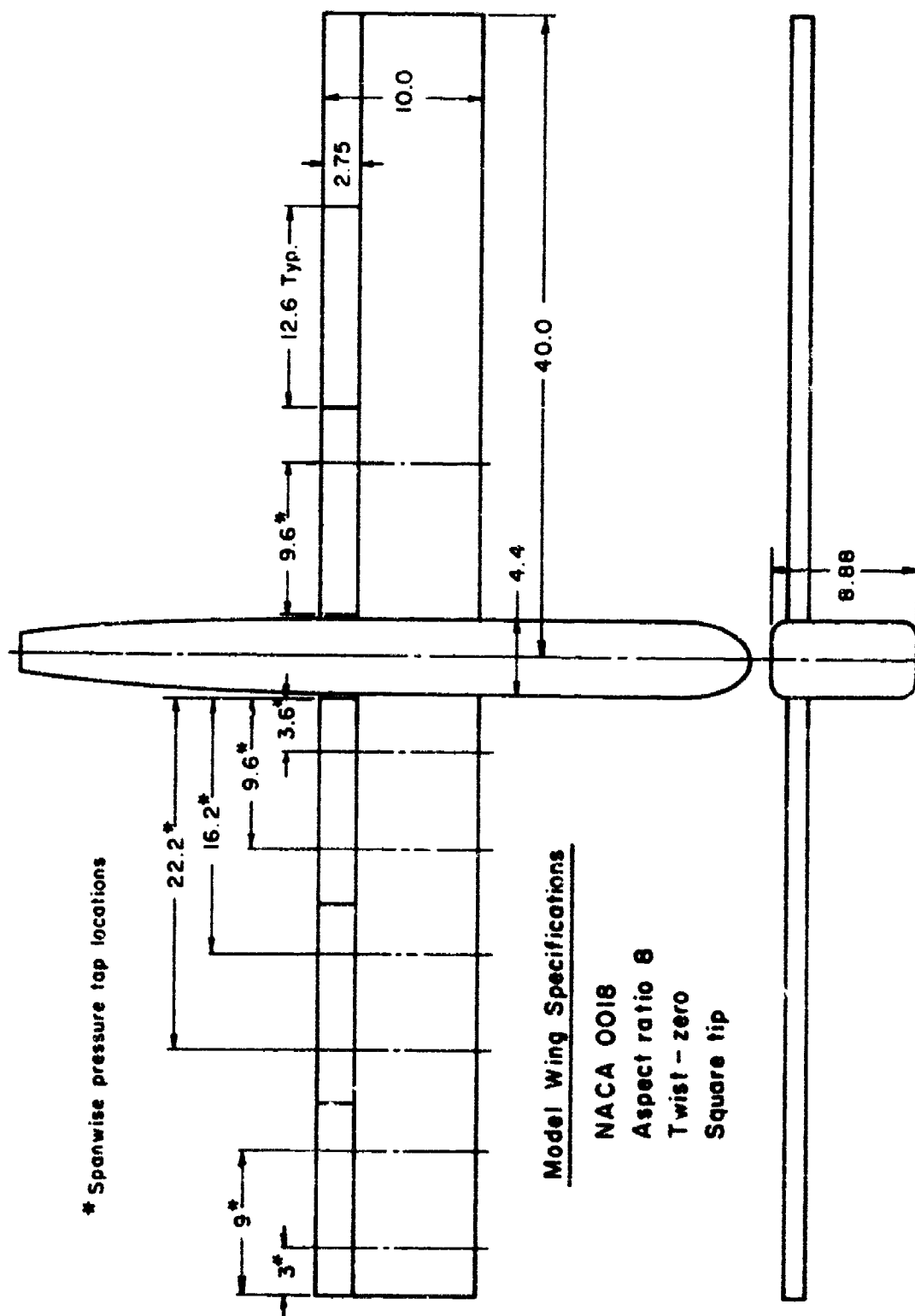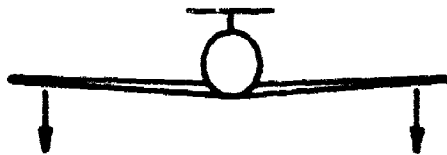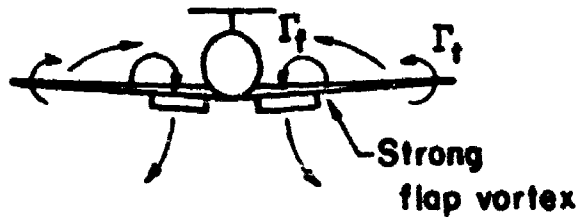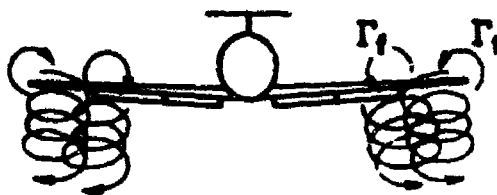
Figure 19. Test model (all dimensions are in inches)

Model Wing Specifications

NACA 0018
Aspect ratio 8
Twist – zero
Square tip

* Spanwise pressure tap locations

Configuration 1

Clean wing

Configuration 2

Inboard flaps $\delta_f = 30°$
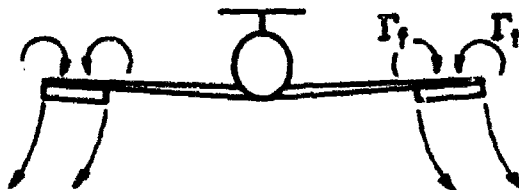
$\Gamma_f > \Gamma_t$

Strong flap vortex

Configuration 3

Inboard & midspan flaps
$\delta_f = 15°$

$\Gamma_f \approx \Gamma_t$

Configuration 4

Outboard flaps $\delta_f = 30°$

$\Gamma_f \approx \Gamma_t$

Figure 20. Model configurations tested in NASA Langley V/STOL tunnel

Figure 21. Test model
sting-mounted in the
V/STOL tunnel at NASA
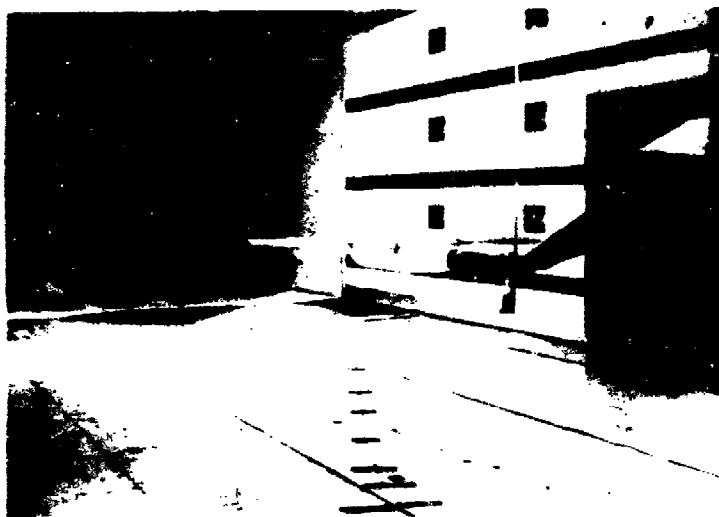Langley Research Center
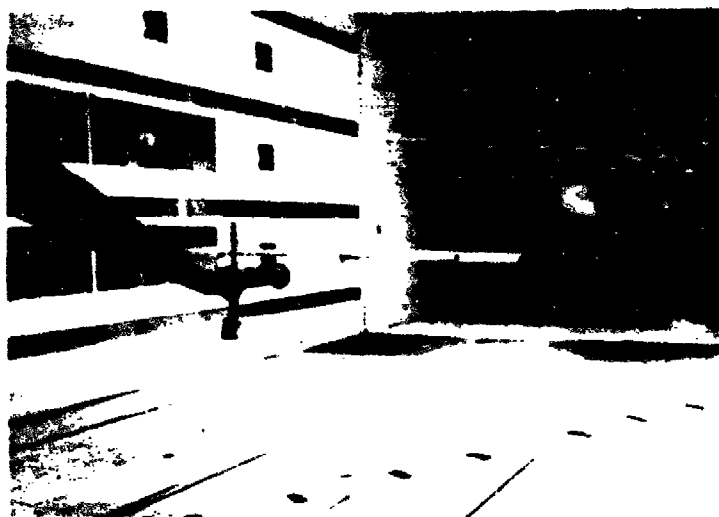
Figure 22. Model test
configuration 4

Figure 23. The wake
traversing mechanism
mounted with the hot-
film probe 5 chords
downstream of the
trailing edge

Downstream wake velocities were measured using a Thermal Systems Model 1050, split-film, three-component anemometer mounted on a traversing mechanism shown in Figure 23. Tunnel test speed was 85 ft/sec (dynamic pressure of 9 lb/ft^2) to avoid structural problems with the traversing mechanism.

Wing load and drag distributions are the inputs to the theoretical models to determine wake structure. Load distribution was determined from integration of pressure data from existing taps located at six spanwise locations. Because of the importance of these data, NASA Langley personnel also performed lifting surface calculations on the geometries to be tested to provide a check on the measured distributions. Profile drag distribution data were obtained by measuring the axial velocity defect at the wing trailing edge and determining the drag from an axial momentum balance. Since lift distribution data would only be given by six spanwise data points, vertical traverses to determine the axial velocity defect were only made at the same six spanwise stations. To assure a turbulent boundary layer on the upper side of the wing, a trip strip (0.06-inch diameter particles) 0.1-inch wide was placed along the wing 1 inch from the leading edge.

Prior to fixing the test model angle of attack and making velocity measurements in the wake, flow visualization studies were undertaken to determine if the chosen model configurations produced the desired wake structure. The trailing vortices were marked with smoke introduced upstream of the wing. The smoke, upon passing around the wing, becomes rolled up with the fluid forming the trailing vortices. Results from prior NASA Langley test programs have shown that this technique gives a very good description of the vortex positions.

Velocity measurements in the wake were to be made at the wing trailing edge, 5 chords, and 30 chords downs   am. However, the 30-chord measurement was subject to being mov $_{\perp}$ closer to the wing if vortex meander was judged so severe that meaningful data could not be obtained. V/STOL tunnel personnel have had considerable experience in making these measurements. Because of the basic unsteadiness in the wake, the anemometer signal was sampled over a time interval of 5 seconds and stored on magnetic tape. Prior test experience has shown that this sample time interval is a good compromise between obtaining meaningful averages and using excessive tape storage capacity. A disadvantage of this system is that no on-line capability was available, and first examination of the velocity data could not be made until after testing was complete.

The procedure used to determine the approximate location of the vortex center downstream was to mount an impact probe above the hot-film sensor and scan until a minimum in total pressure was obtained. Since the vortex is composed of vortical material shed from the boundary layer of the wing, the head in the vortex must be less than the surrounding irrotational flow. To aid in determining the area to be scanned, smoke was again introduced upstream of the

wing which rolled up and marked the vortex center. The hot-film sensor was shielded to avoid contamination and the impact probe was visually lined up with the vortex center.

At the 5-chord and 30-chord downstream positions, three horizontal traverses were made across each vortex. The traverses were spaced 1 inch vertically apart, and velocity data were obtained at approximately 0.5-inch horizontal intervals across the vortex. This grid spacing provides a good description of the vortex structure while not requiring a prohibitively large number of data points. Traverses at the wing trailing edge were made vertically, the distance between data points being approximately 0.1 inch.

2. THE TEST SEQUENCE

The test program was performed in the following sequence.

1) Force, moment, and wing pressure data were obtained for the four model configurations through an angle of attack range which would bracket the estimated test angle of attack. Pressure data were obtained prior to fixing the angle of attack after flow visualization studies to avoid plugging the small pressure orifices with oil residue from the smoke generators.

2) Flow visualization was carried out using smoke and helium-filled soap bubbles to mark the wake flow field. Photographs recorded the trailer positions from cameras which were permanently mounted and hand held. Test angles of attack were fixed upon obtaining the desired wake geometries.

3) Velocity measurements were made in the wake using the hot-film sensor mounted on an existing traversing mechanism which was controlled outside the tunnel test section. Probe calibration was checked prior to and at the completion of each test run.

SECTION IV

TEST RESULTS AND COMPARISON WITH THEORETICAL MODELS

The model test configurations and test conditions are summarized below.

Configuration	Flaps	$\delta_f{}^\circ$	α°	Re_c	q, lb/ft^2
1	None	–	10	2.25×10^5	9
2	Inboard	30	6		
3	Inboard & Midspan	15	6.5		
4	Outboard	30	1.5		

The results of the test program are

1) Wing lift distribution obtained from integration of pressure tap measurements for the four model test configurations;

2) Photographs of the wake structure for the four model test configurations;

3) Three-component mean velocity measurements in the wake at the wing trailing edge and 5 chords downstream for the four model test configurations. Three-component mean velocity measurements in the wake 10 chords downstream for two model test configurations. Wind tunnel scheduling problems prohibited testing two additional configurations at the 10-chord position.

1. WING PRESSURE DATA AND WING LIFT DISTRIBUTIONS

Wing pressure data were supplied by NASA Langley Research Center in pressure coefficient form. Wing lift distribution was obtained by integrating the pressure data over the chord of the airfoil and then taking the vertical component of the resulting force coefficient. In general, pressure data on deflected flaps were difficult to interpret due to the limited number of pressure taps (two) on the underside of the flap. When this problem occurred, data on the flap were faired to yield what were judged to be reasonable chordwise distributions.

The experimentally determined wing lift distributions are shown in Figure 24. The limited number of spanwise pressure tap locations forced some fairing of the results. The distributions are physically very reasonable, however, and will produce the desired wake structures. All configurations had a significant lift drop-off inboard as recorded by the pressure taps at $2y/b \approx 0.15$. This is a result of the rather large model fuselage which is needed to hold instrumentation. The strongly loaded tip in the clean configuration is believed to arise as a consequence
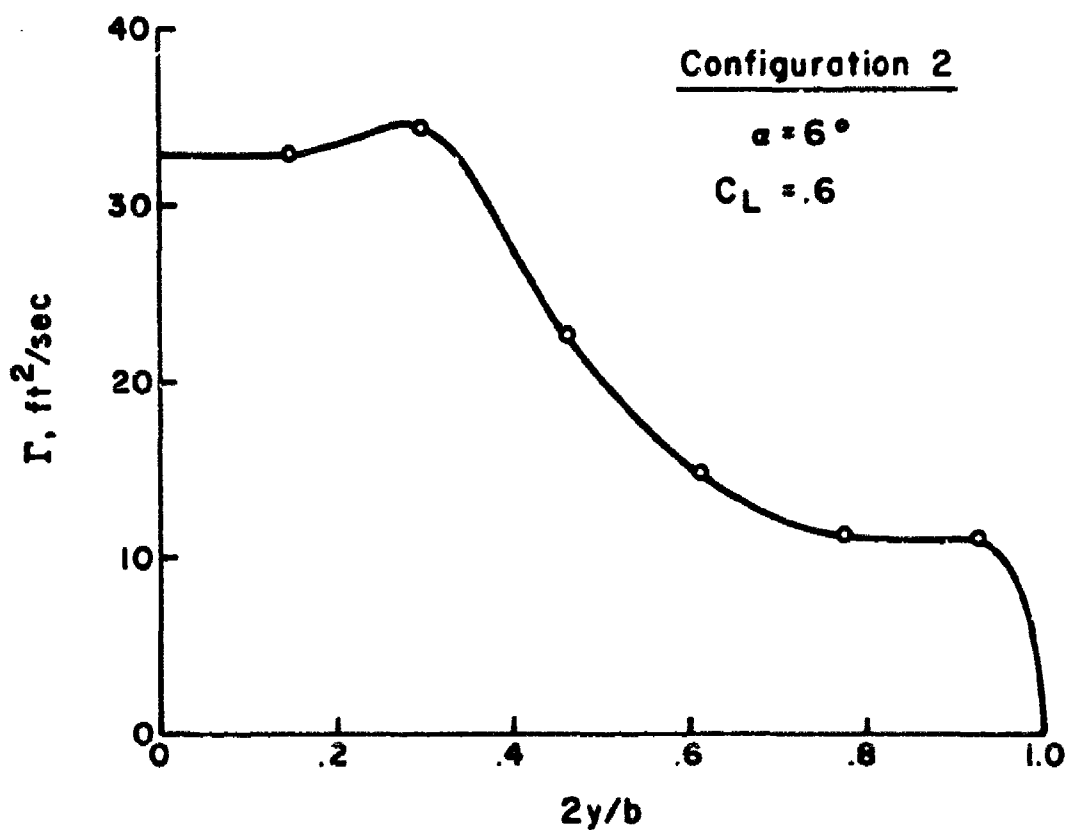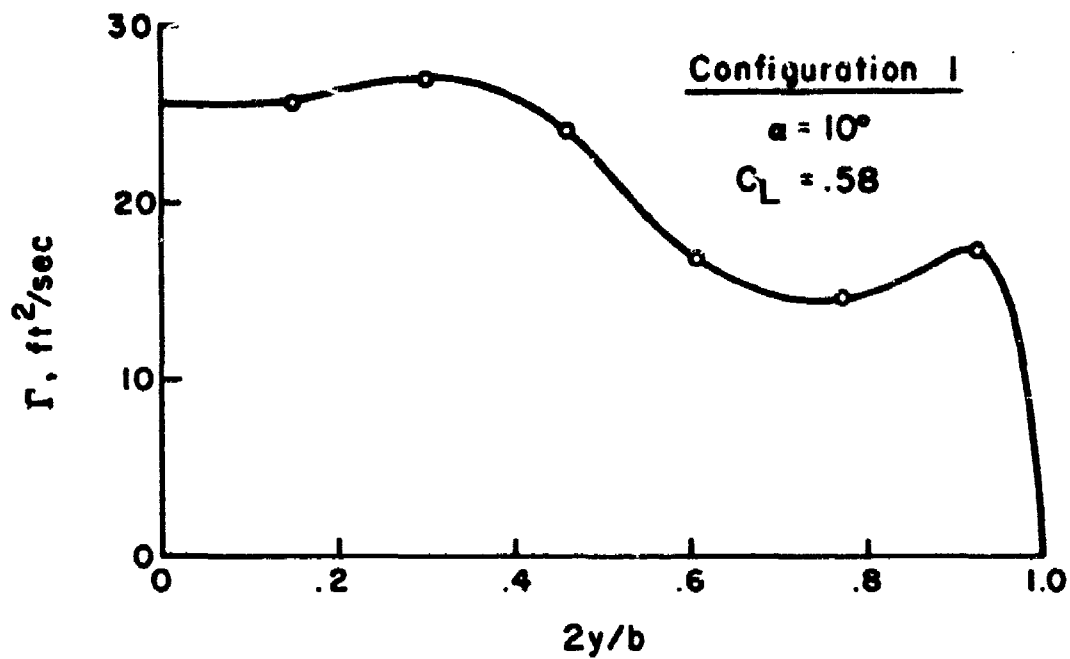
41

Figure 24. Lift distributions from wing surface pressure measurements

Configuration 3

$a = 6.5°$
$C_L = .57$
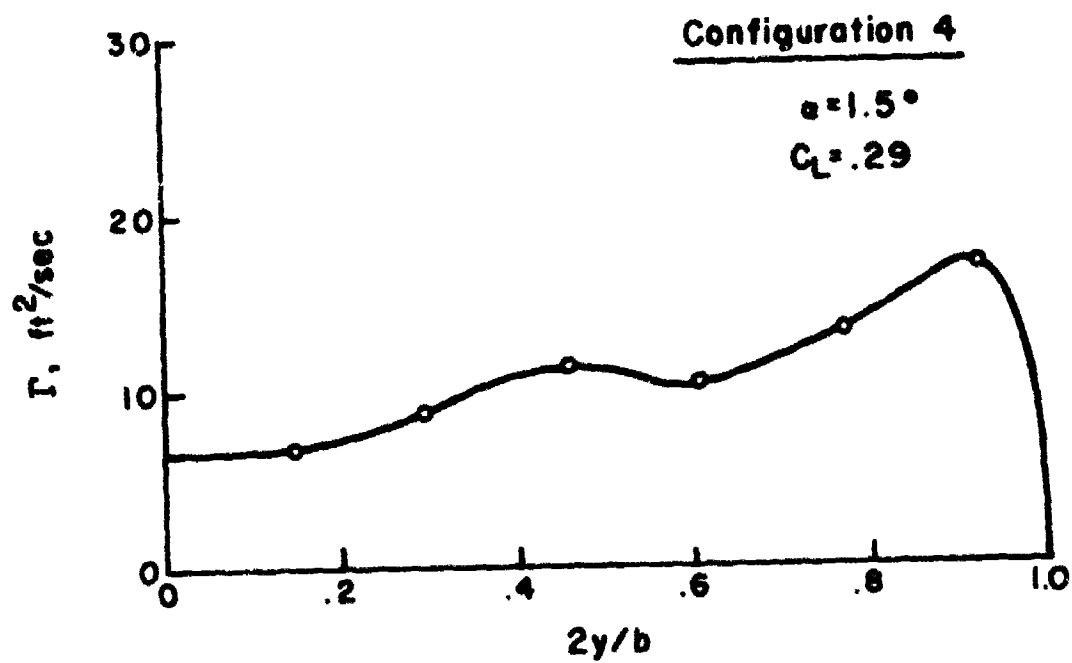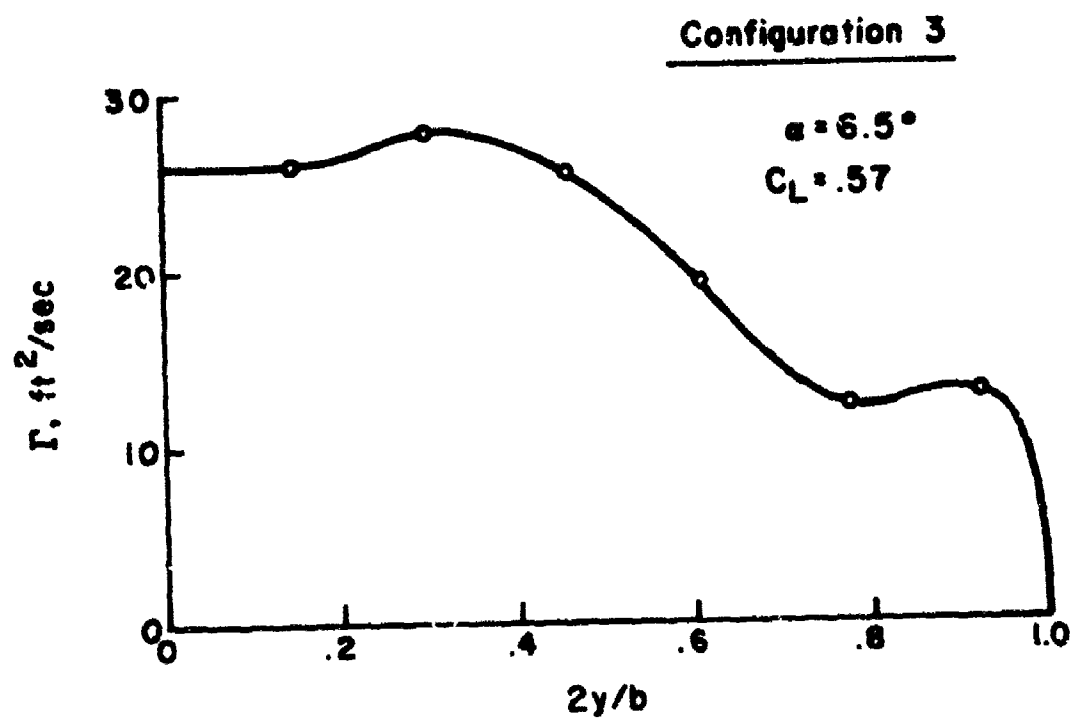
Configuration 4

$a = 1.5°$
$C_L = .29$

Figure 24 (continued)

43

of vortex lift much like that which results on a delta wing.
Smoke flow visualization of this configuration indicates that the
flow separates at the square tip, and roll-up actually proceeds
from the wing tip near the leading edge.

The experimentally determined lift distributions may be
compared with lifting surface calculations supplied by the V/STOL
tunnel staff. The calculations are shown in Figure 25 and match
model geometry and measured lift coefficient. It is obvious that
there are some differences between these results. Both results
are subject to error, and it is likely that the true lift distri-
bution is somewhere between the two results. We view both results
cautiously for several reasons. On one hand, the lifting surface
calculation neglected the rather large fuselage. Perhaps more
significant is the fact that the test Reynolds number was moderate
and the airfoil section had a thickness ratio of 0.18. On the
other hand, however, experimentally determined distributions, as
previously mentioned, suffered from a limited number of pressure
taps. So that no bias would be shown in the comparison of measured
wake velocity fields with those calculated from wing lift and drag
distributions, calculations were performed using both experimental
and lifting surface results.

2. FLOW VISUALIZATION

Results of the flow visualization studies and calculated vortex
positions are shown in Figures 26-33. The vortices were made
visible with smoke, as previously described. Vortex centroid posi-
tions were calculated using the model developed in Section II.4 and
are shown on consecutive figures. As an input to the calculation,
the lifting surface load distributions were divided into flap and
tip vortices according to the criterion previously described. For
the small downstream distances observed here, the results are quite
insensitive and differ little from the results obtained using the
experimentally determined lift distributions. The calculated
trajectories are presented in perspective with the viewing position
taken to be the camera location. As can be seen, the agreement is,
in general, very good.

Photographs taken with cameras permanently mounted in the
tunnel provided somewhat less information than those taken with
hand held cameras. In Figure 34 are shown side views of the wakes
of configurations 2 and 4 taken with a permanently mounted camera.

Helium filled soap bubbles were also introduced upstream of
the wing in an effort to visualize the downstream wake. Although
the bubbles did roll up into the vortex, observation was hampered by
the low density of bubbles and difficulties with illumination.

3. COMPARISON OF COMPUTED AND MEASURED WAKE VELOCITY DISTRIBUTIONS

Wake velocities were received in Cartesian tunnel coordinates,
positive x measured downstream from the trailing edge and positive
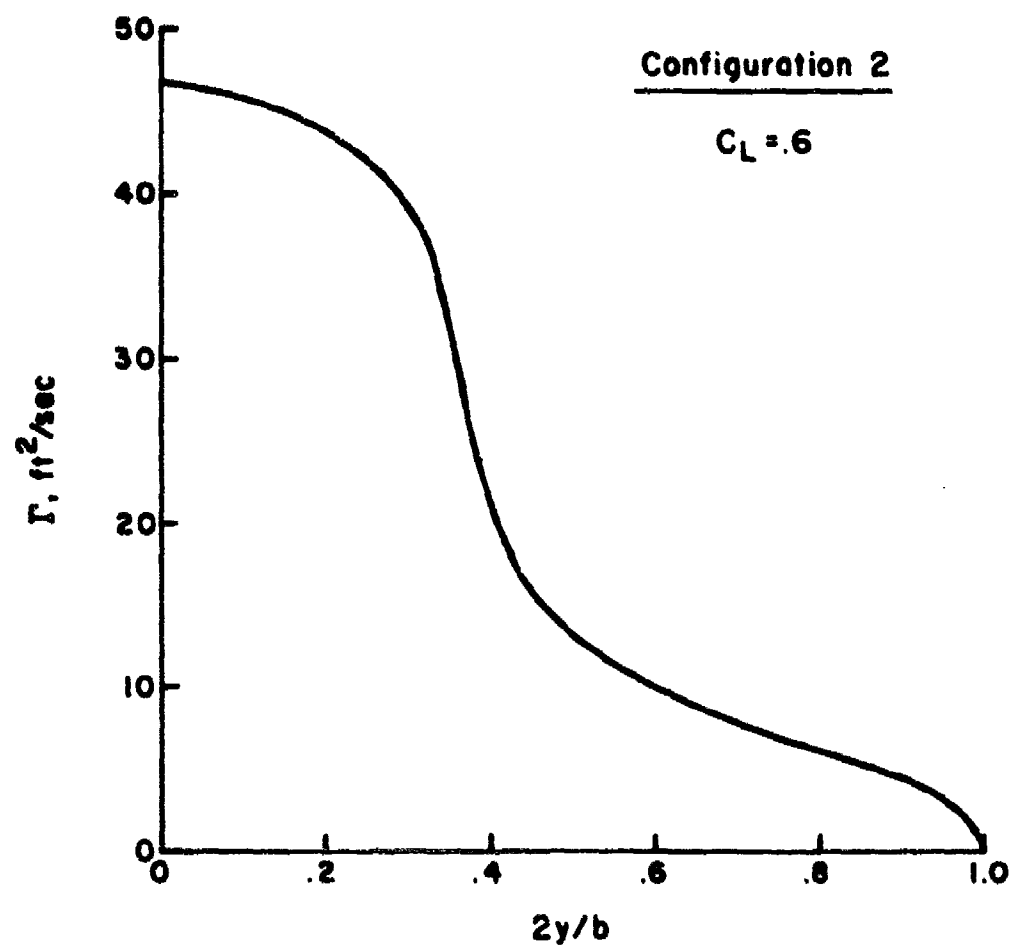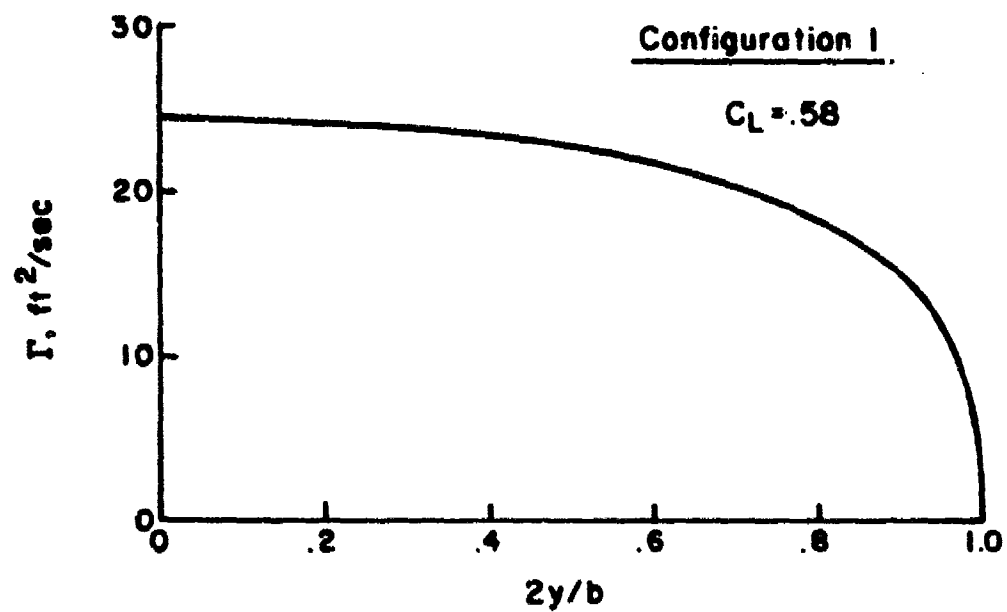
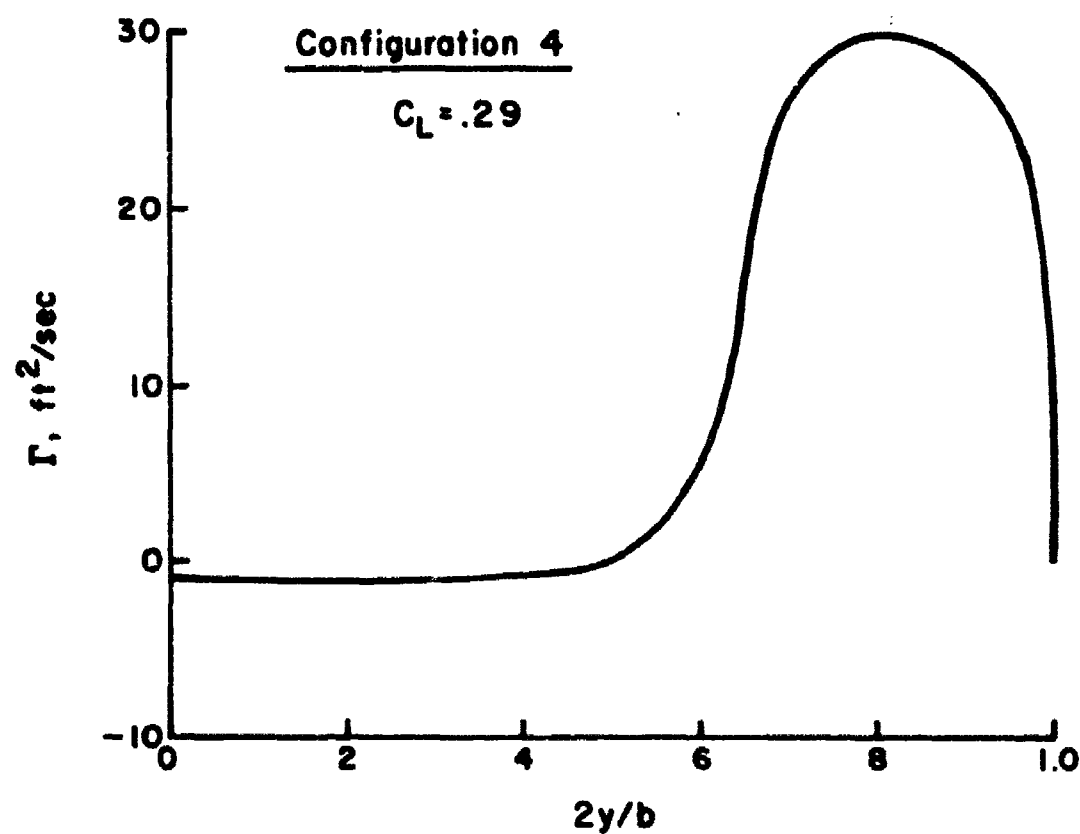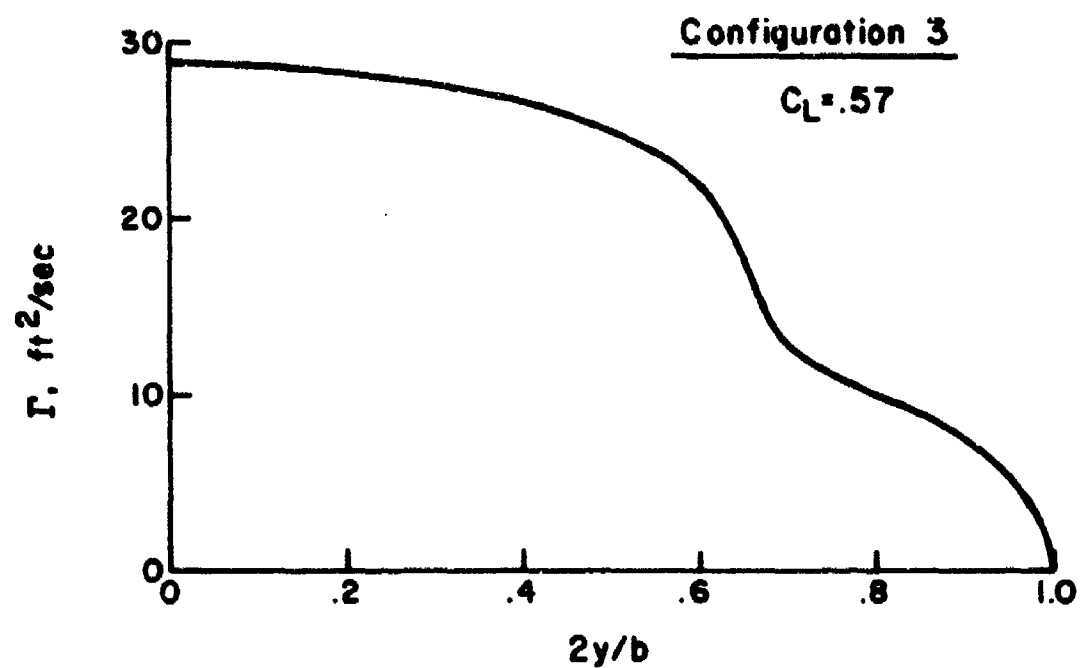Figure 25.   Lift distributions from lifting surface theory

Configuration 3
$C_L = .57$

Configuration 4
$C_L = .29$

Figure 25 (continued)

Figure 26.   Smoke visualization; configuration 1; overhead view
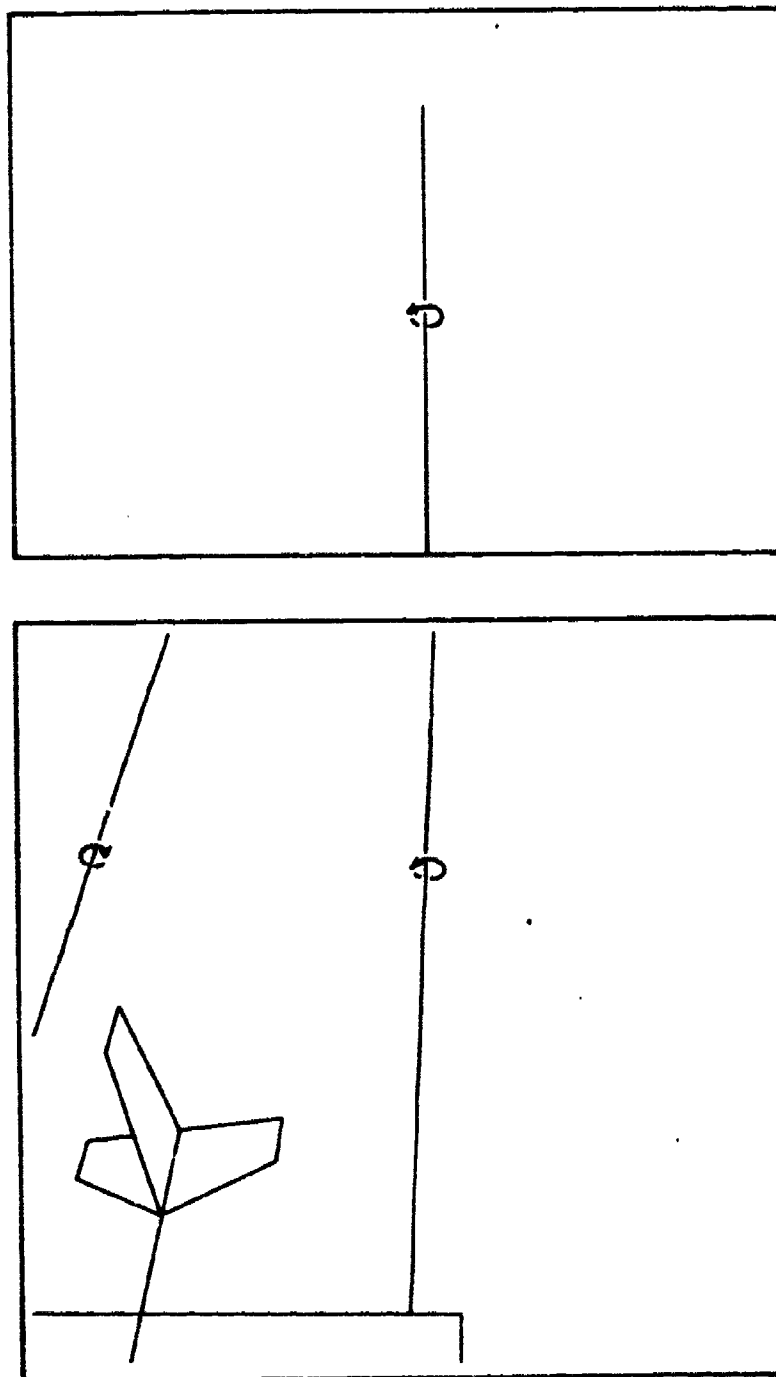
Figure 27. Computed vortex centroid location to be compared
with Figure 26

Figure 28. Smoke visualization; configuration 2. (a) viewed from downstream; (b) viewed from downstream and above
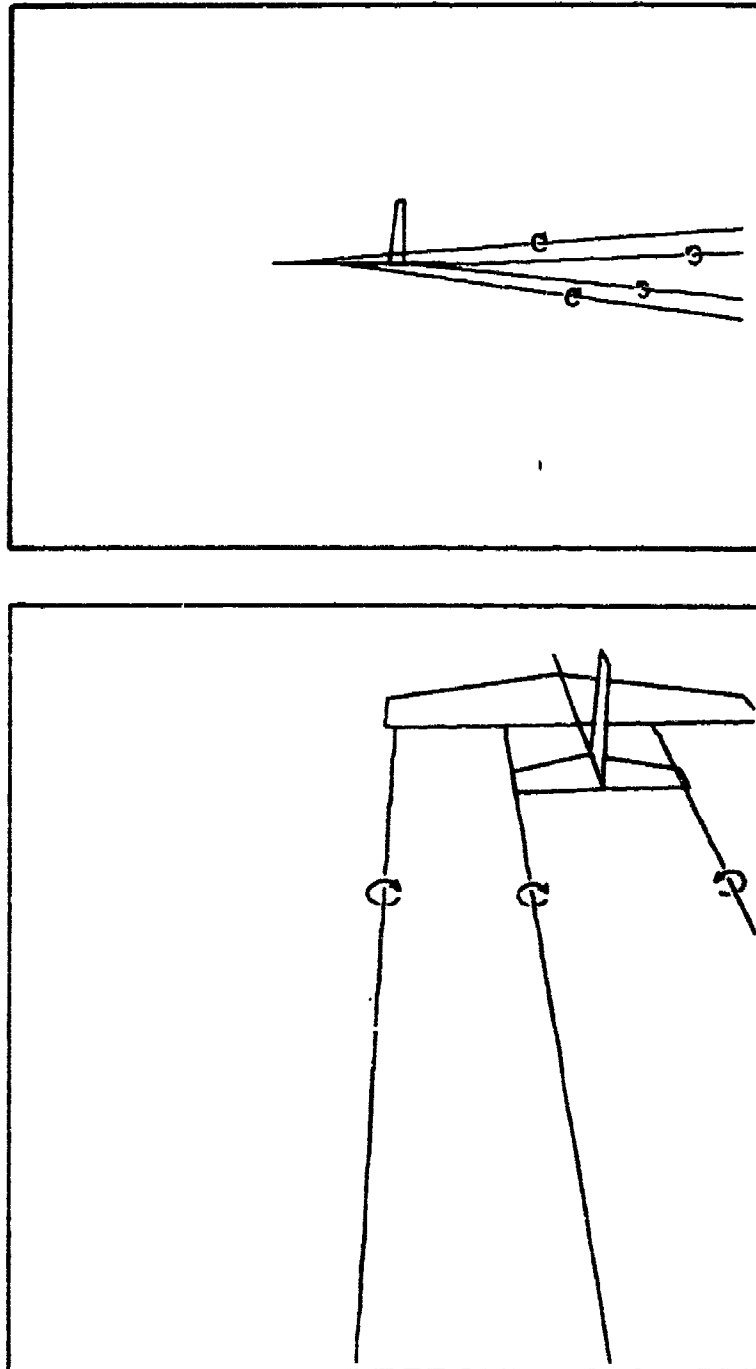
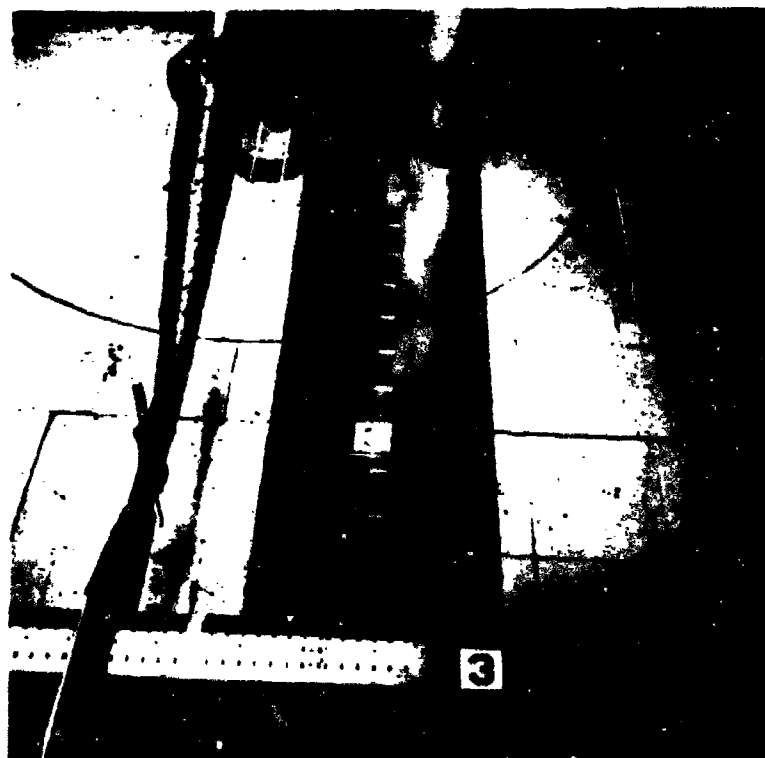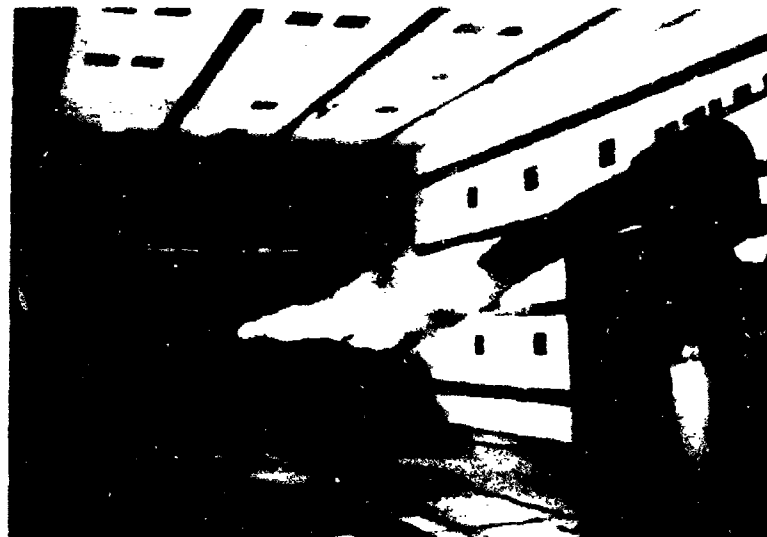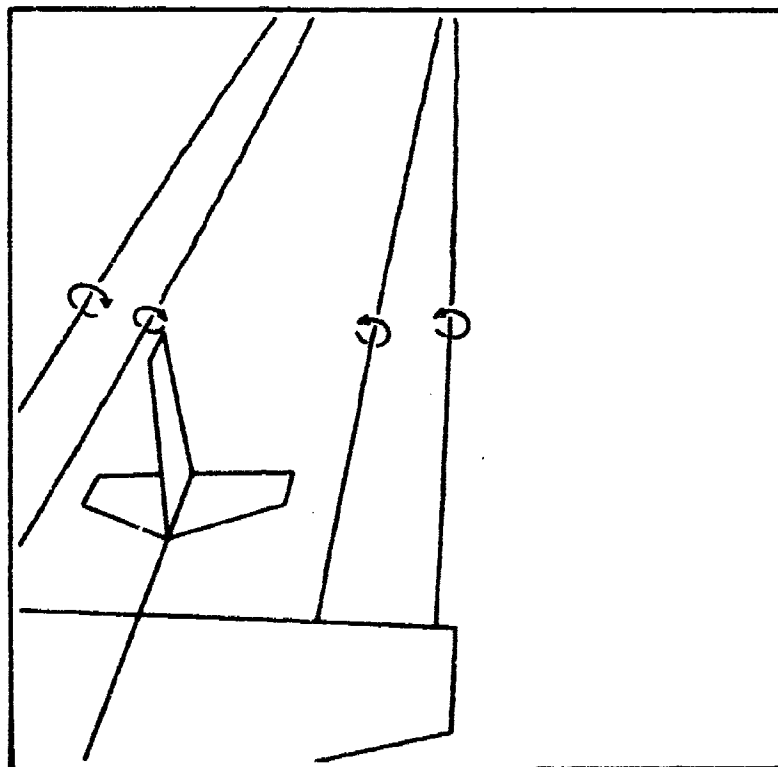Figure 29. Computed vortex centroids to be compared with Figure 28

Figure 30. Smoke visualization; configuration 3. (a) viewed from downstream; (b) viewed from overhead
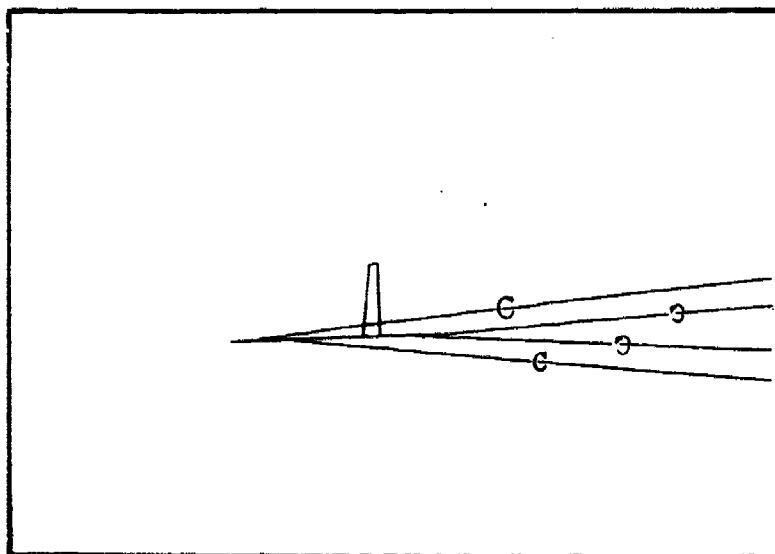
Figure 31. Computed vortex centroids to be compared with
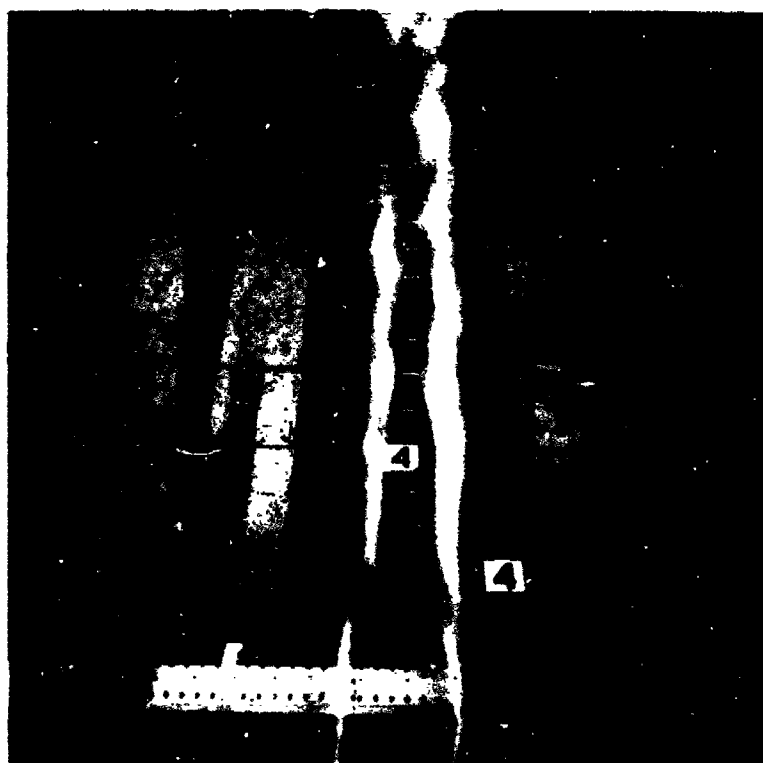Figure 30

Figure 32.   Smoke visualization, configuration 4.   (a) viewed from
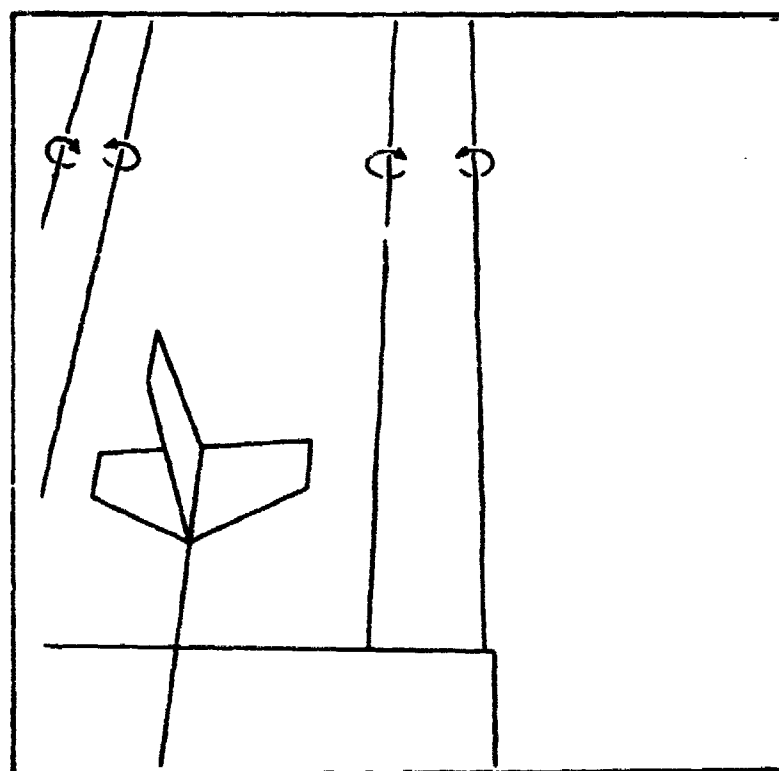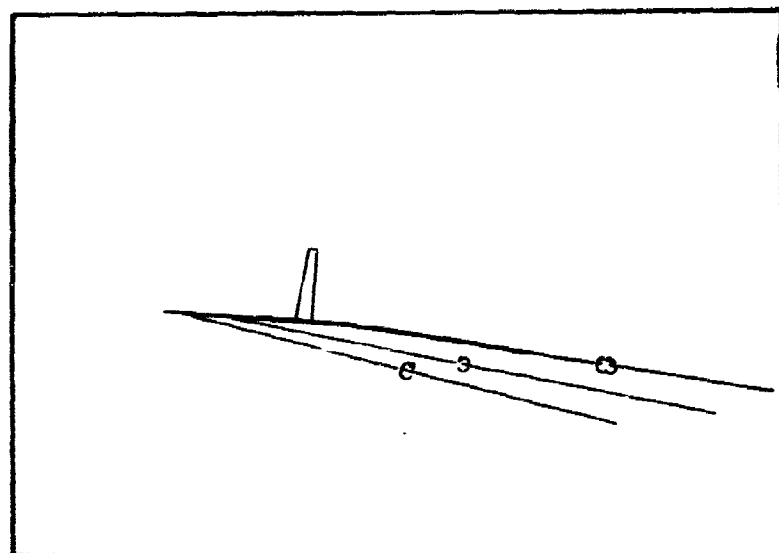downstream; (b) viewed from above

Figure 33   Computed vortex centroids to be compared with
             Figure 32

Figure 34. Side view photographs (upper – configuration 2;
lower – configuration 4)

y measured from the tunnel centerline to the right wing tip
(facing upstream). Positive z is measured vertically upward
from the tunnel floor. Velocity measurements were made behind the
left half of the wing, the wing tip being located at y = -40 in.
The velocity traverses made at the wing trailing edge (actually
within 3 inches of the trailing edge) were reduced to estimate the
profile drag of the wing. Profile drag distributions were calcula-
ted from the axial velocity deficits shown in Figures 35 and 36
for configurations 1 and 2, respectively. The computed sectional
drag coefficients are shown in Figure 37. The large value of
profile drag at the inboard stations for the clean configuration
suggests that the flow is beginning to separate.

NASA tunnel staff members have confirmed (with tuft studies)
separated flow at the unfaired fuselage wing junction for this
model at moderate angles of attack.

Wake velocity measurements at distances further than 10 chords
downstream were precluded by severe wake meander. Vortex centers
marked by smoke had excursions whose amplitudes were visually
estimated to be nearly 1 foot at downstream distances of 30 chords.
The validity of averaged velocity data under such circumstances was
doubted, and measurements were made at 5 and 10 chords downstream
where meander was judged to be moderate. Experimental velocity
data are shown in Figures 38-61 and Figures B.1-B.4. At each down-
stream station, three horizontal traverses were made at three
elevations across each vortex. The traverses, in principle, were
to pass above, through, and below the vortex center, a task not
easily achieved.

Since three traverses were made across each vortex, it was
decided to check the Betz model and extensions by trying to dupli-
cate the velocities measured with each traverse by computation.
Comparison in this way is a more stringent check of the models than
has previously been used in the literature where it is often the
practice to use the velocity measurements from only one traverse
and to fit the computed results to the experimental data by adjus-
ting the location of the vortex center. Even small changes in the
location of the vortex center can result in large changes in the
velocities computed at a point due to the large gradients which
occur near the vortex center. When two or more traverses at differ-
ent elevations are available, the freedom to choose vortex center
locations is limited in that only one location will distribute the
error in a prescribed manner.

Swirling velocity distributions in the wake were calculated
from the Betz model for tip vortices and with the extension by
Ref. 13 for flap vortices (wing drag is neglected here). The wing
load distributions which would result in multiple vortex wakes were
divided according to the criterion given in Ref. 13 and in Section
II.1. A computer program was then developed to best fit the
experimental velocity measurements with the computed values. The
procedure was to minimize the square of the difference between the
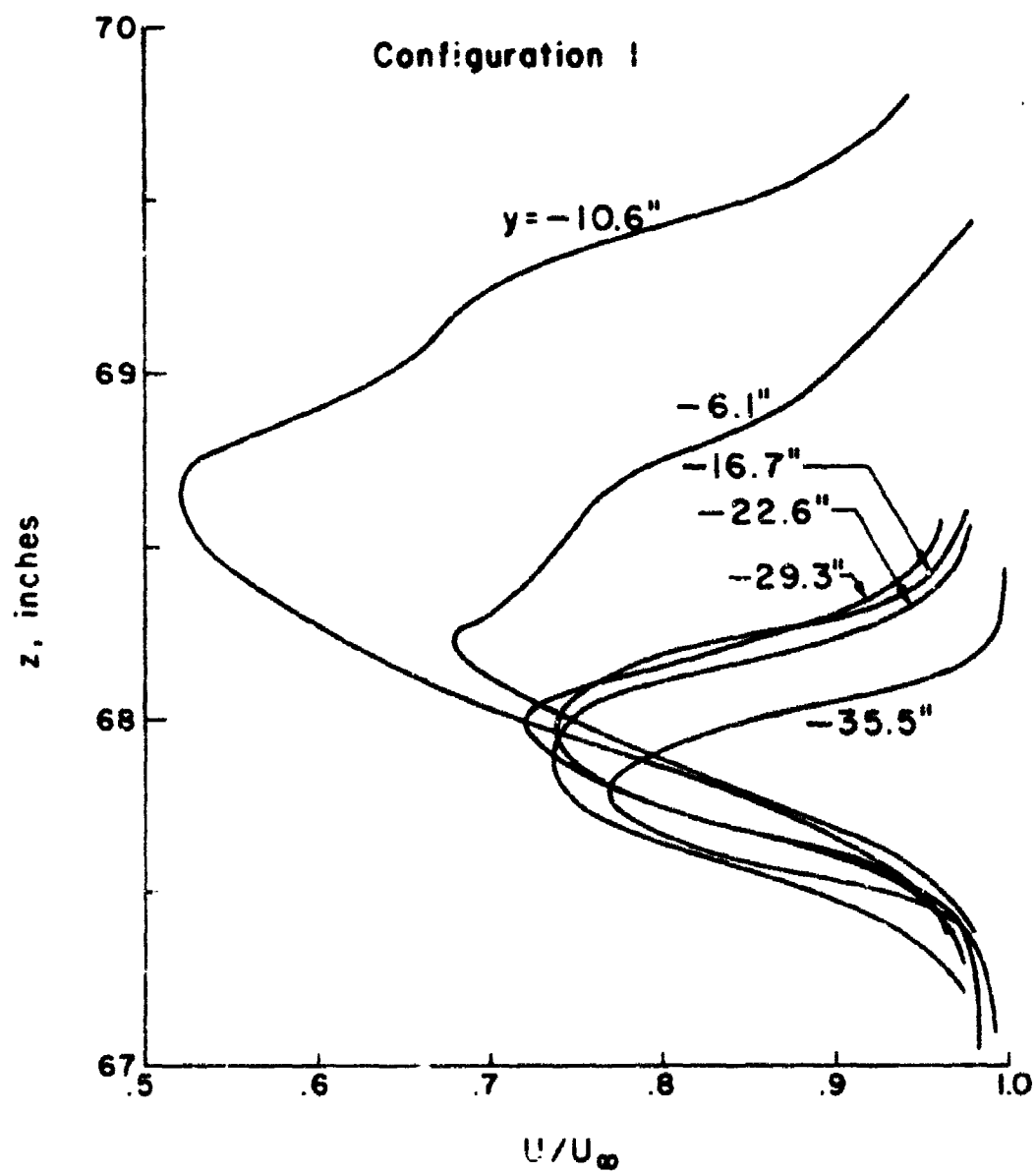experimental measured velocity at a point and the computed value.

Figure 35. Faired measured axial velocity defect; z = 3 in.
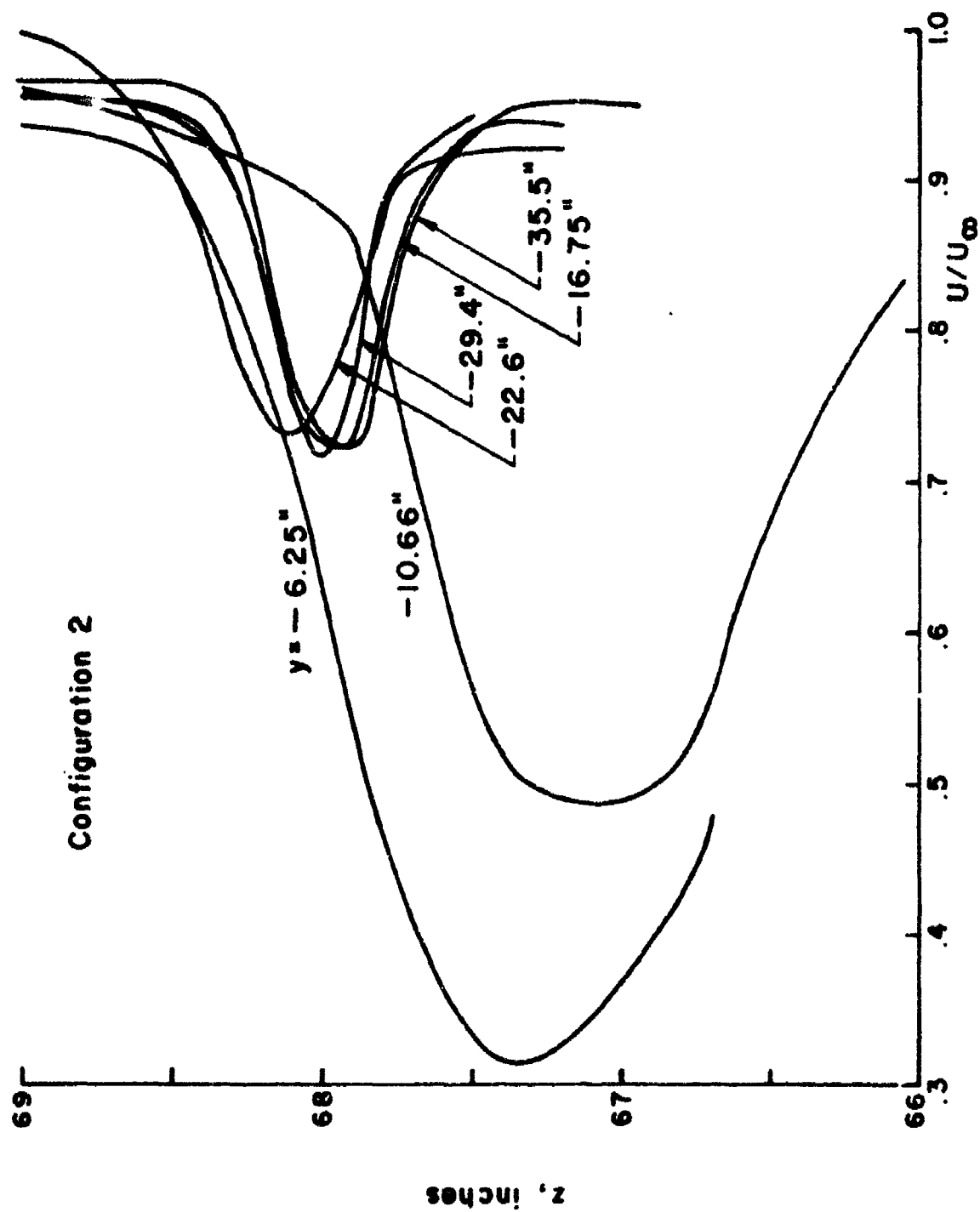
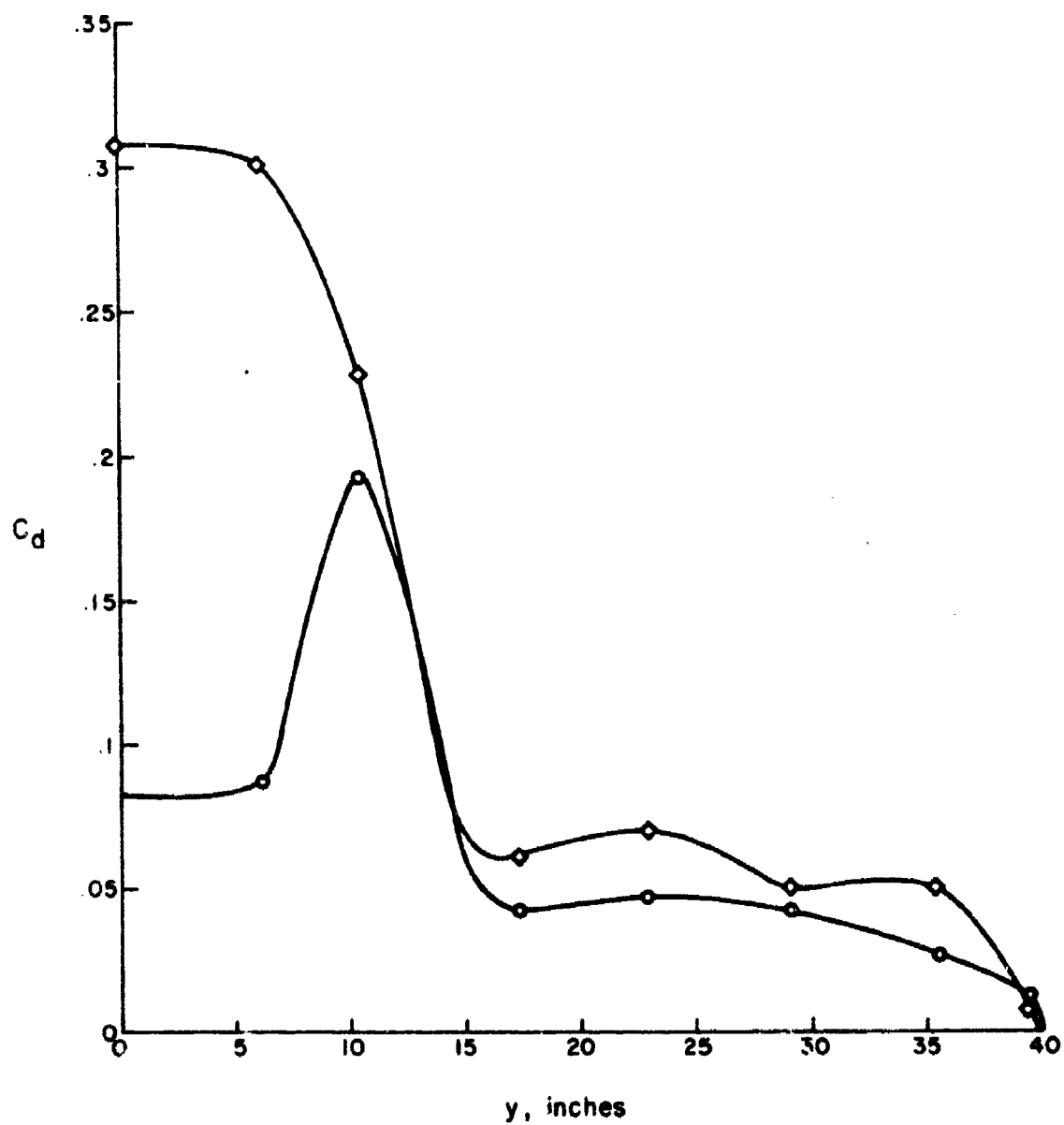Figure 36. Faired measured axial velocity defect; z = 3 in.

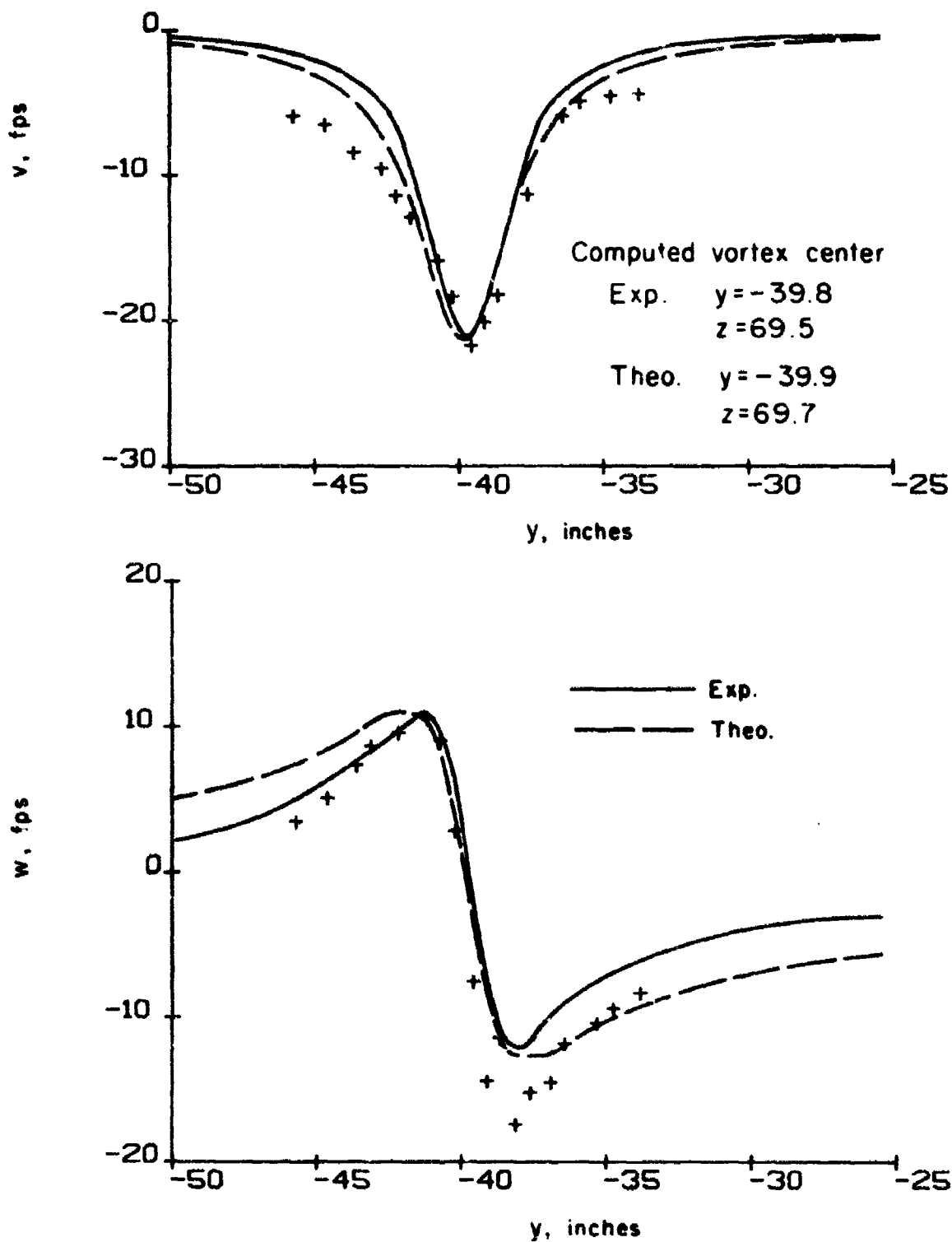Figure 37. Computed sectional profile drag coefficients from
Figures 35 and 36

Figure 38. Configuration 1; comparison of measured and computed horizontal and vertical velocities (x = 50 in., z = 67.95 in.)
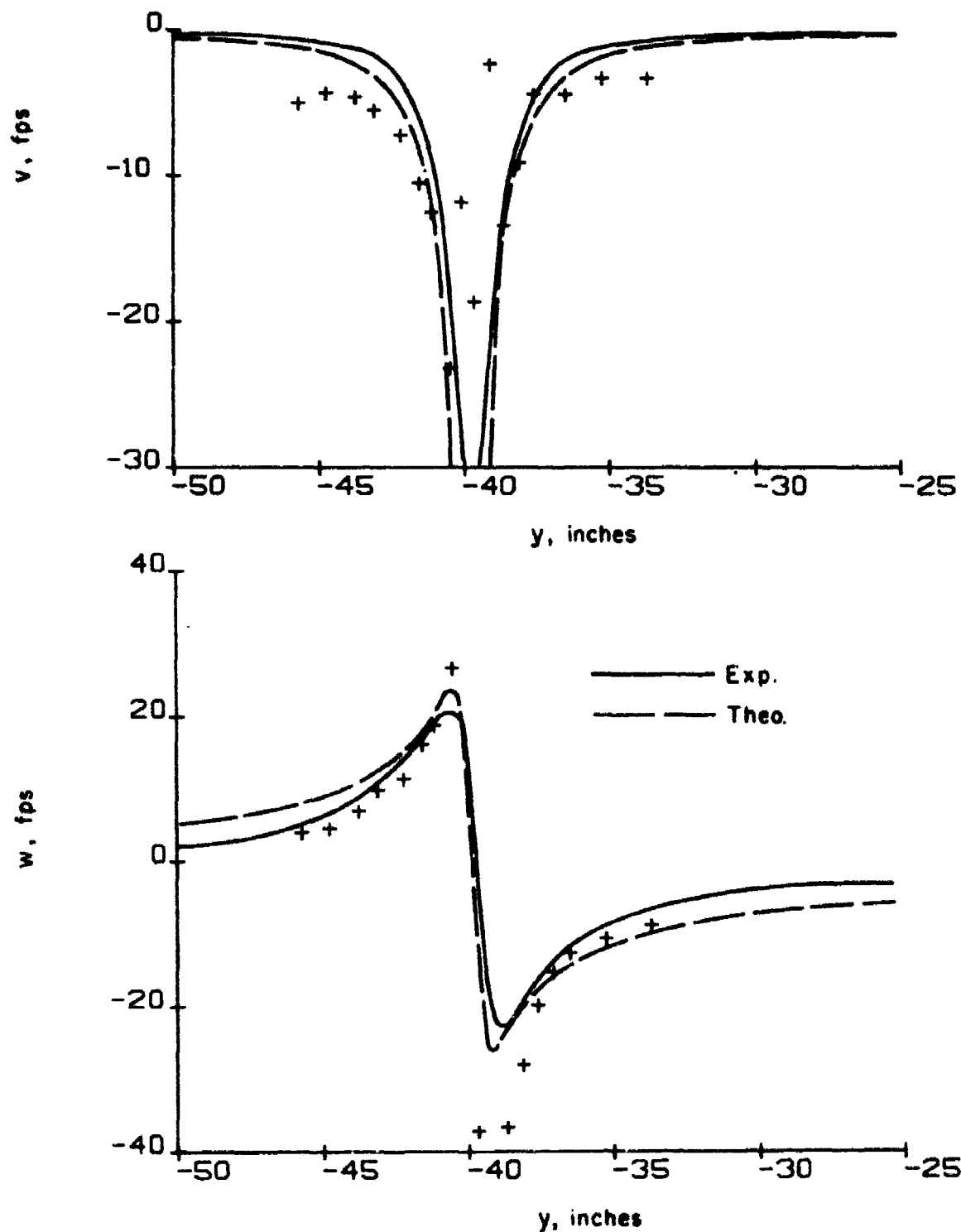
60

Figure 39. Configuration 1; comparison of measured and computed
horizontal and vertical velocities (x = 50 in.,
z = 68.9 in.)
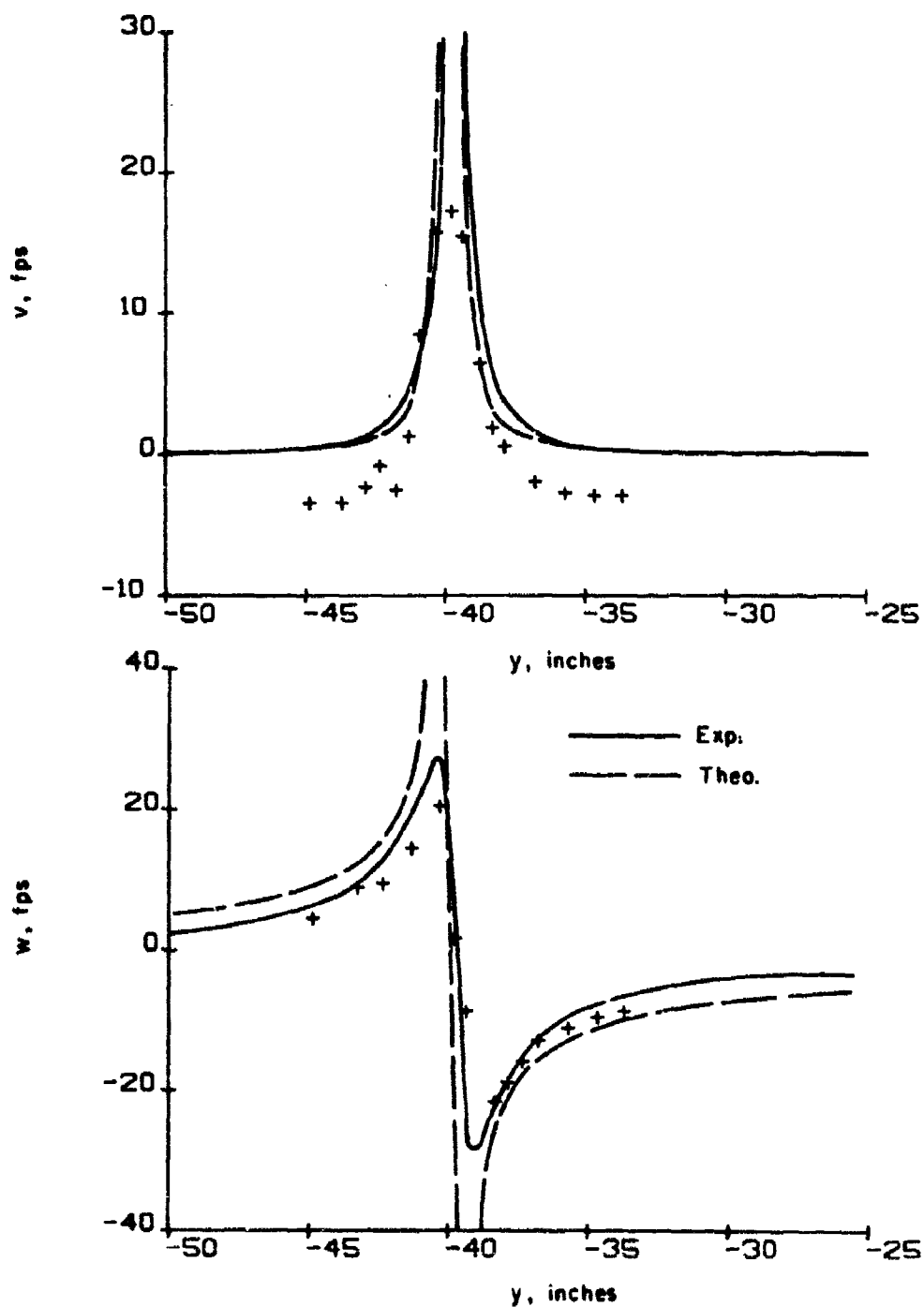
Figure 40. Configuration 1; comparison of measured and computed horizontal and vertical velocities (x = 50 in., z = 69.96 in.)
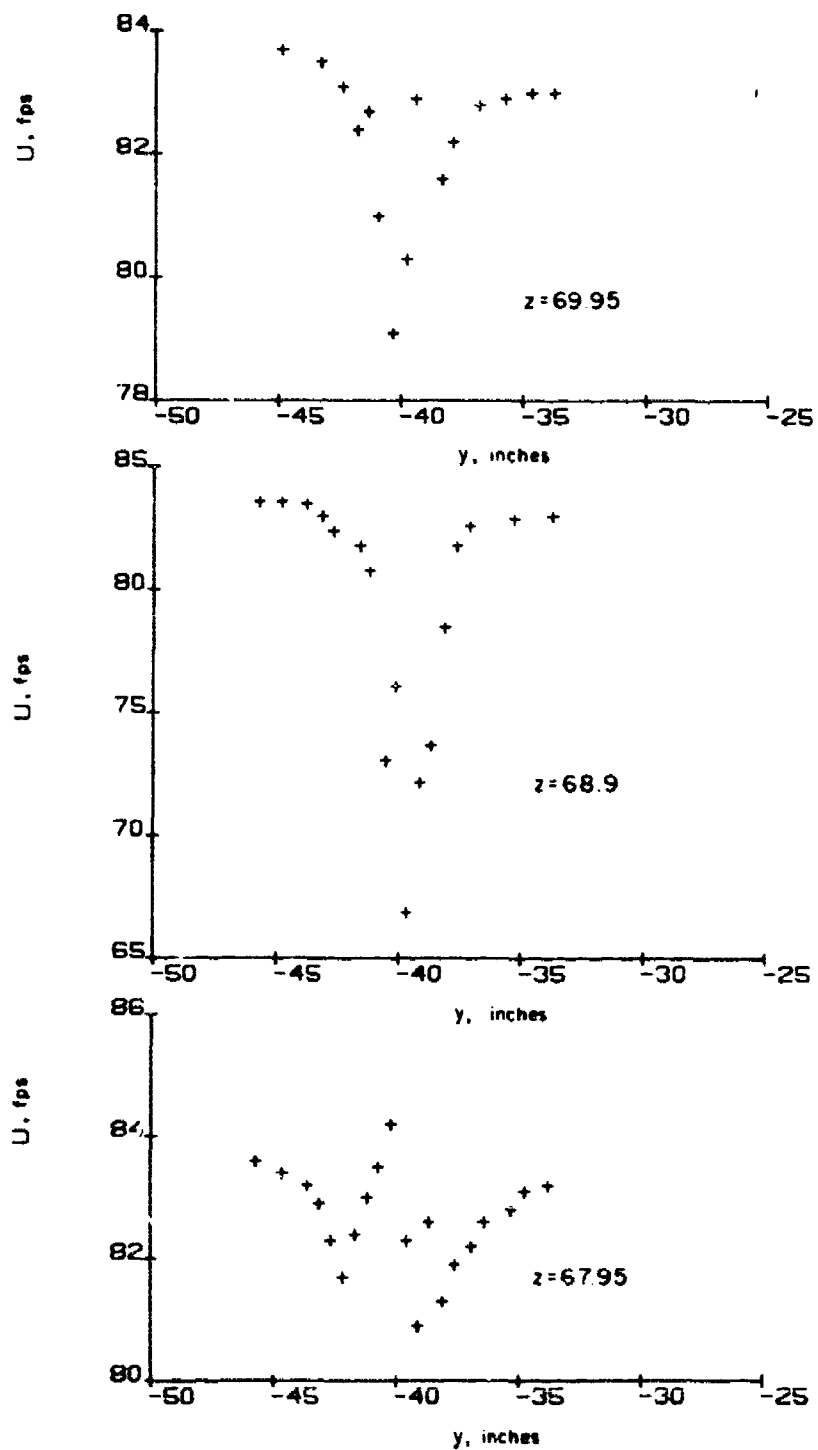
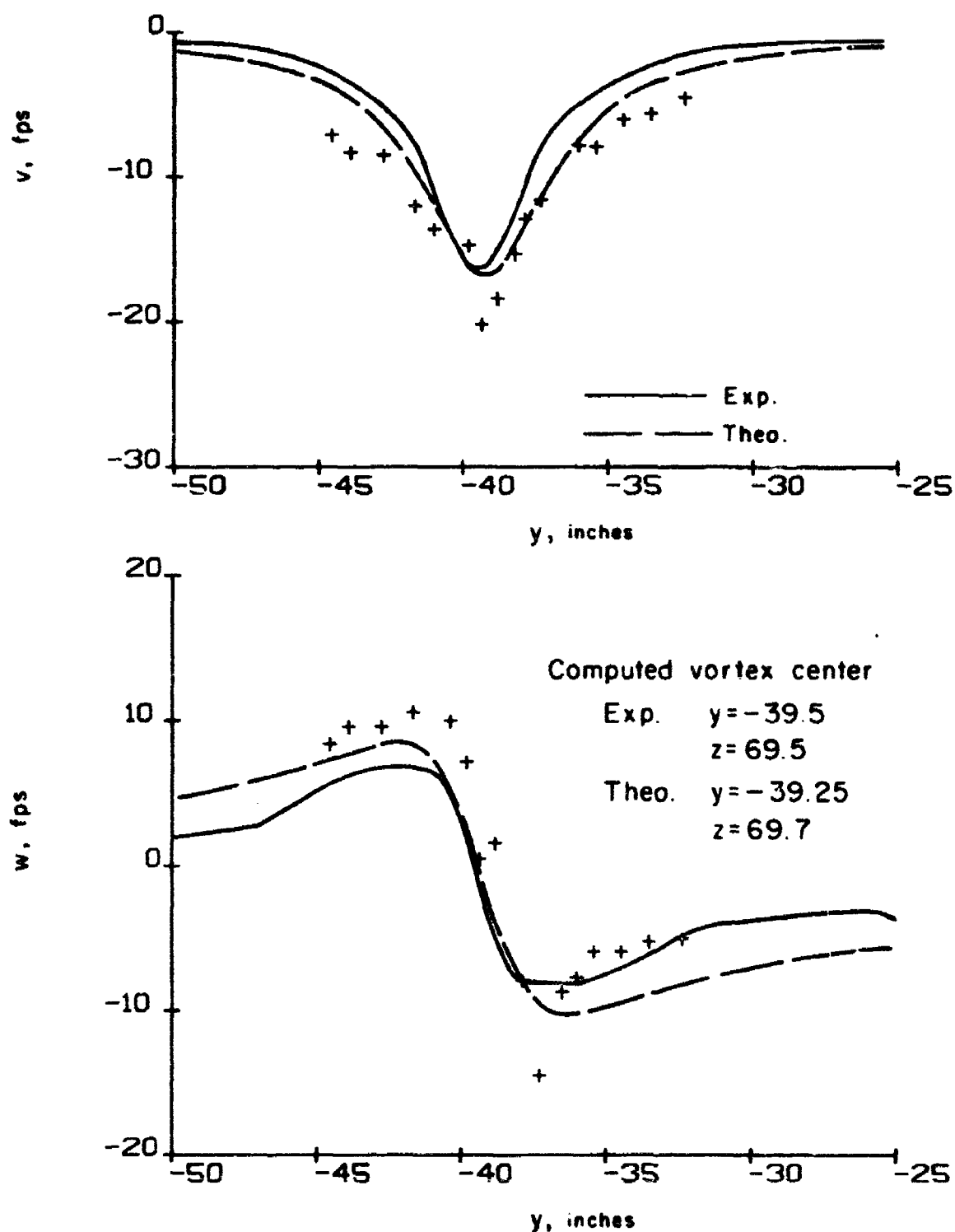Figure 41.   Configuration 1; measured axial velocities (x = 50 in.)

Figure 42.   Configuration 1; comparison of measured and computed horizontal and vertical velocities (x = 100 in., z = 67.2 in.)
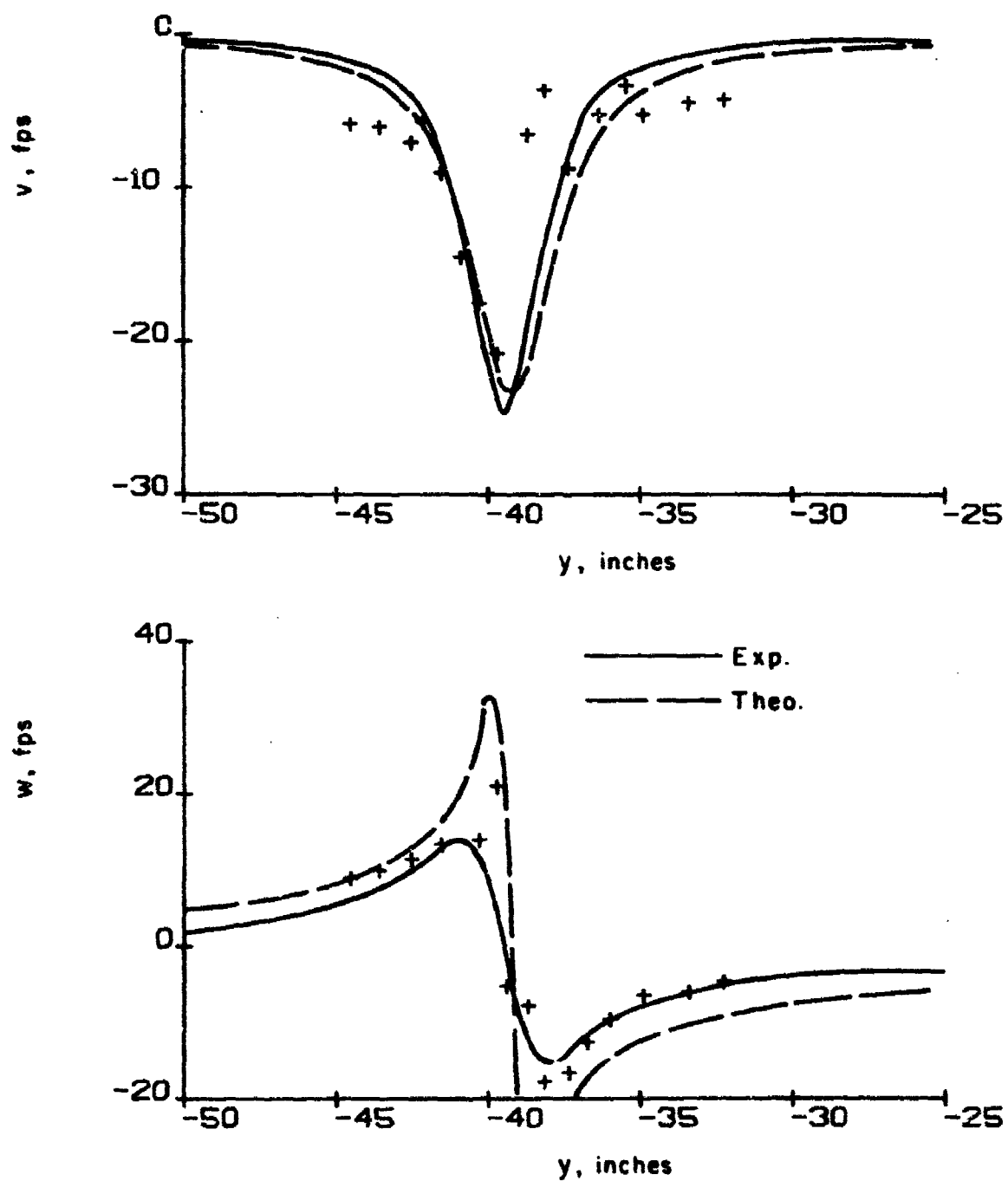
Figure 43. Configuration 1; comparison of measured and computed horizontal and vertical velocities (x = 100 in., z = 68.3 in.)
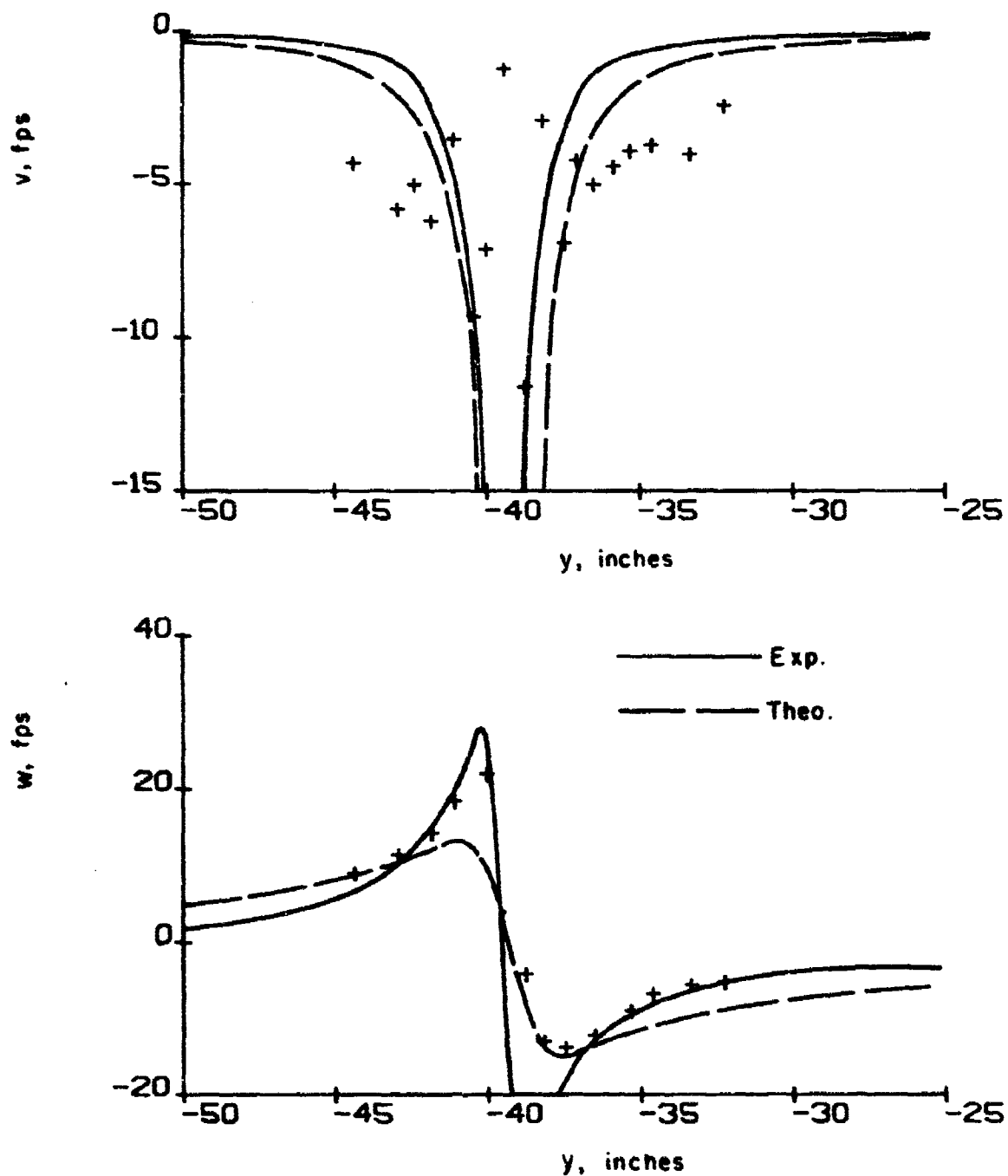
Figure 44. Configuration 3; comparison of measured and computed horizontal and vertical velocities (x = 100 in., z = 69.1 in.)
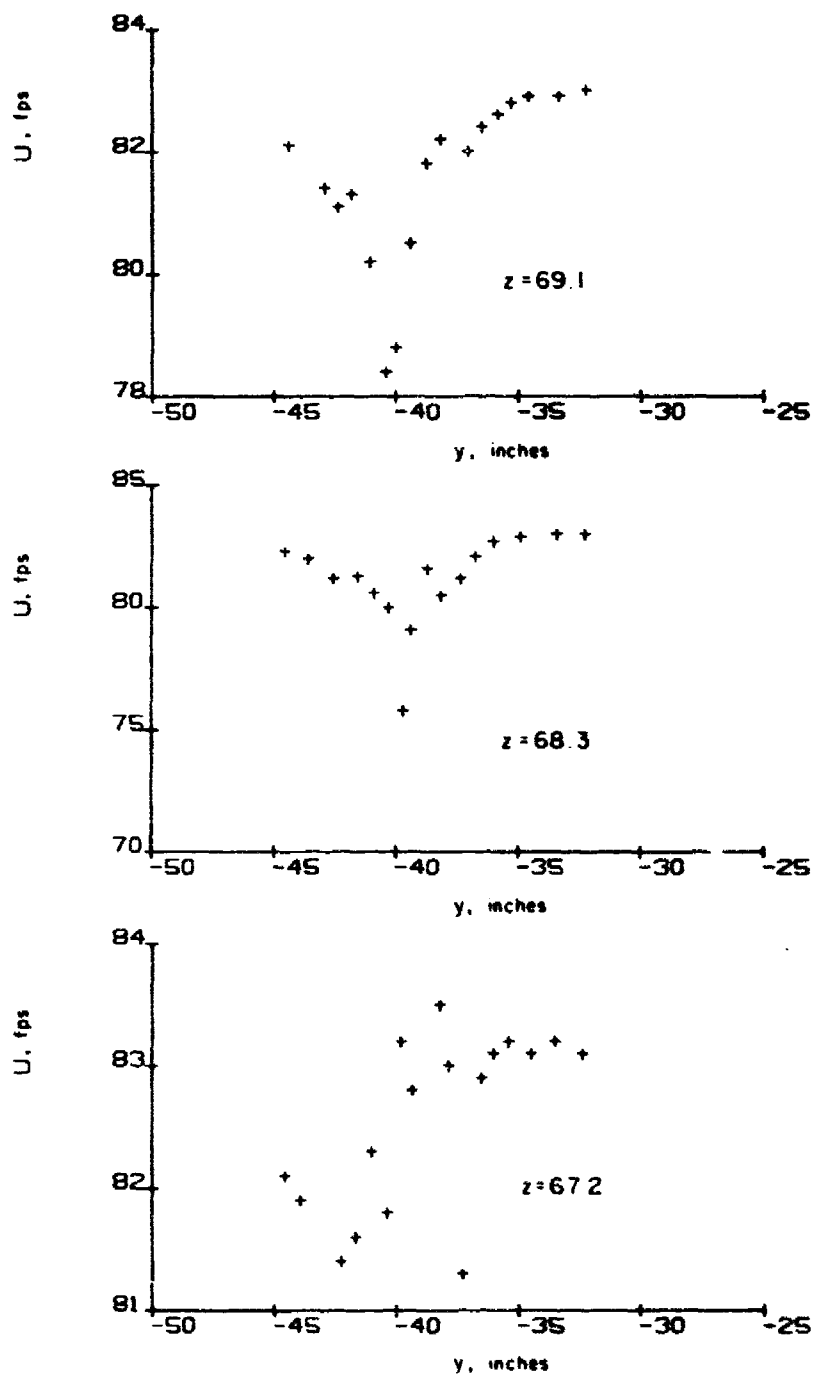
Figure 45. Configuration 1; measured axial velocities (x = 100 in.)

Figure 46. Configuration 2; tip vortex. Comparison of measured and computed horizontal and vertical velocities (x = 50 in., z = 69 in.)

Figure 47. Configuration 2; tip vortex. Comparison of measured
and computed horizontal and vertical velocities
(x = 50 in., z = 70 in.)

Figure 48.   Configuration 2; tip vortex.   Comparison of measured
and computed horizontal and vertical velocities
(x = 50 in., z = 71 in.)

70

Figure 49.   Configuration 2; measured axial velocities (x = 50 in.)

Figure 50. Configuration 2; flap vortex. Comparison of measured and computed horizontal and vertical velocities (x = 50 in., z = 59.2 in.)

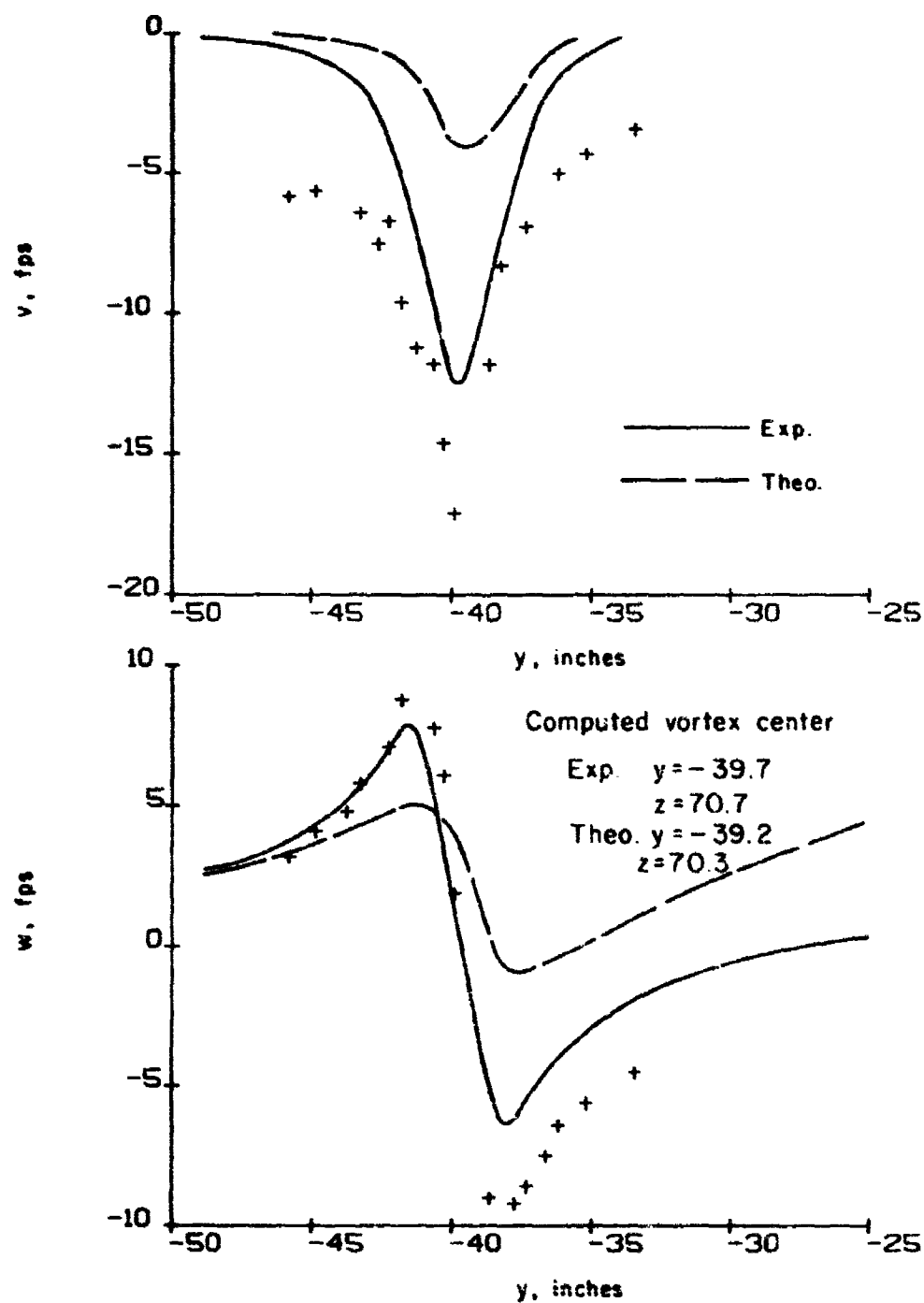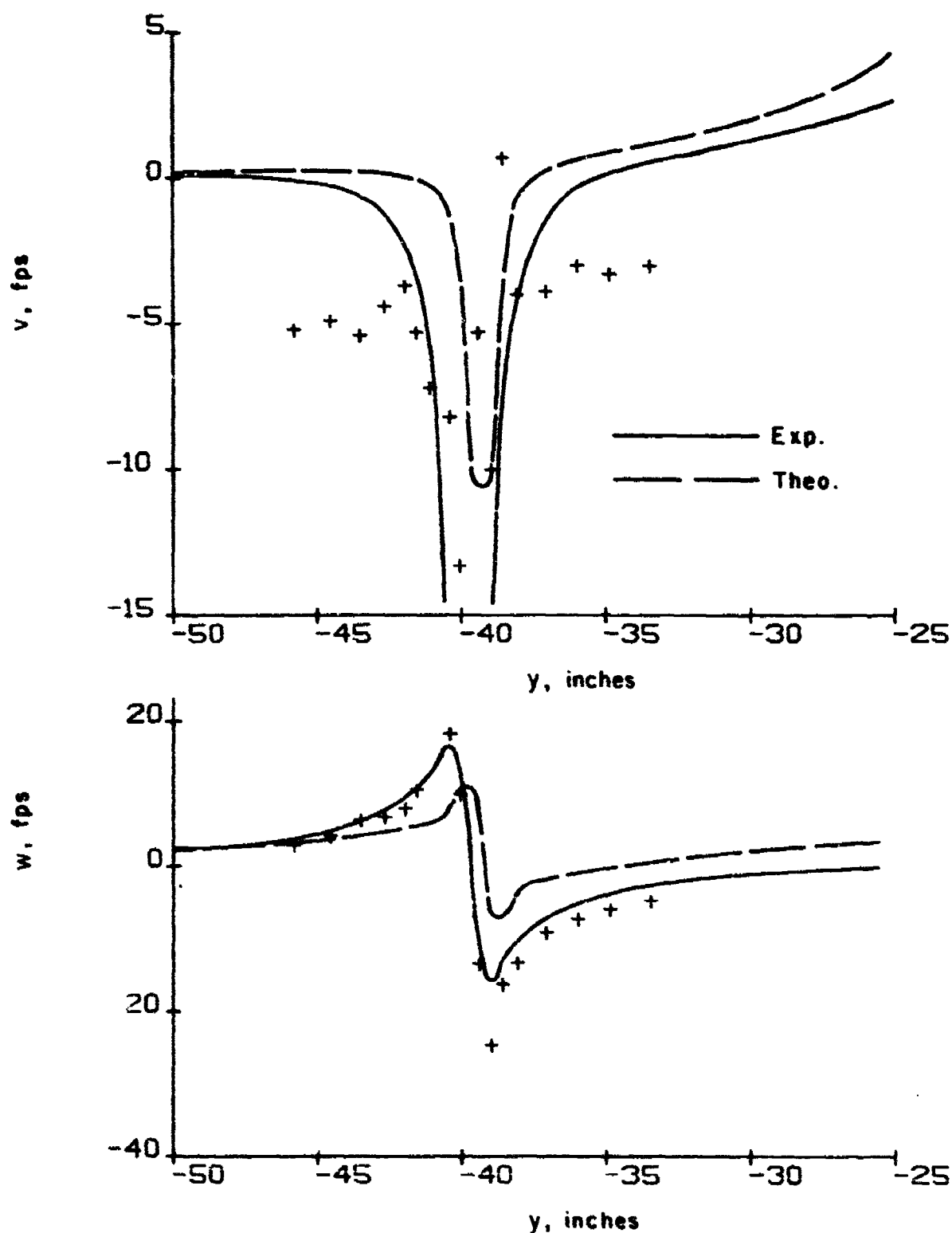Figure 51.   Configuration 2; flap vortex.   Comparison of measured
and computed horizontal and vertical velocities
(x = 50 in., z = 60.3 in.)

Figure 52. Configuration 2; flap vortex. Comparison of measured
and computed horizontal and vertical velocities
(x = 50 in., 61.4 in.)

74

Figure 53.   Configuration 2; measured axial velocities (x = 50 in.)

Figure 54. Configuration 2; tip vortex. Comparison of measured and computed horizontal and vertical velocities (x = 100 in., z = 70.5 in.)
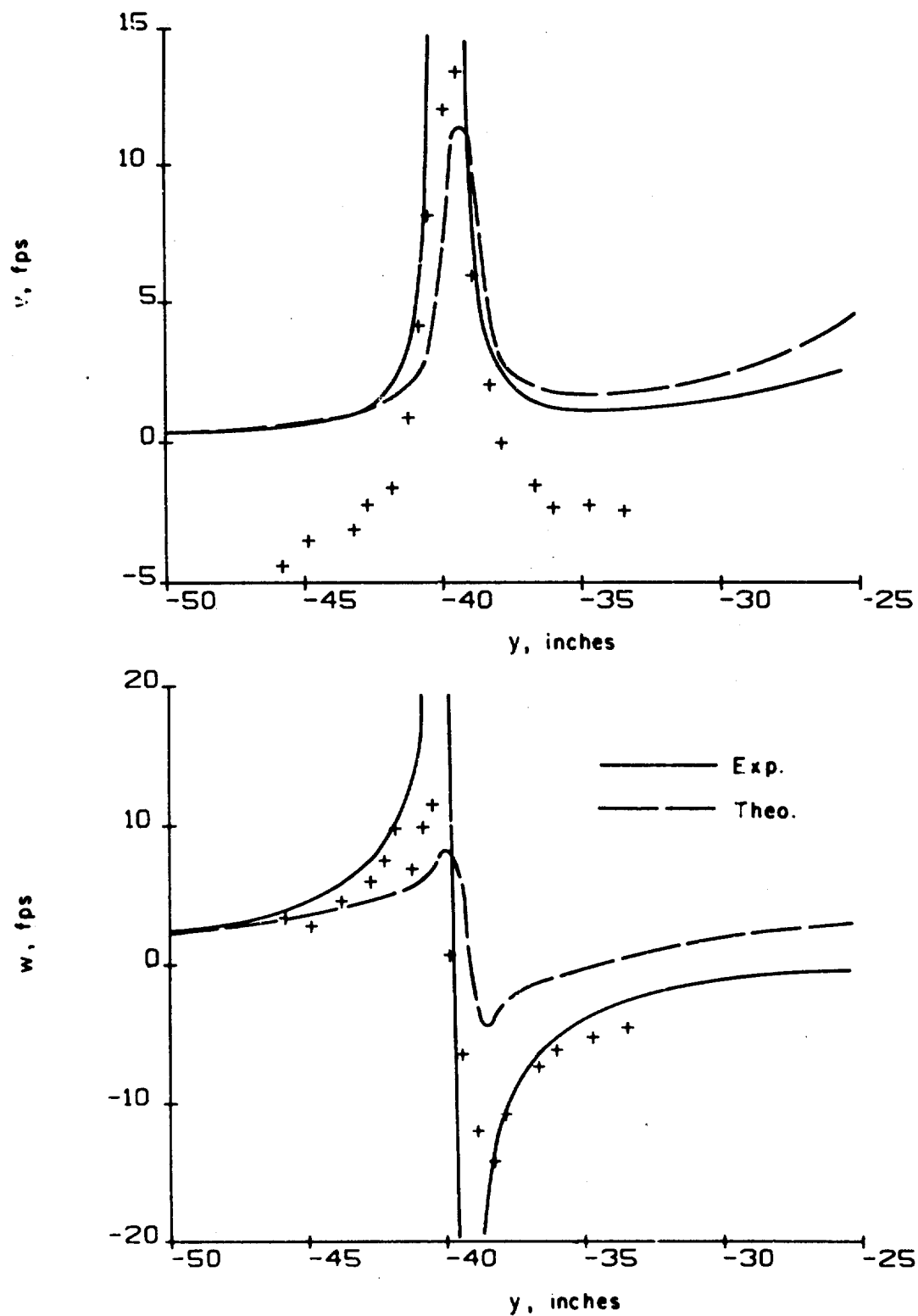
Figure 55. Configuration 2; tip vortex. Comparison of measured and computed horizontal and vertical velocities (x = 100 in., z = 71.5 in.)

Figure 56. Configuration 2; tip vortex. Comparison of measured and computed horizontal and vertical velocities (x = 100 in., z = 72.5 in.)
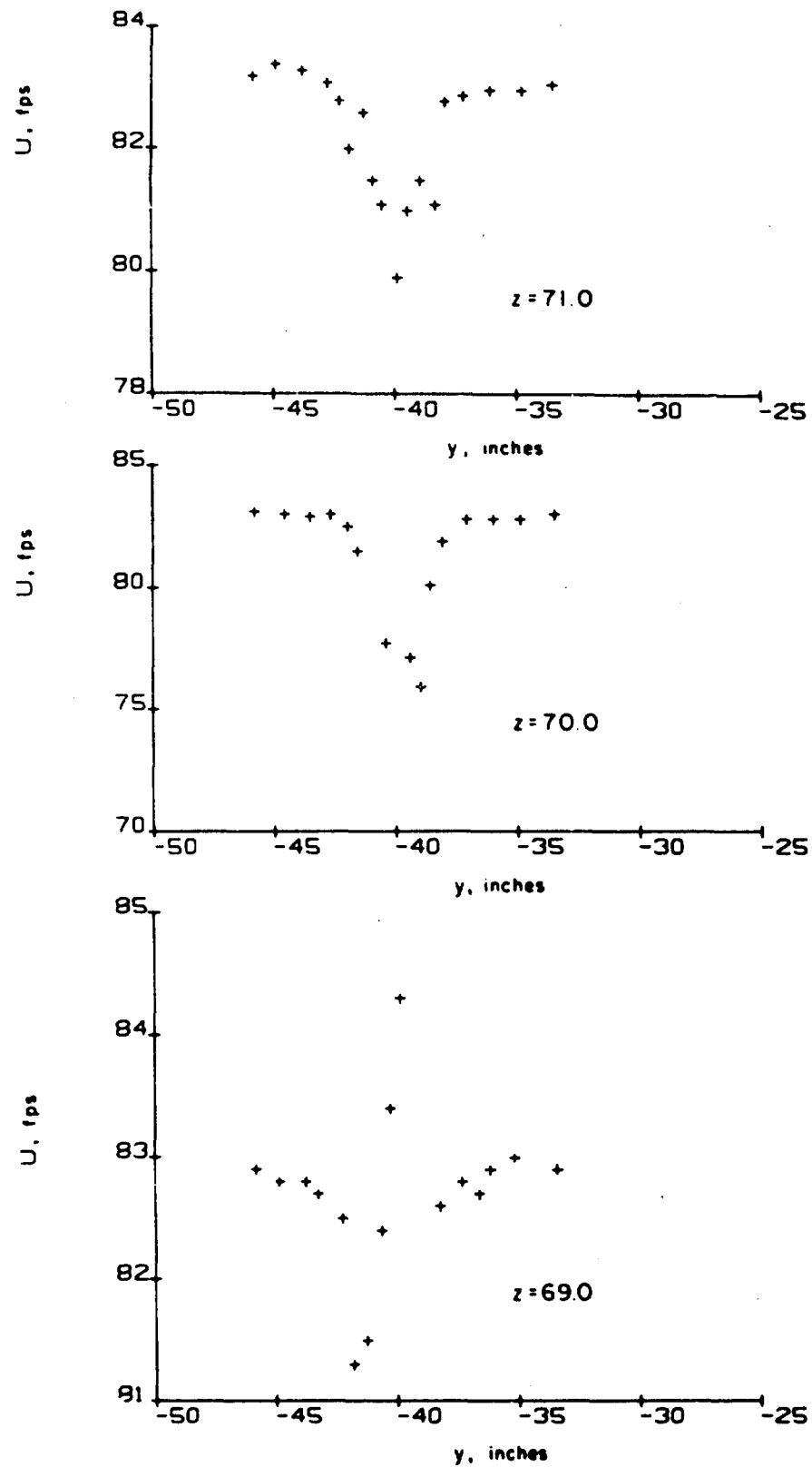
78

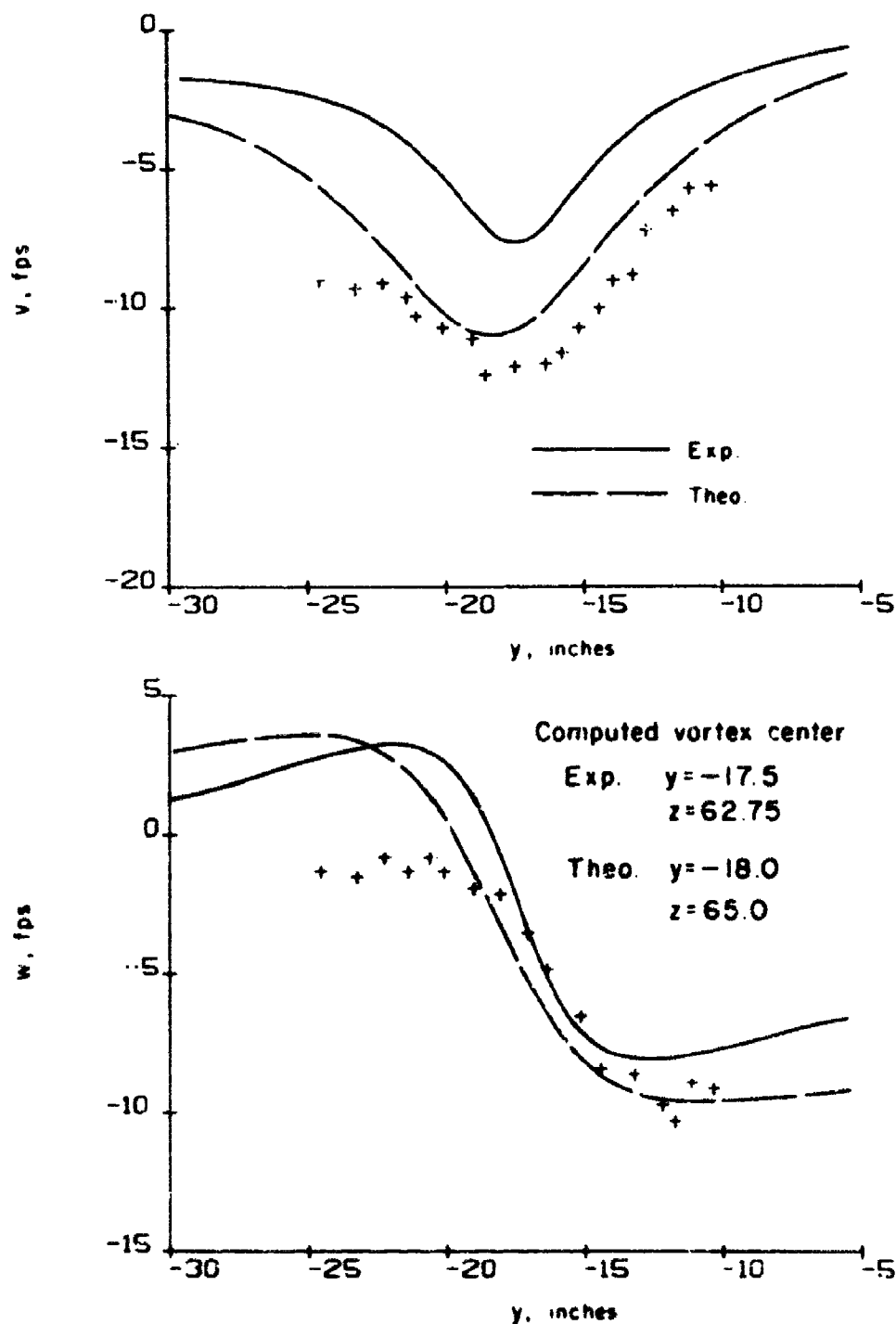Figure 57. Configuration 2; measured axial velocities (x = 100 in.)

Figure 58. Configuration 2; flap vortex. Comparison of measured and computed horizontal and vertical velocities (x = 100 in., z = 57.5 in.)

Figure 59. Configuration 2; flap vortex. Comparison of measured and computed horizontal and vertical velocities (x = 100 in., z = 58.5 in.)

Figure 60. Configuration 2; flap vortex. Comparison of measured and computed horizontal and vertical velocities (x = .00 In., z = 59.5 In.)

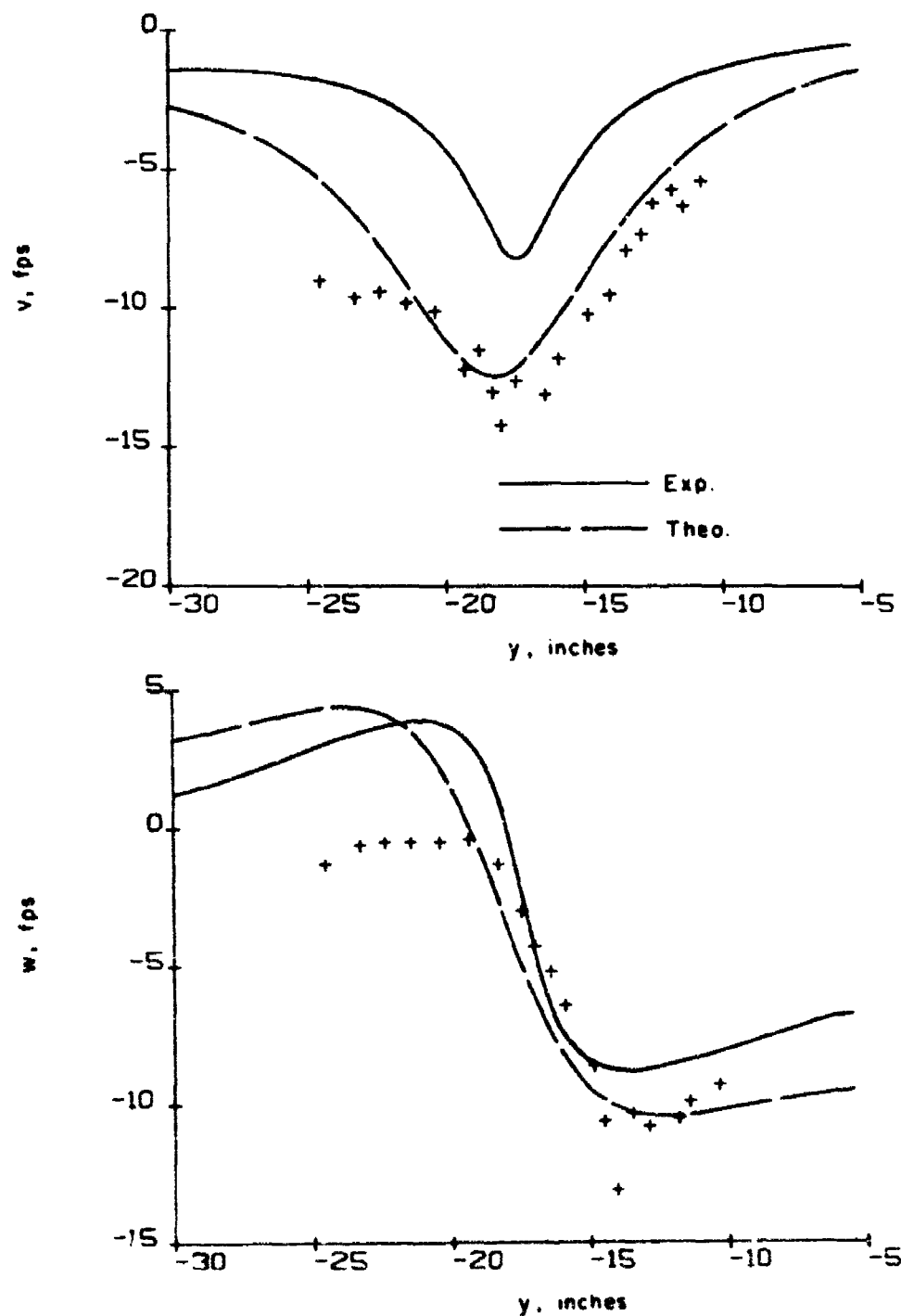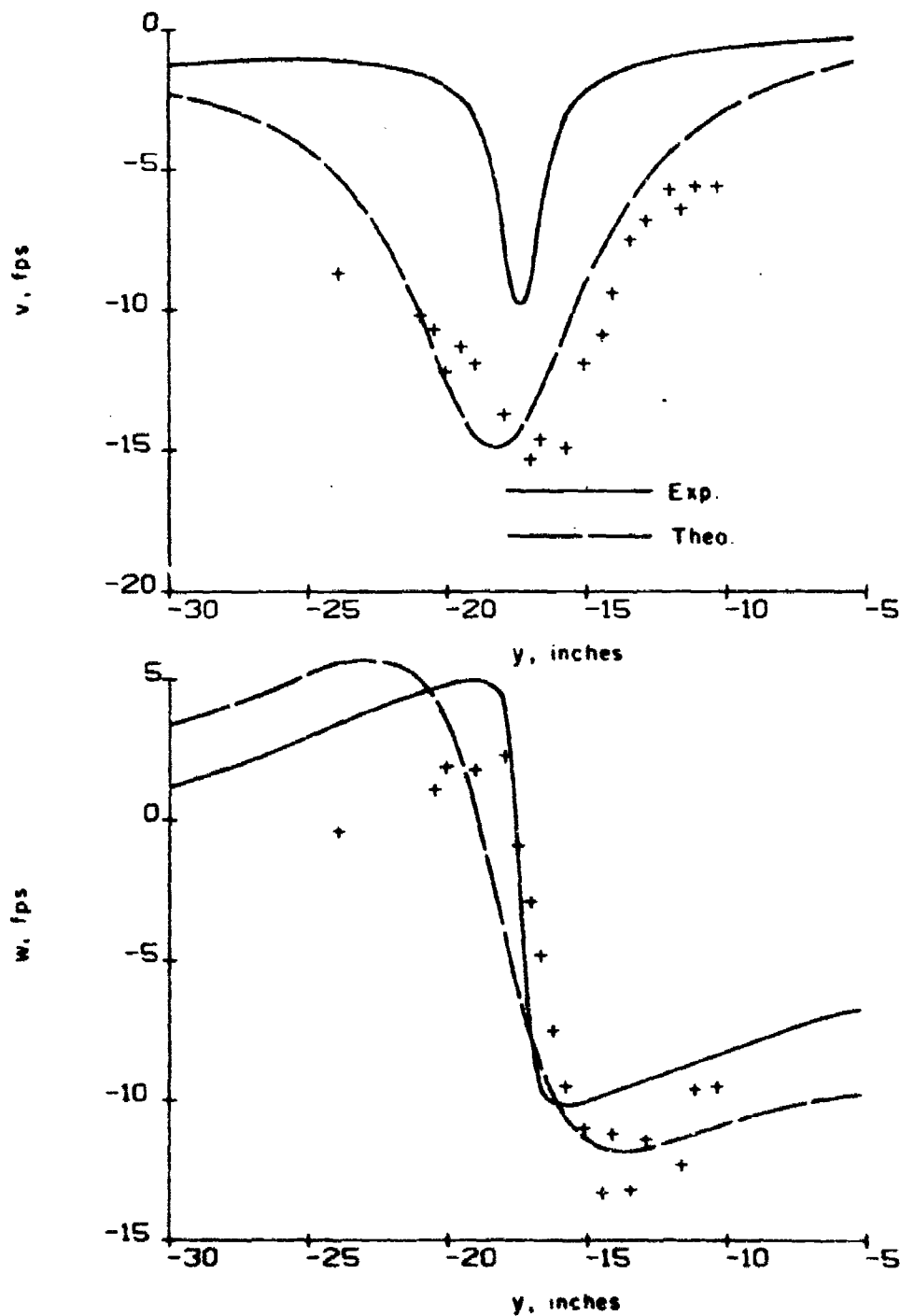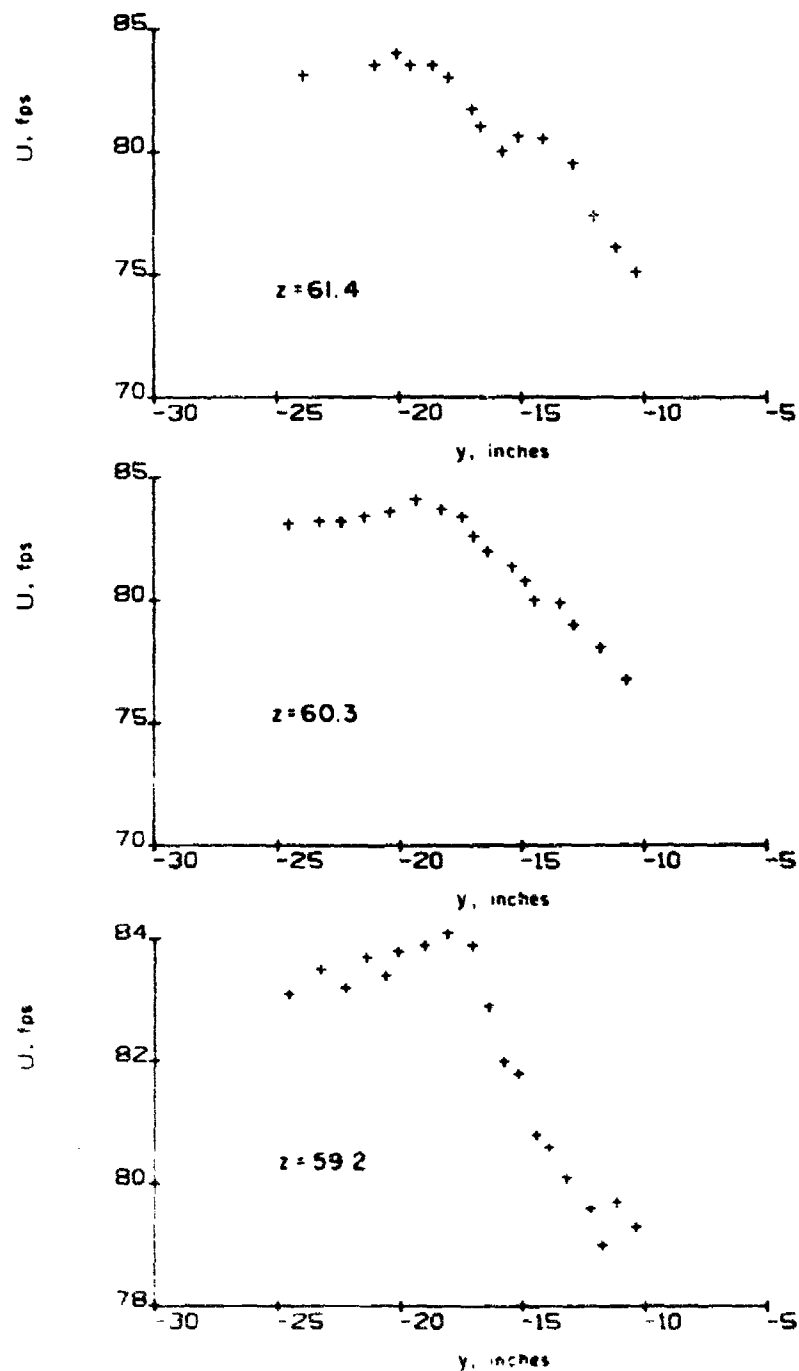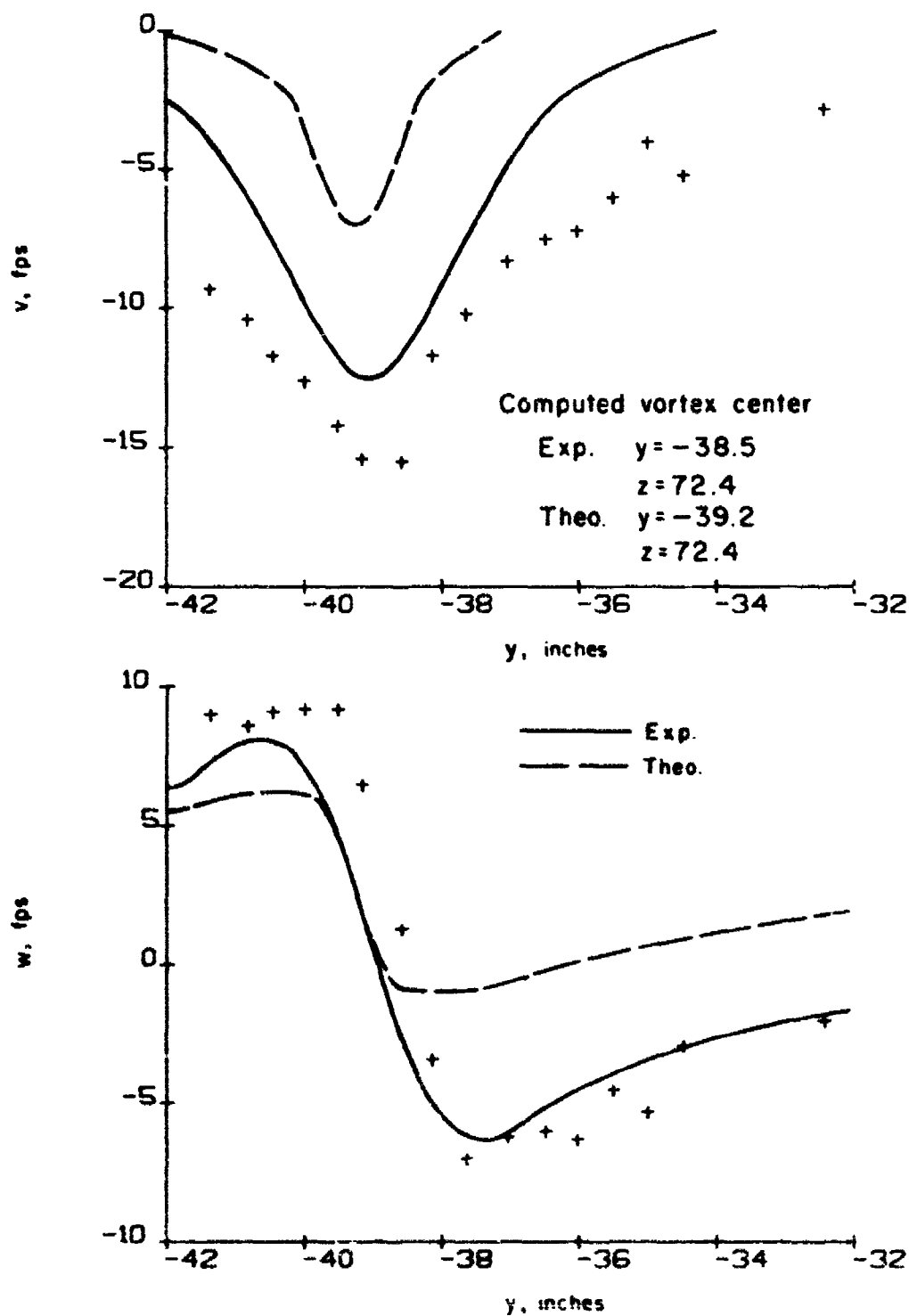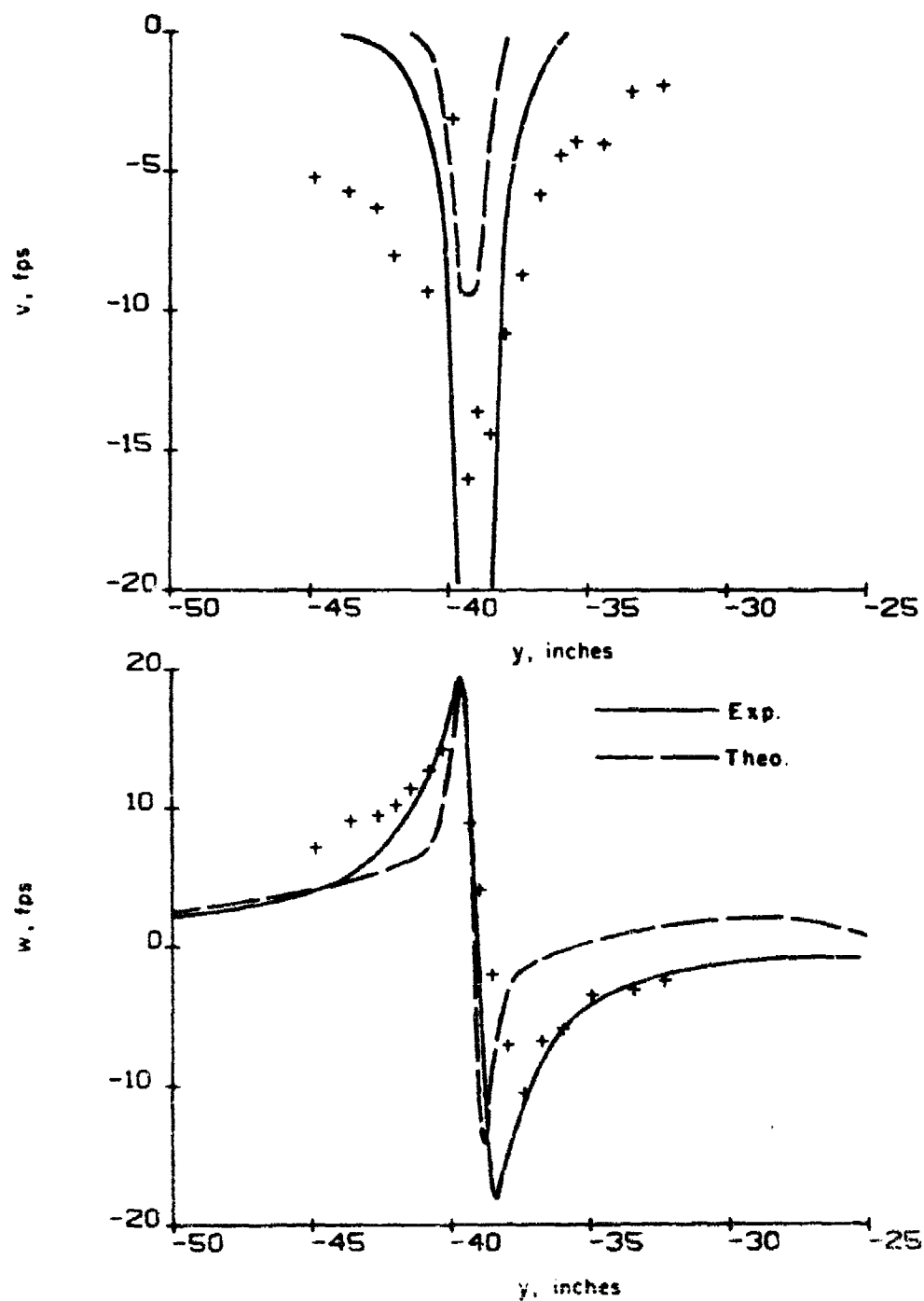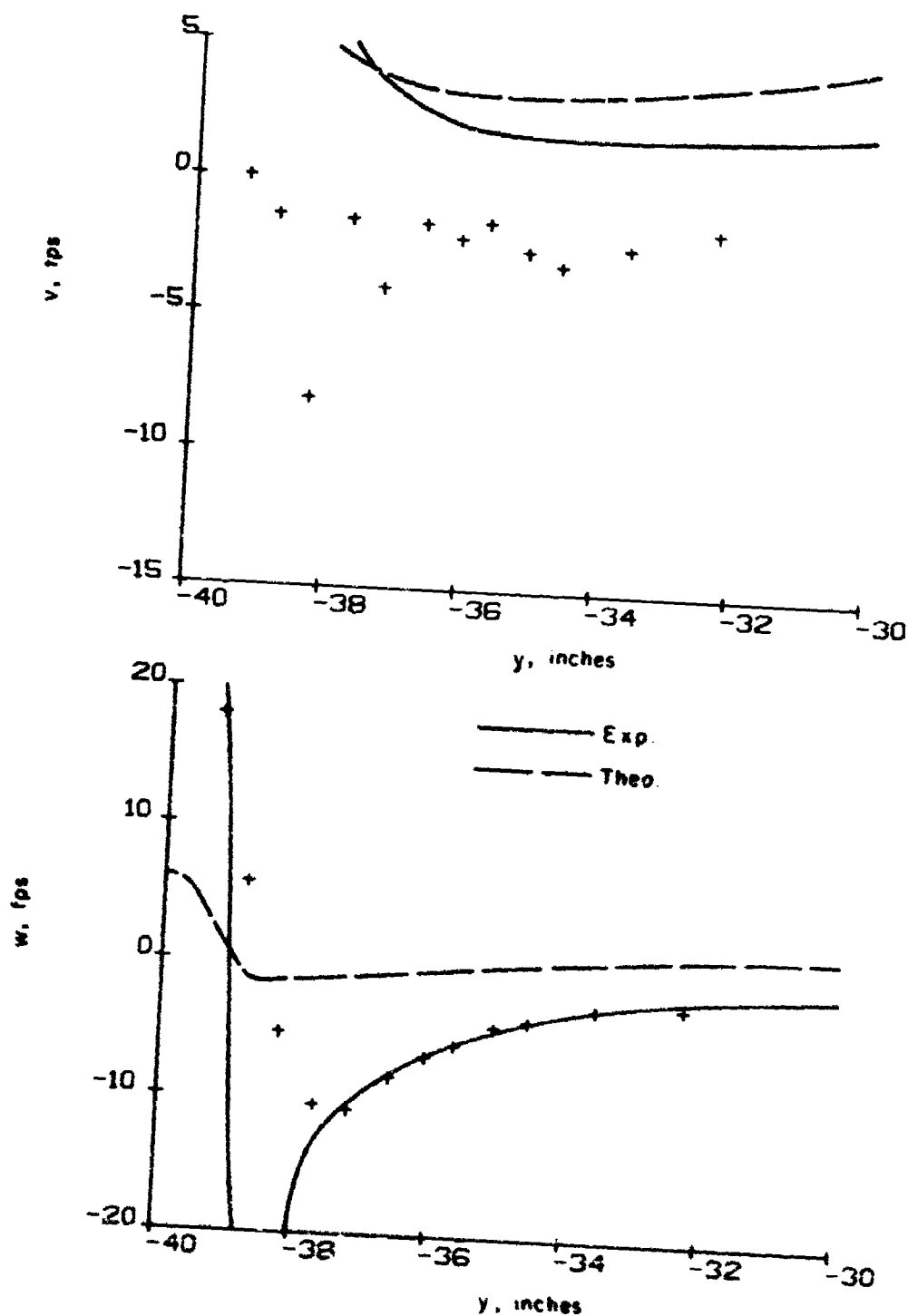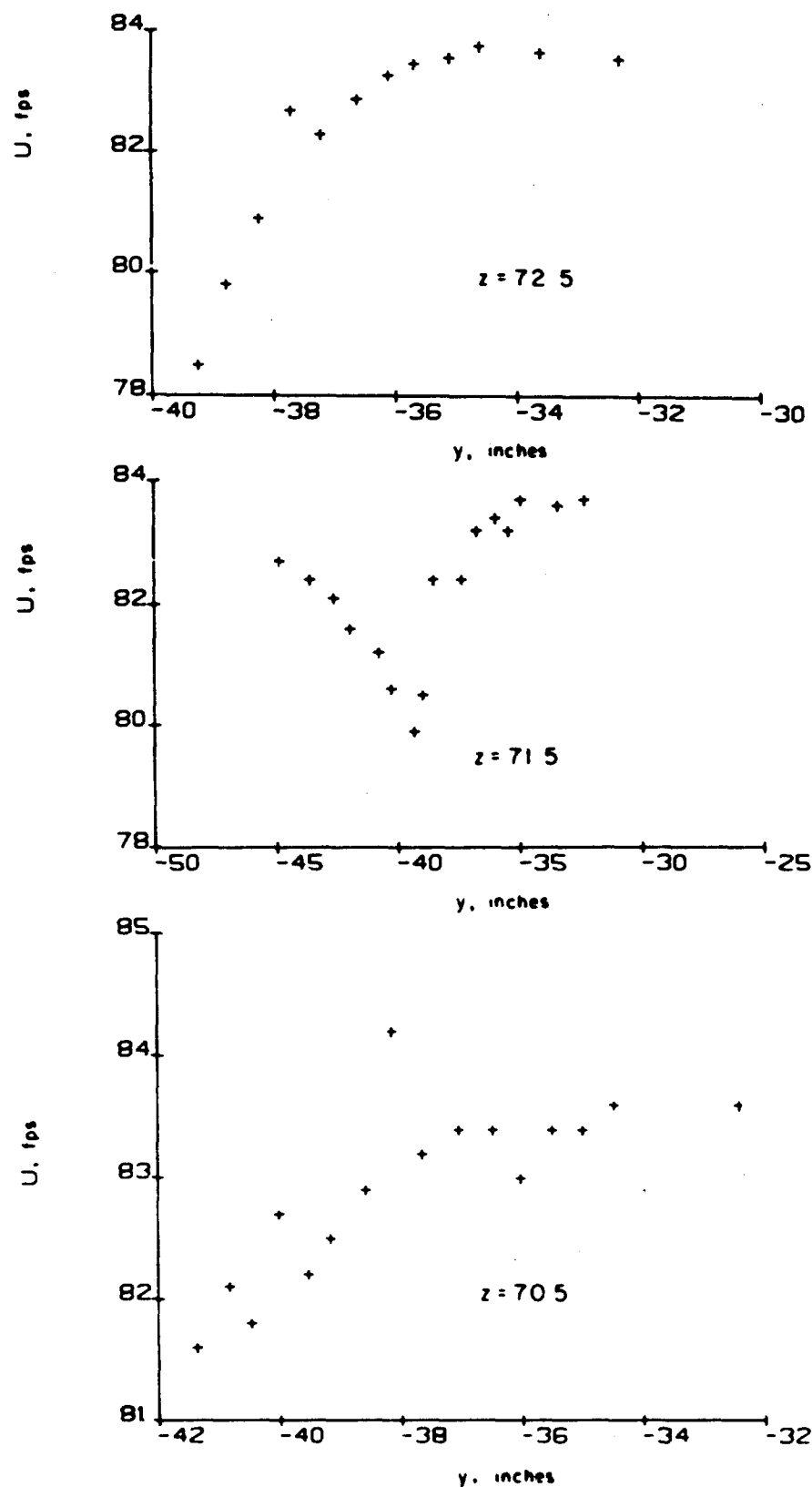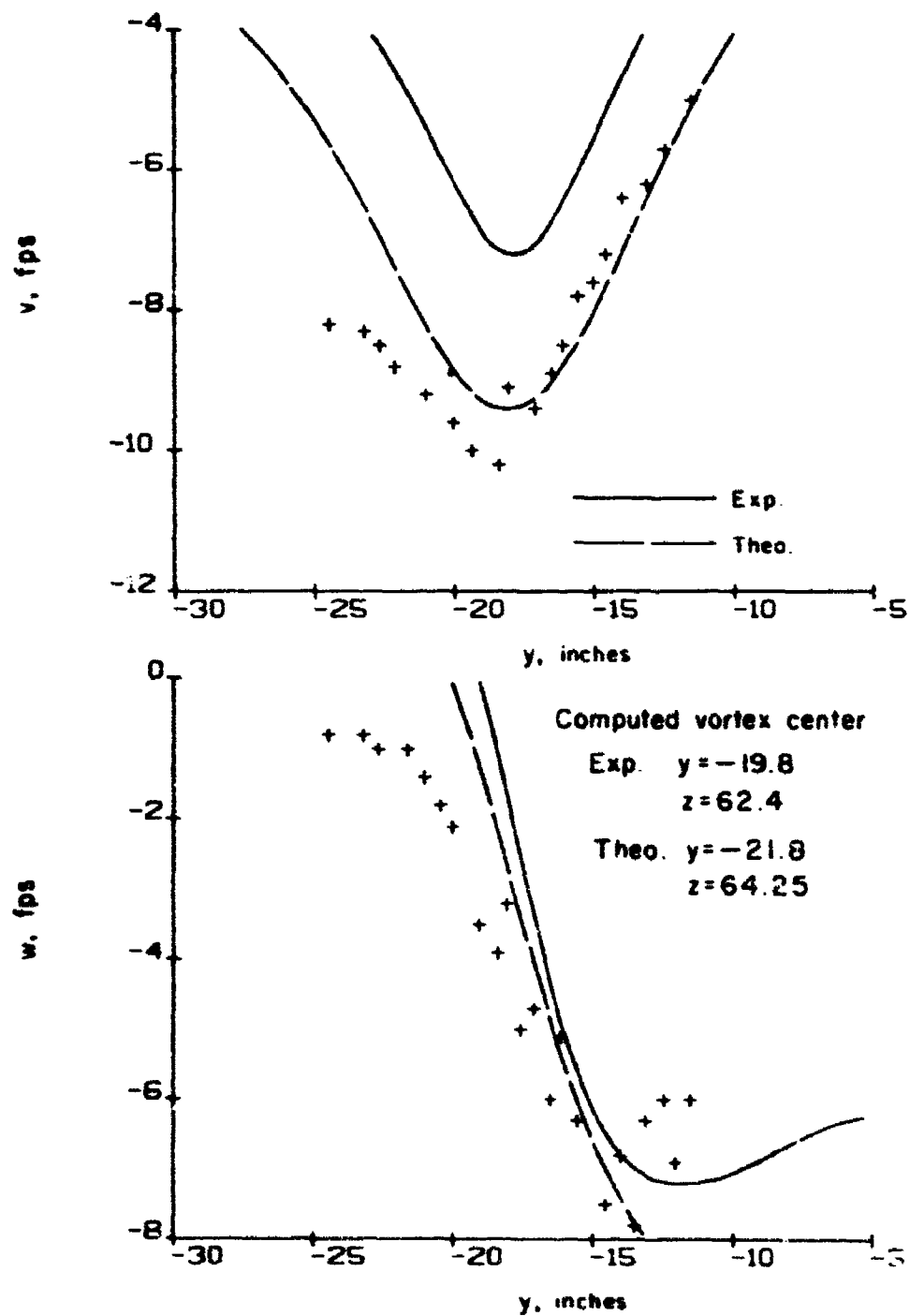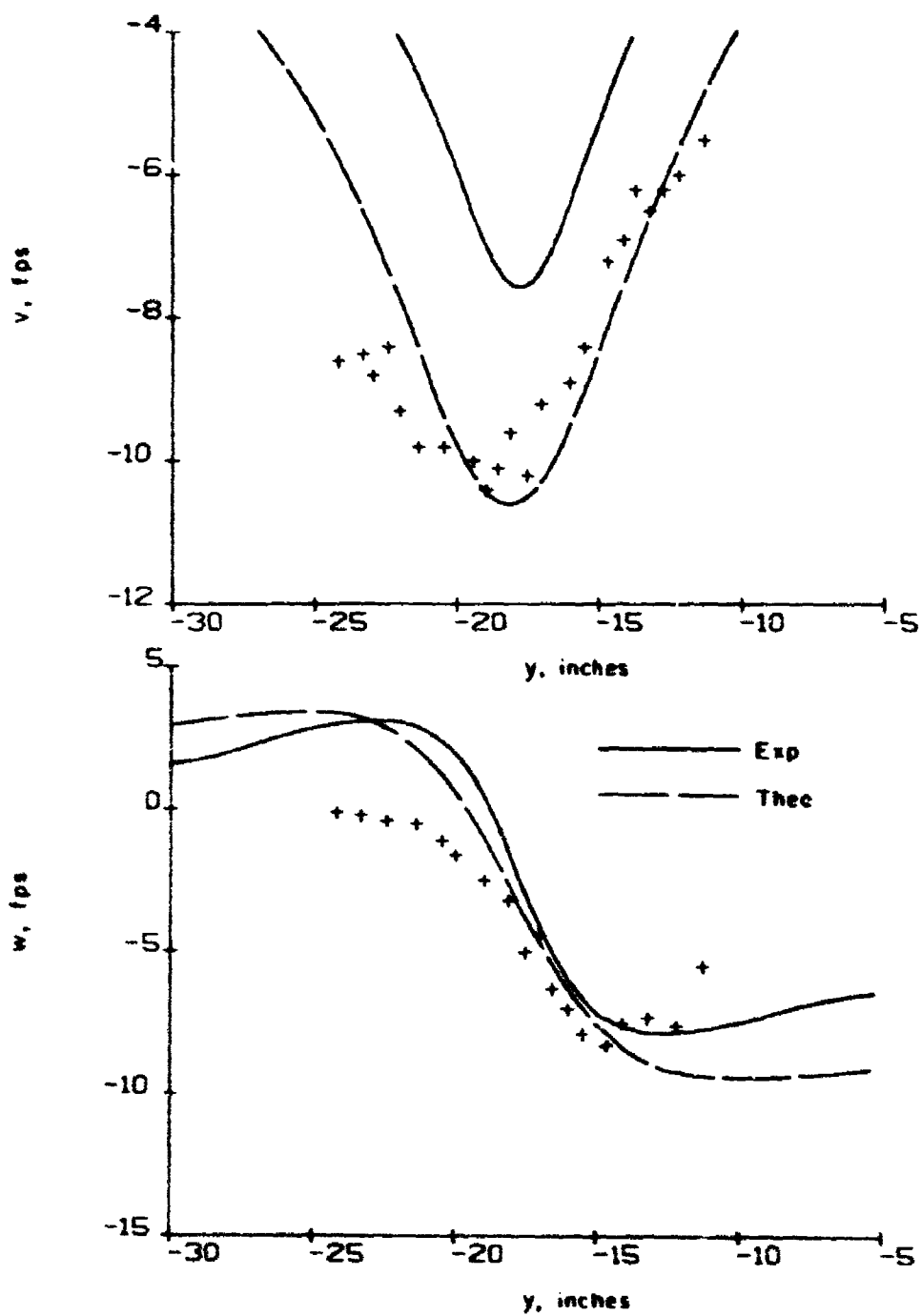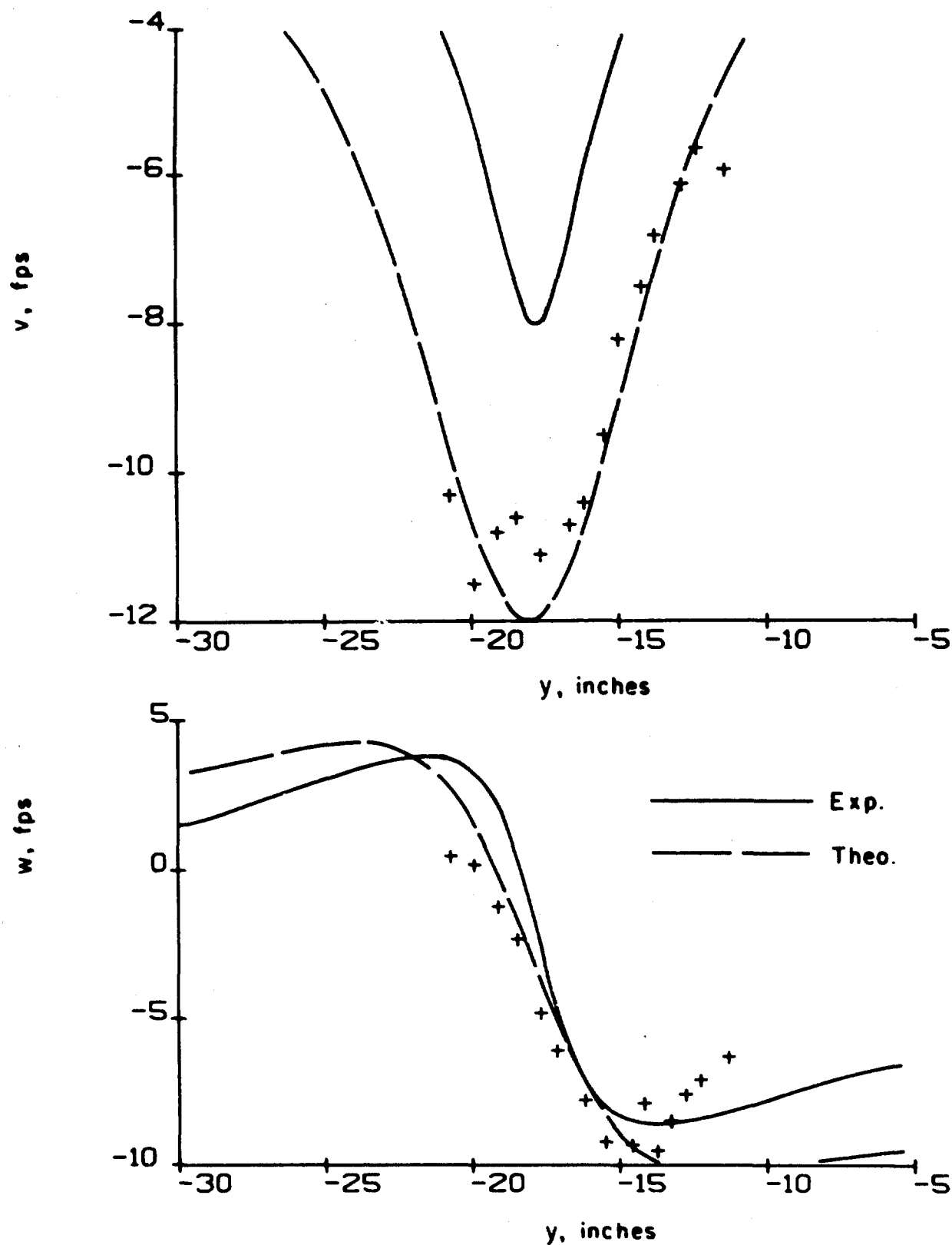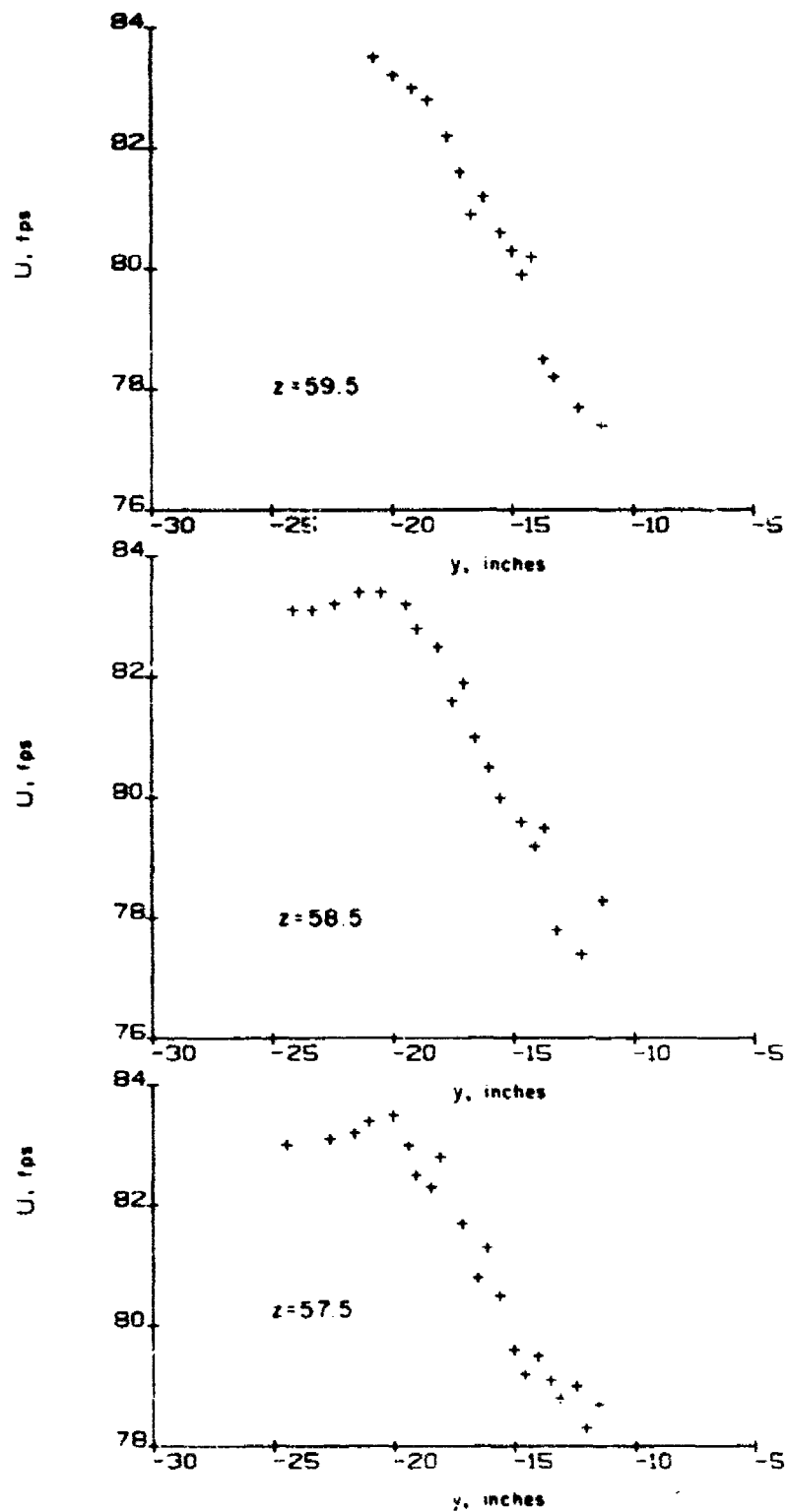Figure 61.   Configuration 2; measured axial velocities (x = 100 in.)

A weighting function, which was simply the radial distance from the assumed vortex center to the point at which the measurement was made, was used to bias the most distant data (from the vortex center). The output of the program was the vortex center or centers (when both a tip and flap vortex were present). When the weighting function was taken to be unity, the vortex centers only changed slightly. The horizontal and vertical velocity components were then computed from the Betz model and extension for flap vortices. The results are shown in Figures 38-61 and in Figures B.1 and B.3. The calculation was performed with the load distributions obtained from pressure measurements (labeled experimental) and lifting surface theory (labeled theoretical).

Computations of the horizontal and vertical velocity components for the flap vortices of configurations 3 and 4 were not in good agreement with experimental velocity measurements and are not shown in Figures B.2 and B.4. The explanation of this discrepancy is most easily seen in Figures 62 and 63. Here the measured velocity vectors in the Trefftz plane located at 5 chords downstream have been plotted. The flap vortex velocity fields are markedly nonsymmetric; roll-up apparently is not complete. Yates (Ref. 14) has shown that the initial rate of roll-up is strongly dependent on the maximum value of $d\Gamma/dy$. Referring back to the wing lift distributions shown in Figures 24 and 25, it is clear that the flap vortices will develop at a lesser rate than the tip vortices. Also, it is expected that the flap vortex in configuration 2 will develop more rapidly than those of configurations 3 and 4. In Appendix A, a simple model which estimates rate of roll-up has been developed for simple load distributions. This model also shows how roll-up rate is related to rate of change of the wing load distributions. While the results of this model, in its present form, cannot be directly applied to flap vortices, it is reasonable to assume that at axial stations near the wing, tip vortices will, in general, be better defined (roll-up will be more nearly complete) than flap vortices. Figures 38-61 support this assertion.

4. ROLL-UP OF THE WING DRAG DISTRIBUTION

The vortex axial and swirl velocity distributions were calculated for the clean wing configuration only, using the extended Betz model developed in Section II.2. The sectional induced drag coefficient for $C_L = 0.58$ was obtained from a lifting surface calculation and is shown in Figure 64. The section drag coefficient is the sum of the profile drag and induced drag and is also shown in Figure 64. The results of the calculation for the axial and swirl velocity distributions are shown in Figure 65. As can be seen, the axial velocity is nearly the free stream value. This result is surprising and significant in that it shows that the drag on a typical airfoil is nearly that required to keep the axial velocity uniform and equal to the free stream value across the vortex. In the absence of drag, the axial velocity is in excess of the free stream value as discussed by Batchelor (Ref. 17). This
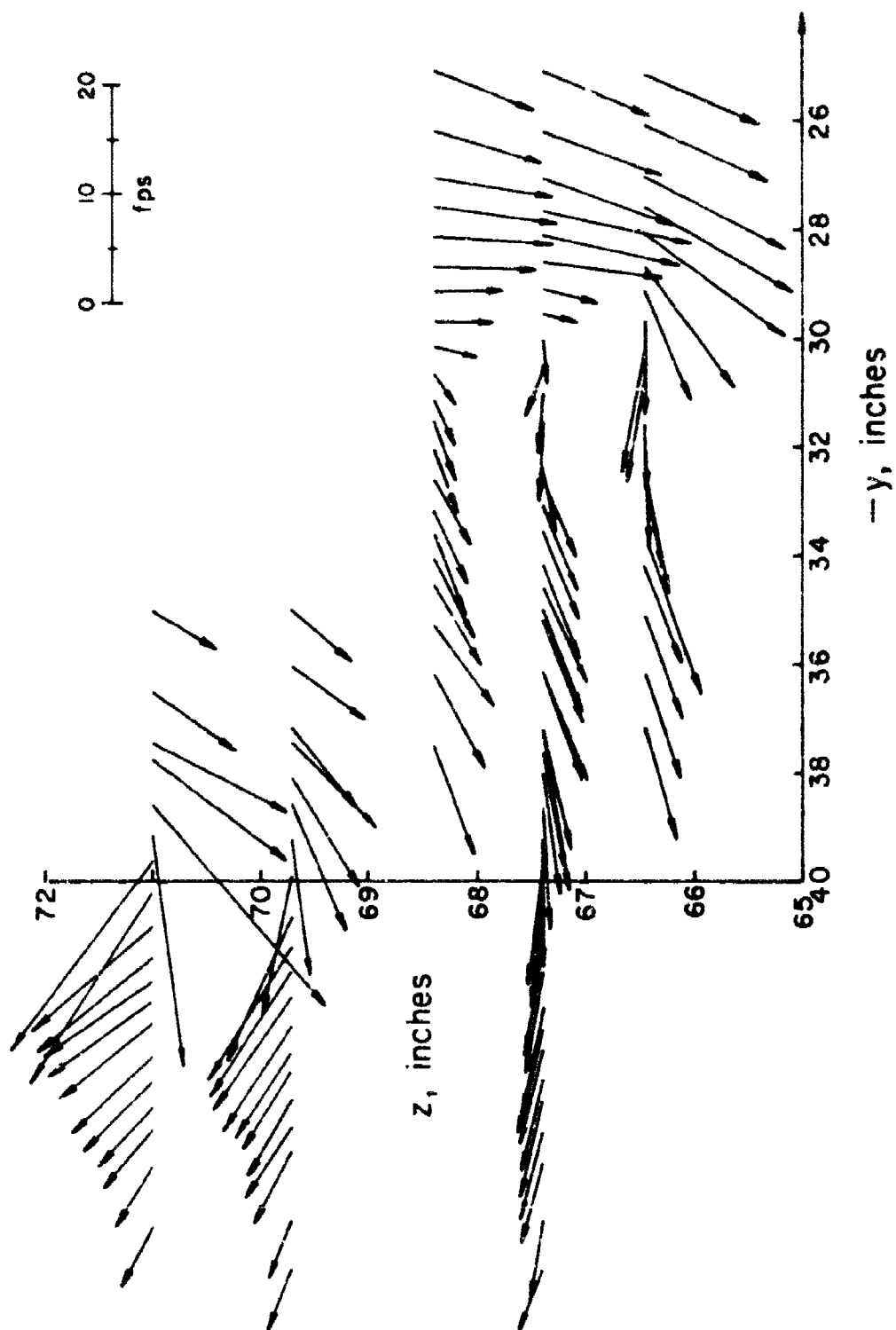
84

Figure 62. Measured velocities in the Trefftz plane; configuration 3)z = 50 in.)
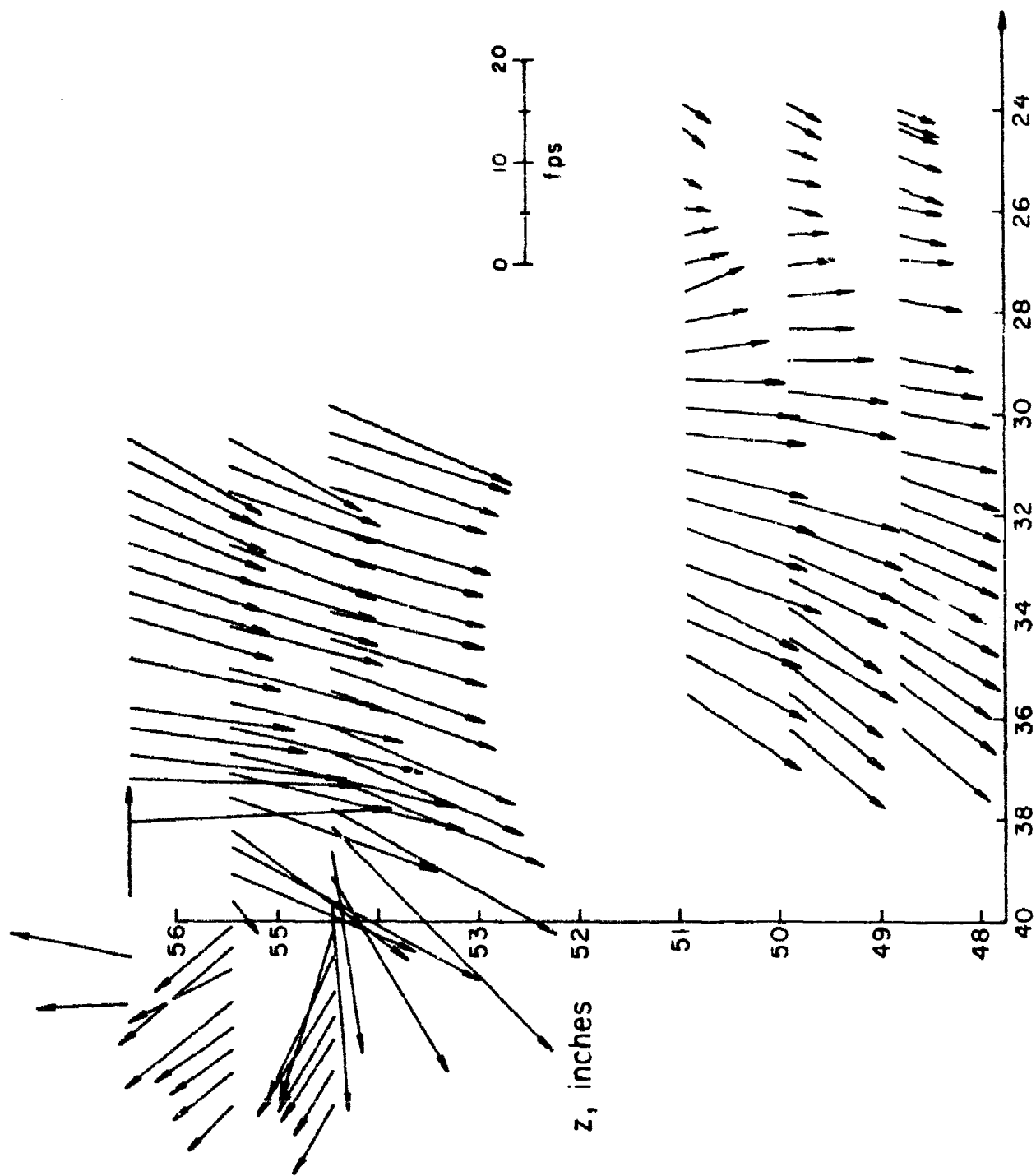
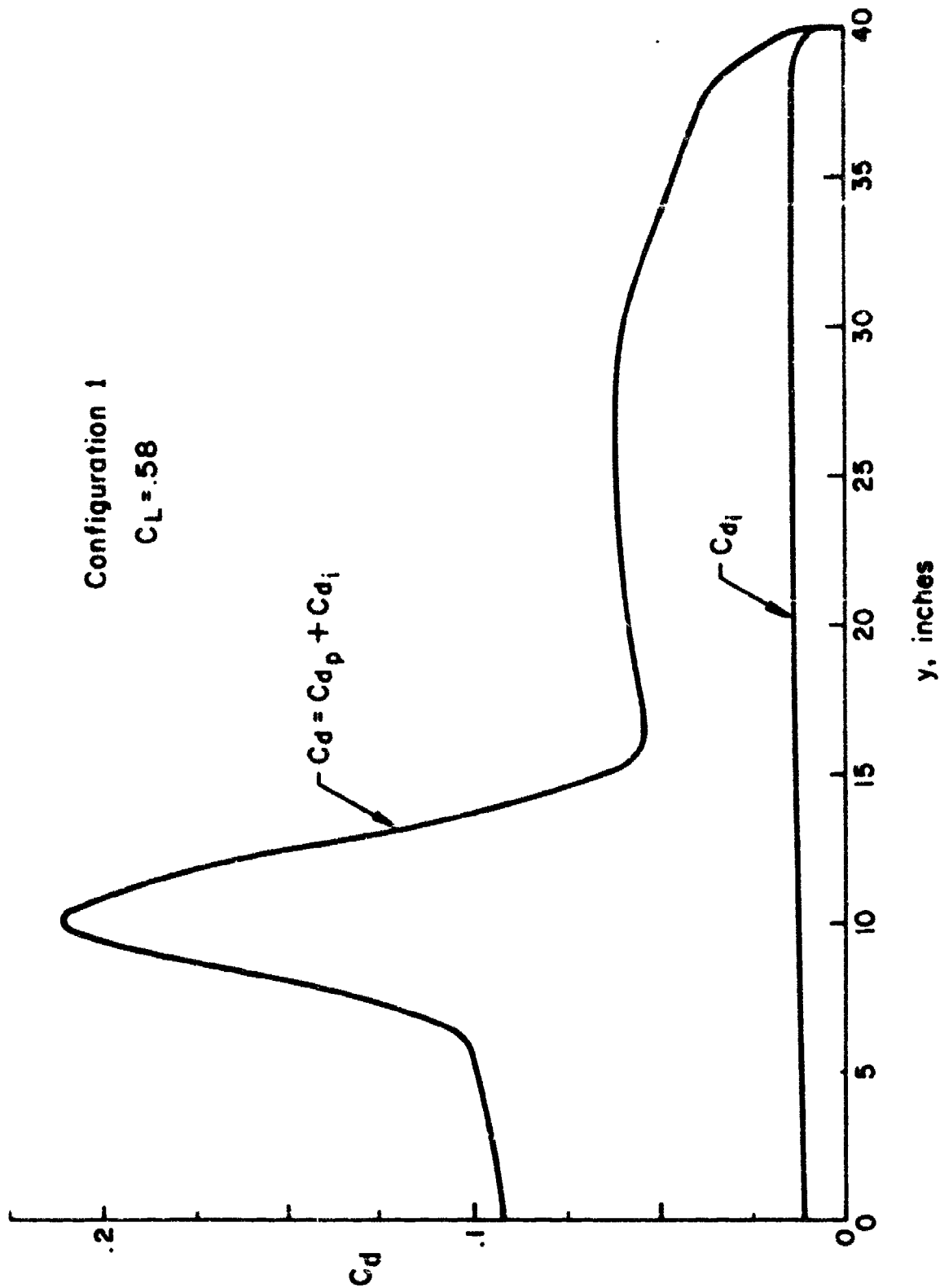Figure 53. Measured velocities in the Trefftz plane; configuration 4 ($z = 50$ in.)

Figure 64. The sectional induced drag coefficient for configuration 1 (from a lifting surface calculation)
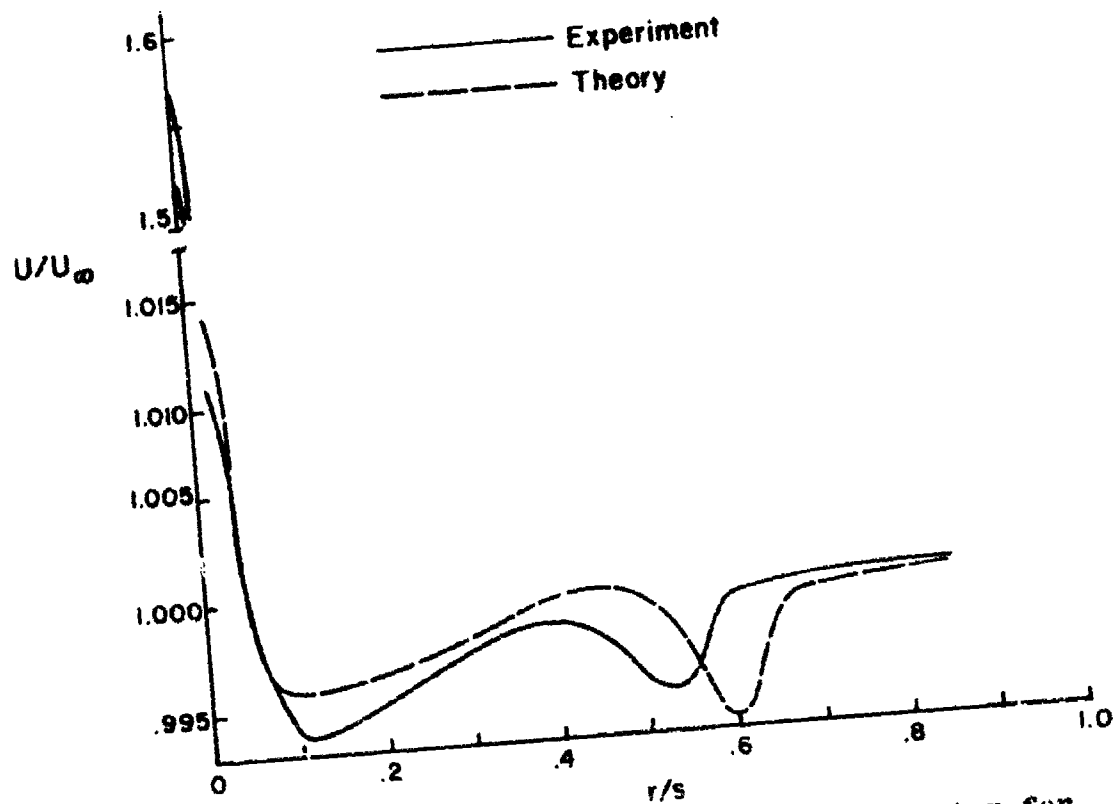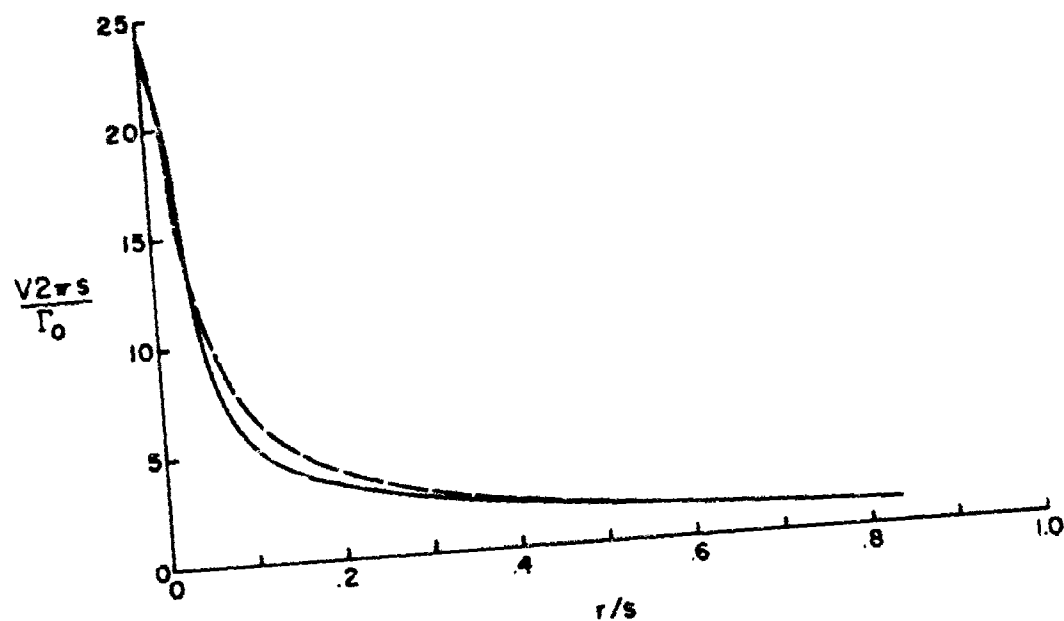
87

Figure 65. The downstream structure of the tip vortex for configuration 1

suggests to us that unless large drag-producing devices, such as spoilers, are present on the wing, an adequate description of the downstream vortex may be obtained by setting $U(r) = U_\infty$ in Eqs. (13) and (14). The vortex structure is then given by the Betz model and the extension given by Donaldson, et al. There is often a strong axial velocity excess or defect on the vortex centerline; however, this is not significant in that the actual mass flux or axial momentum flux departure over the uniform axial velocity vortex is small when compared to these quantities over the whole vortex (defined as that region in which all the axial vorticity may be found). As will be shown, this large excess or deficit on the vortex centerline is rapidly diminished by viscous processes.

5. ROLL-UP OF WING TURBULENT KINETIC ENERGY

The initial turbulent kinetic energy distribution in the rolled-up vortex for the clean wing configuration was estimated with the procedure given in Section II.3. The turbulent kinetic energy distribution at the trailing edge of the wing was calculated from a turbulent boundary layer program developed at A.R.A.P. (Ref. 19). The distribution of q^2 computed at the trailing edge is shown in Figure 66a; the maximum value of q/U_∞ was nearly 0.09. It was assumed that the distribution of kinetic energy was even in z (where z was measured vertically from the wing). The distribution of q'^2 in the vortex is shown in Figure 66b. Note that the maximum (at $r = 0$) is the same maximum value in the boundary layer. The sudden drop-off, as mentioned earlier, is brought about by the mixing of turbulent boundary layer fluid with increasing amounts of fluid which do not contain turbulent kinetic energy as roll-up proceeds from the tip.

6. DECAY OF AN ISOLATED TURBULENT VORTEX

A three-dimensional turbulent vortex program was developed at A.R.A.P. under contract to ARL. This program is described in detail in Ref. 15. Given the axial, swirl, and second-order velocity correlation radial distributions, the program will calculate the entire mean and turbulent vortex structure at subsequent positions downstream. Output at designated downstream stations are the mean velocity distributions and second-order velocity correlation distributions. In addition, the torque exerted by the vortex on a flat rectangular airfoil of prescribed span may be calculated at designated downstream distances. We have run the program for the clean wing configuration using the axial and swirl velocities shown in Figure 65 as calculated from the experimentally measured wing load distribution. The initial turbulent quantities were specified with auto-correlations taken to be $q'^2(r)/3$ ($q'^2(r)$ is given in Figure 66) and cross-correlations equal to zero.

The results of the calculation are summarized in Figures 67-72. Note that the initial swirl and axial velocity distributions were smoothed near $r = 0$ to avoid numerical problems with the number of grid points needed to adequately represent this region.
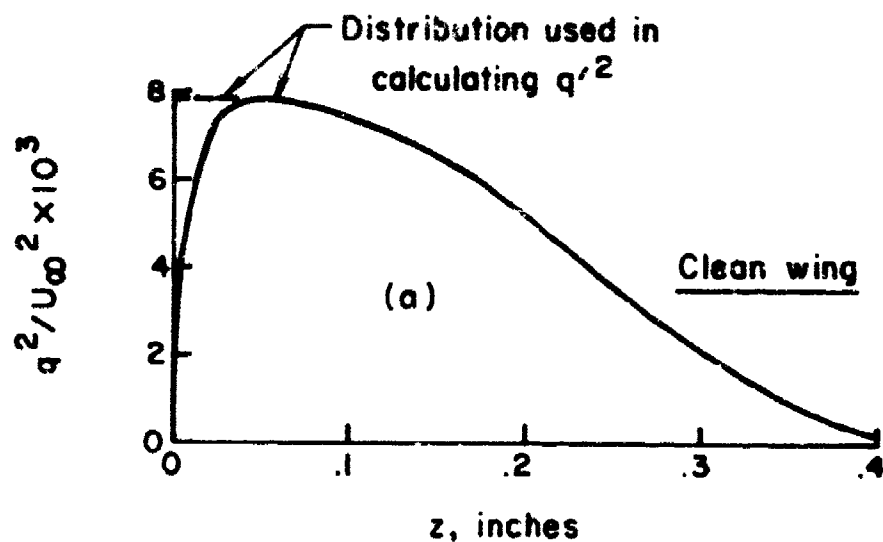
Figure 66a.   Estimated distribution of turbulent kinetic energy
at the wing trailing edge
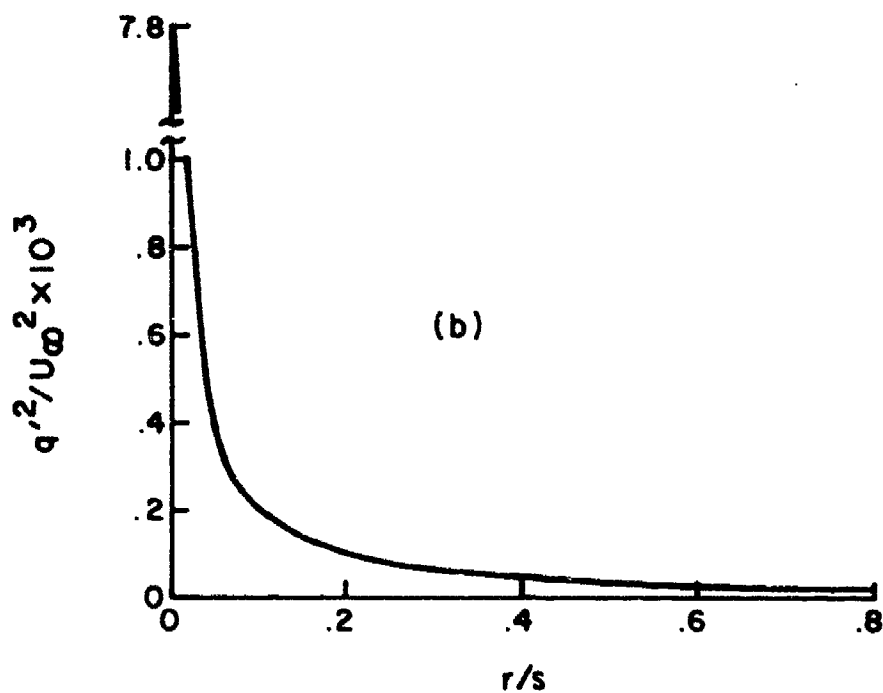
Figure 66b.   The computed distribution of turbulent kinetic energy
in the Betz vortex
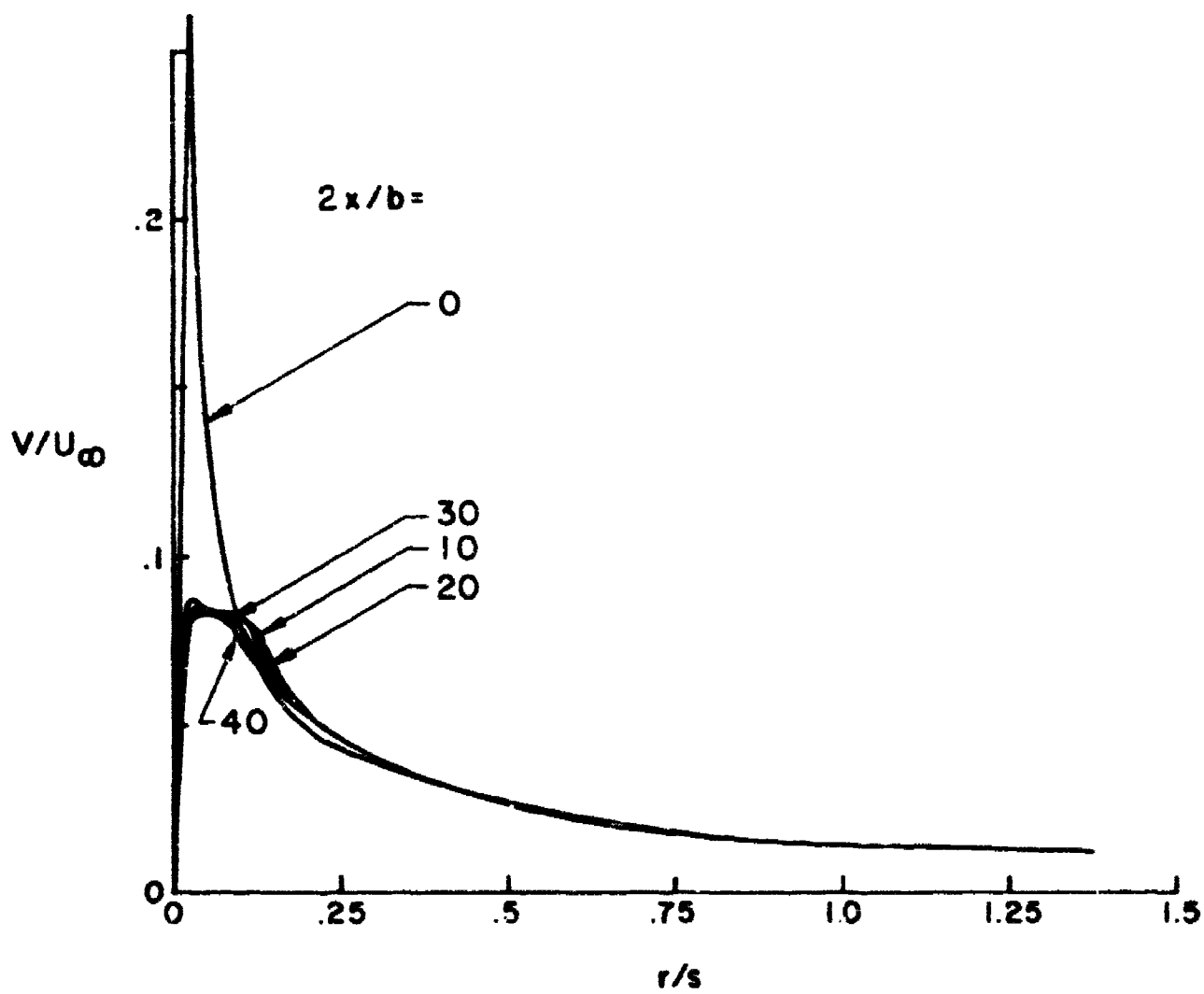
Figure 67.   Computed swirl velocity distributions
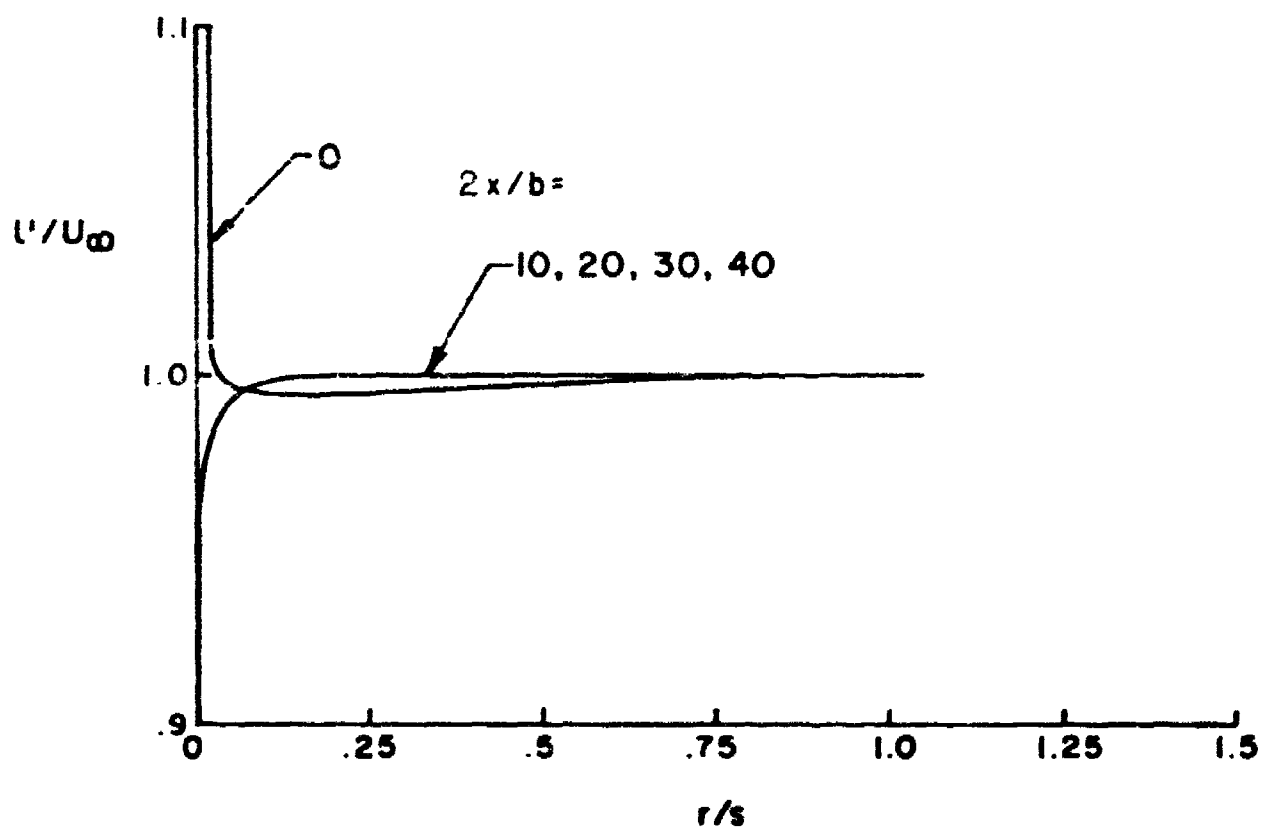
Figure 68. Computed axial velocity distributions
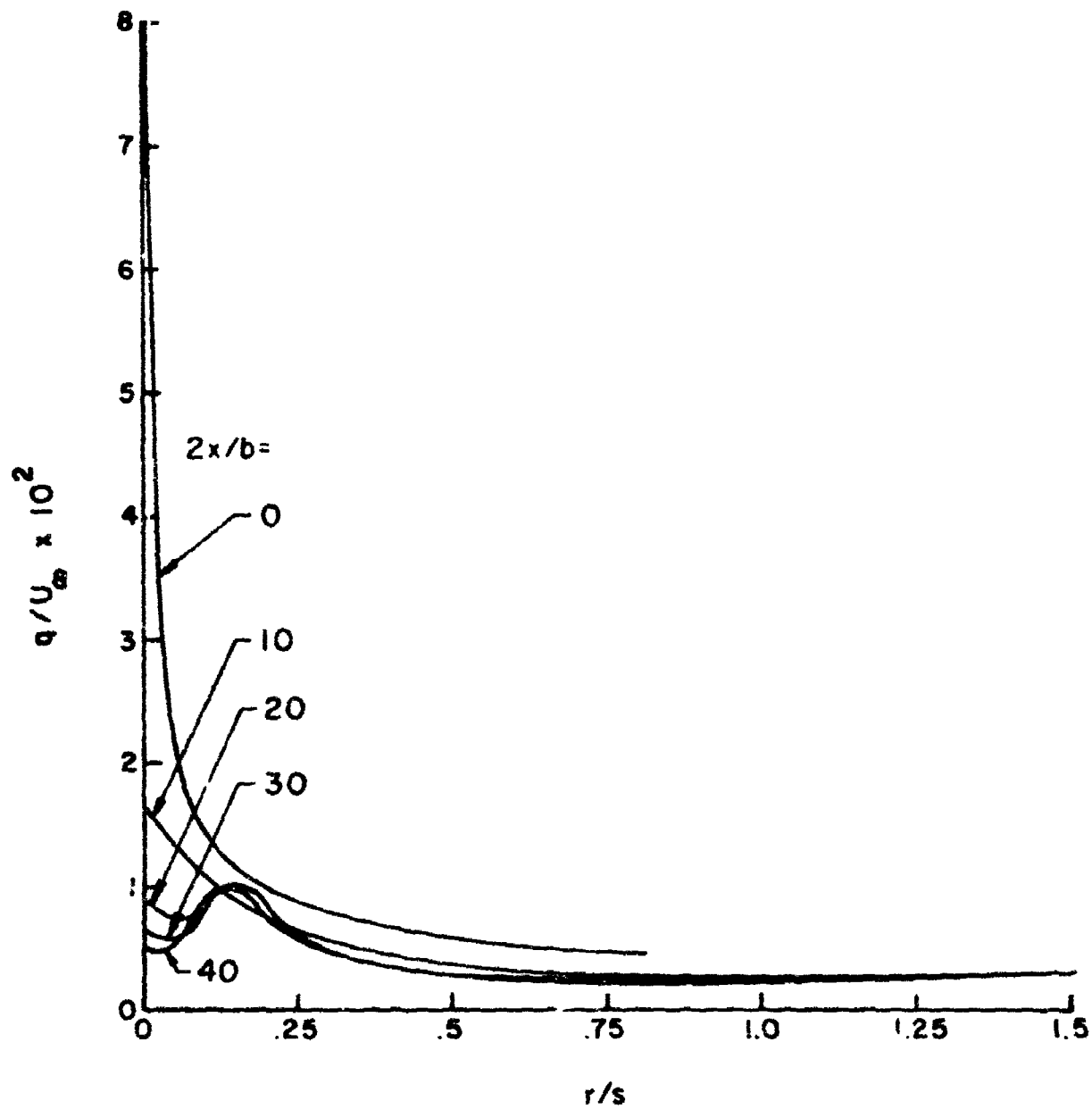
Figure 69. Computed distribution of $q' = \sqrt{\overline{u'^2} + \overline{v'^2} + \overline{w'^2}}$

93
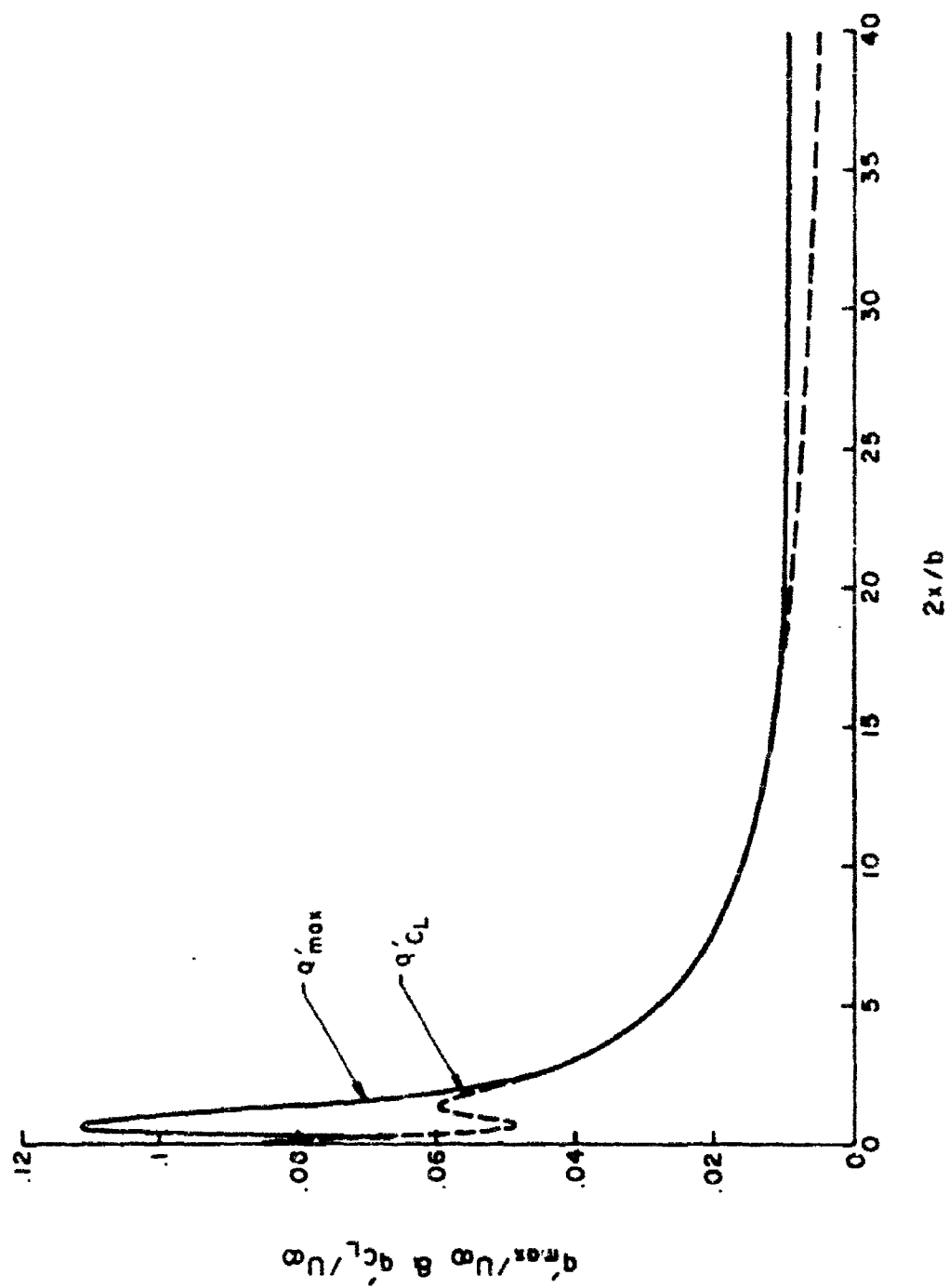
Figure 70. Computed centerline and maximum value of q'
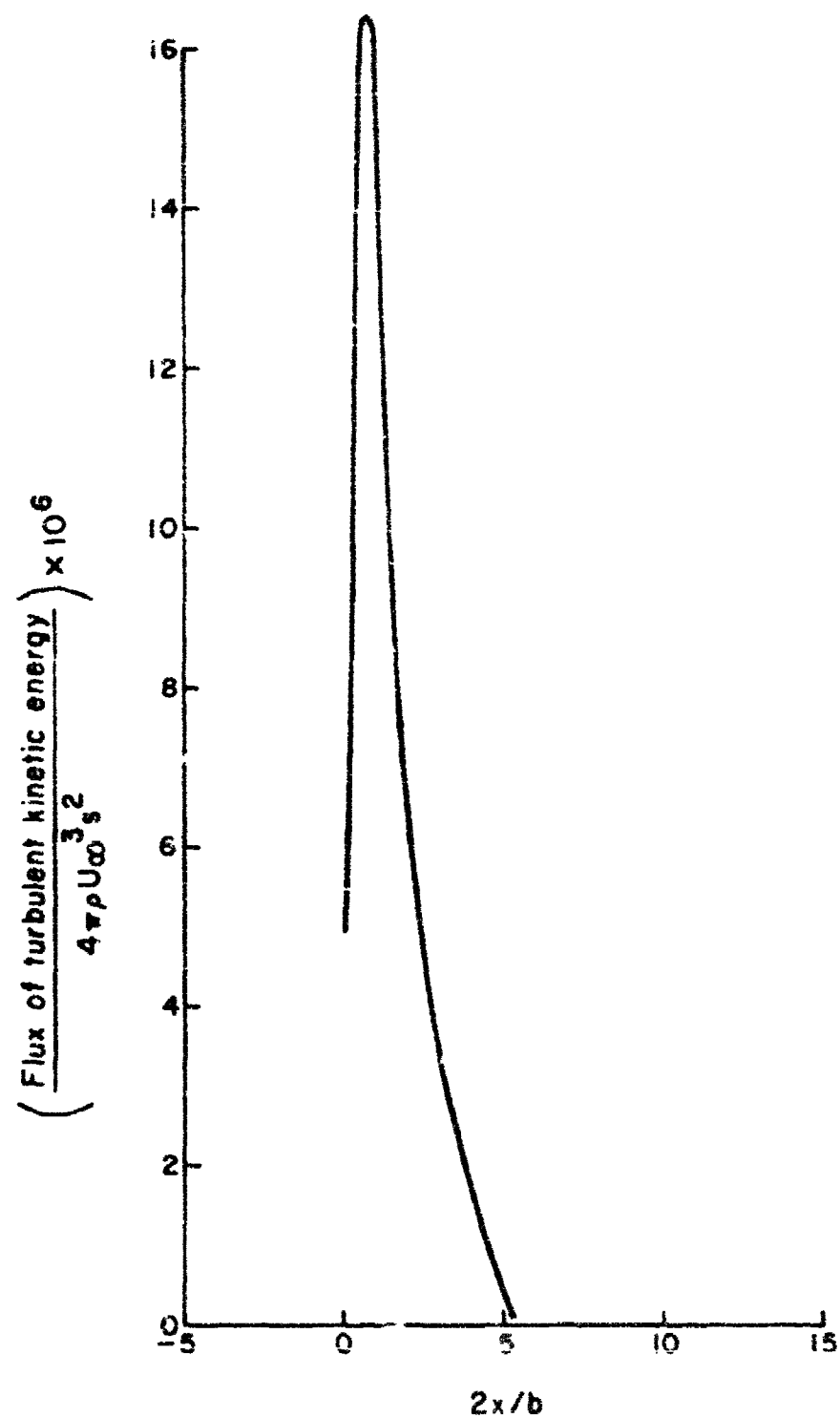
Figure 71. Computed flux of turbulent kinetic energy

95
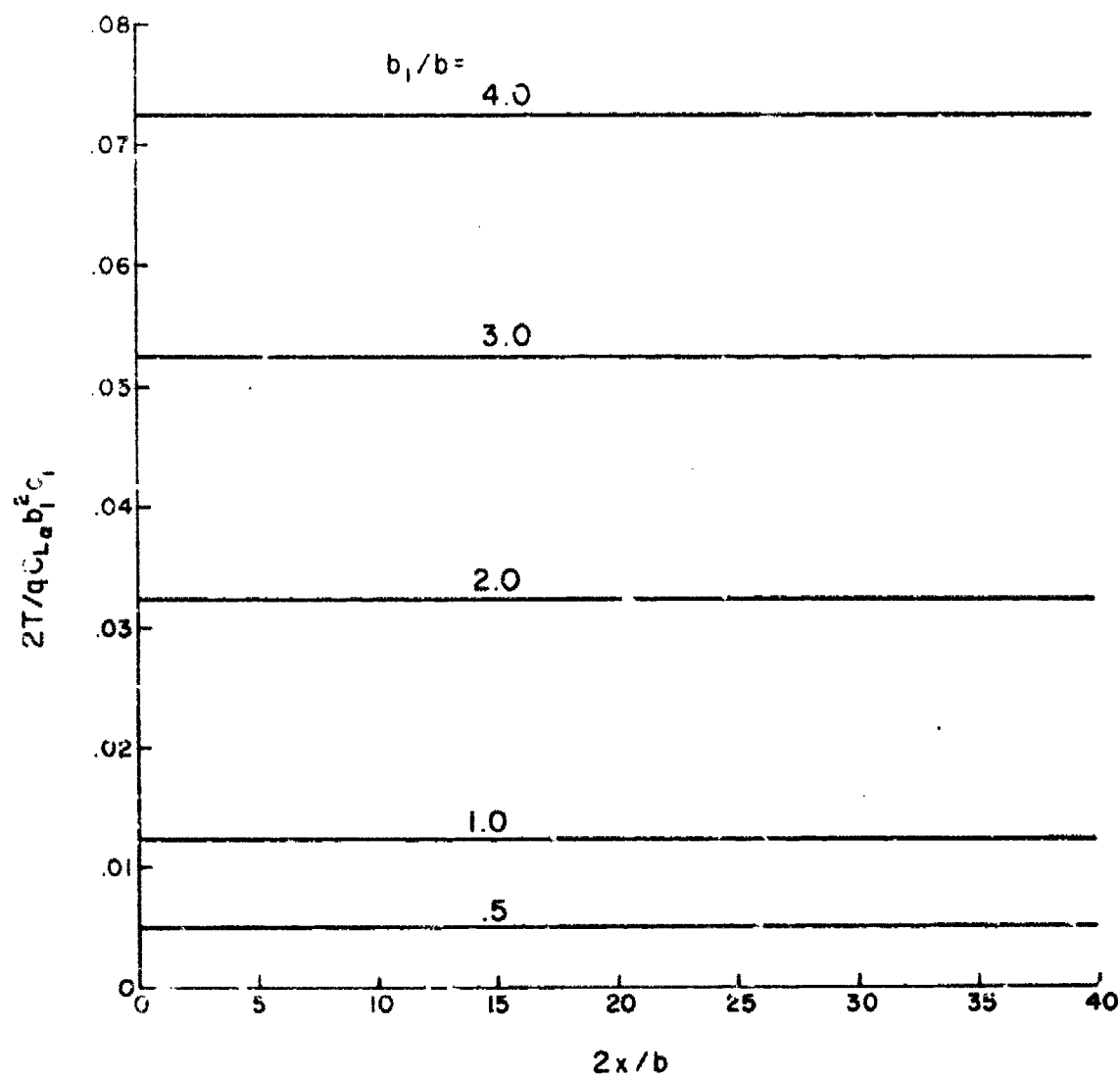
Figure 72.   Computed torque on a rectangular flat plate airfoil

In general, the calculation is not sensitive to this type of fairing since the actual axial flux of linear and angular momentum is negligible through the region.

Two results of this calculation are significant. The first concerns the level of turbulence which is supported by the vortex. In Figure 71 we see that the axial flux of q'^2, after the adjustment of the inviscid profiles (two semispans), drops far below the initial value. This result is not surprising since, if the production terms for the second-order correlations are examined for a turbulent boundary layer, production is proportional to the shear and of the order of the free stream velocity divided by the boundary layer thickness. In a vortex in which radial gradients of axial velocity are small, turbulent production is proportional to $r(V/r)_r$, a term which vanishes in the viscous core of the vortex (where V goes like r) and decays as r^{-2} in the irrotational region. At the maximum in swirl velocity, production is proportional to V_{max}/r_{max}, a quantity which is small when compared to U_∞/δ_{bl} on the wing. The fact that no turbulent production is possible at the vortex centerline suggests an explanation for the fact that the maximum value of q' does not occur at $r = 0$ as shown in Figure 70.

The second result concerns the slow decay of the vortex as measured by the torque calculated on a flat plate airfoil (Fig. 72). We do not want this result to imply that the rate of decay of an isolated vortex represents the decay rates to be expected in an aircraft wake. The assumption of axial symmetry and assumptions regarding the nature of the boundary conditions on the correlations for large r are idealizations which become invalid as the vortex pair ages. We note that the calculation was carried downstream to a nondimensional distance of 40 semispans. Investigations to determine the amplification rate of sinusoidal instability have shown that initial disturbances grow to e times their initial amplitude in time $\Theta(2\pi b^2/\Gamma)$ or, in terms of downstream distance, $\Theta(8AR/C_L)$ wing spans. For this configuration, the downstream e-folding distance is of the order of 40 semispans, and at 40 semispans the wake is, indeed, still very young.

The axial velocity distribution shown in Figure 68 can be compared with that measured for the clean wing (Fig. 45) at 10 chords downstream. The comparison is made in Figure 73 and, as can be seen, is in general agreement.
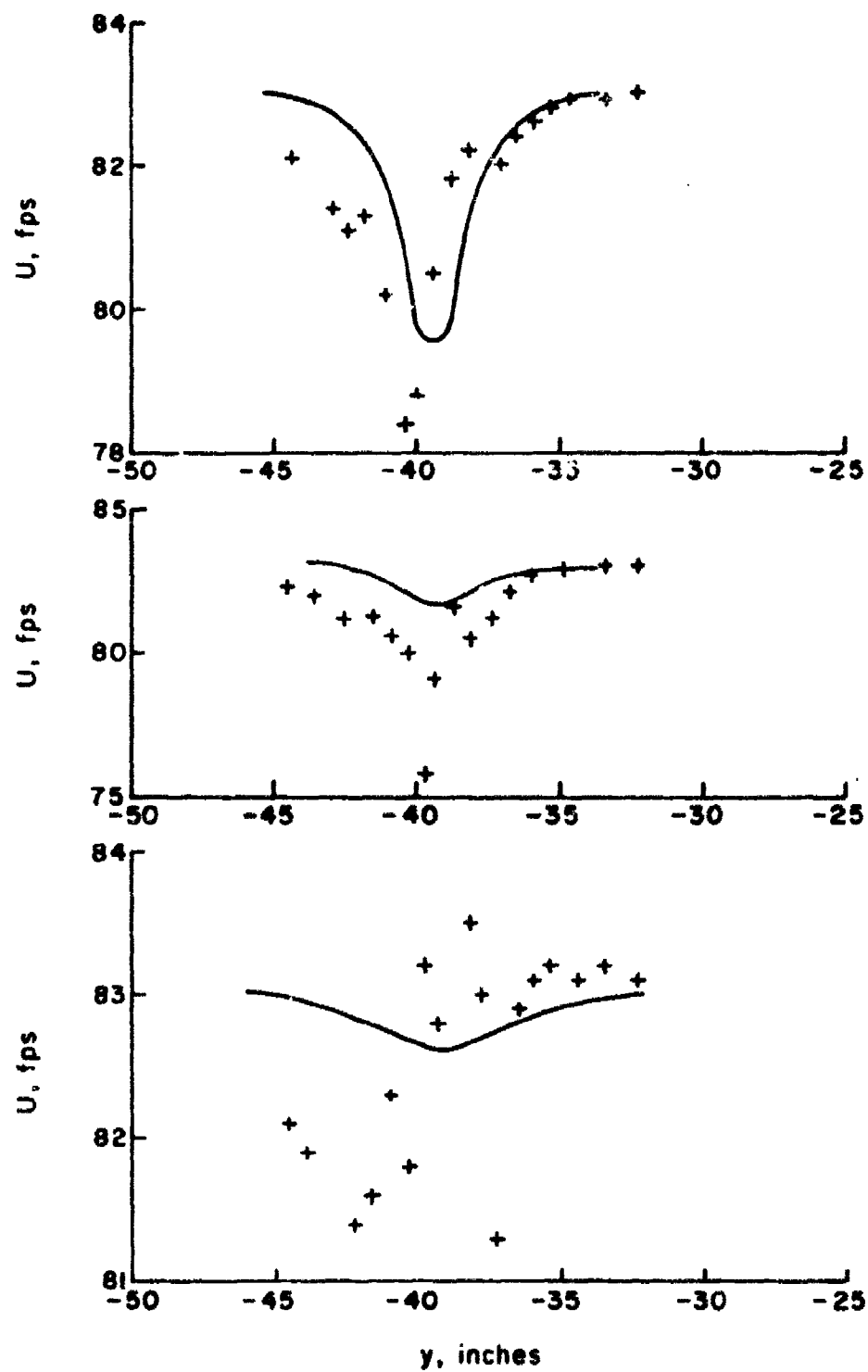
Figure 73. Comparison of the computed and measured axial
velocities at x = 100 in. (configuration 1)

98

SECTION V

CONCLUSIONS AND RECOMMENDATIONS

1. CONCLUSIONS

Several conclusions from this study can now be made regarding the structure of aircraft wakes.

1) The Betz model and extension to include "interior" vortices give a good description of the circulation distribution in wake vortices outside the viscous core and after roll-up is complete. At distances closer to the aircraft, a more detailed model is needed. One approach would be to treat the roll-up region as a growing vortex and stretching sheet, as described in Appendix A. At distances far downstream, aging alters the vortex structure, and descriptions of the decaying vortex must be obtained by deliberate calculation.

2) Distributed wing drag of the magnitude typical of clean airfoil sections has only a small effect on the inviscid tip vortex structure. This results primarily from the fact that typical values of drag reduce the axial velocity in the vortex so that it is nearly uniform and equal to the free stream value. This result, while obtained by direct calculation for a tip vortex, is expected to be approximately correct for "interior" roll-ups as well. When large drag devices are deployed on a wing, significant structural changes in the wake vortex can result. Drag devices which leave the lift distribution unchanged result in vortex structural changes which are a consequence of redistributing the axial flux of angular momentum in the vortex. The total flux of angular momentum remains unchanged in the region containing axial vorticity. The inviscid model suggests that vortex deintensification brought about solely by increased drag will be expensive in terms of drag penalty. It is likely that drag devices will significantly raise the turbulent level in the wake vortex which will lead to increased rates at which the angular momentum is redistributed outward. Therefore, estimates of the power required to reduce the intensity of a wake vortex, as calculated from an inviscid model, are likely to be high.

3) Based on the models used in this study, the flux of turbulent kinetic energy in the wing boundary layer which rolls-up into a vortex is greater than the flux of turbulent kinetic energy that is to be found in the downstream vortex. Since asymmetries exist in the flow field of a vortex pair or pairs, it is likely that aging will occur more rapidly than is predicted here by computing the decay of an isolated turbulent vortex.

99

4) The technique developed to calculate the location of the centroids of the discrete concentrations of vorticity in the wake have been shown to be quite accurate by comparison with flow visualization studies made here and by others. It has been shown that the structure of two-vortex-pair wakes can be obtained from a simple classification chart. Descriptions of the relative positions of the centroids of three of more pair wakes must be obtained, in general, by direct calculation.

2. RECOMMENDATIONS

Our recommendations cf additional work which should be undertaken in the area of vortex wake dynamics are divided into two categories:

1) Application of the technology developed in this and previous studies;

2) Additional research to understand the complete vortex wake behavior.

1) Application of New Technology

It has been shown that in the spirit of Betz mean discrete vortex structure may be calculated from the wing span load and drag distributions, and a simple model may be used to calculate the relative positions of these vortices. This in itself provides a description of the rolled-up aircraft wake with a precision that was previously unavailable. In addition, the model developed in Appendix A provides a first step in a description of the wake during roll-up, from which the velocity field in the vicinity of the wing may now be calculated in detail. These models have immediate application to the design and evaluation of the performance and stability of lifting surfaces in vortex wake flow fields. Some obvious applications of these wake models are

1) The design of tails, canards, side force generators, and wings in vortex flow fields produced by upstream lifting surfaces. The longitudinal instability of the E.B.F. V/ STOL model is but one example of the need for the application of this new technology.

2) The use of velocity fields as input to flight simulators. Pilots could then train for wake encounters; military pilots could simulate aircraft upset due to wake turbulence under close-interval take-off, formation flying, and refueling conditions.

3) The design of a low hazard wake. By specifying the vortex wake structure, the wing lift and drag distribution which generates the desired wake may be calculated. Estimates of the induced and profile drag penalties to obtain a specified level of wake intensity may be obtained by a direct calculation.

2) Additional Research

The wake models presented in this study provide an important step in developing techniques to describe the complete vortex wake history. However, several important aspects of the problem still remain unsolved. We have proposed that a complete description of the aircraft wake must answer three basic questions — roll-up, aging, and instability. The Betz model and extensions, including the roll-up model, can only be used with confidence before aging and instability become important. The areas of wake aging and vortex breakdown need additional study.

Our understanding of the phenomenon of vortex pair or pairs aging is just in its infancy. Although fundamental contributions have been made to our understanding of the aging of an axisymmetric isolated turbulent line vortex, few of the conclusions which may be drawn can be directly applied to the pair. Advances in numerical computation procedures ɛt A.R.A.P. and increased confidence in the invariant modeling technique have recently made the calculation of turbulent decay of a complete vortex wake possible. We strongly recommend that this unique capability be exploited to make more realistic calculations of wake decay than have previously been possible.

Vortex breakdown occurring in proximity to lifting surfaces can have adverse effects on the performance of those surfaces. New advances in our understanding of the phenomenon can now predict conditions conducive to breakdown. As advanced technology aircraft use favorable lifting surface vortex interaction effects to improve performance, the ability to predict and control breakdown will have important consequences. Favorable vortex-surface interaction, when exploited, will undoubtedly improve many aspects of aircraft performance.

APPENDIX A

ESTIMATED TIME TO ROLL UP A TWO-DIMENSIONAL SHEET

The assumptions made by Betz can be used to develop a model to estimate the time required to roll up the vorticity behind a simply loaded wing. In the spirit of Betz, we consider the roll-up of a two-dimensional vortex sheet of strength $\gamma(y,t)$.

Referring to Figure A-1, we assume that vorticity which has been convected past station A is rolled up in the vortex and is distributed according to Eq. (4). Further, we assume that the portion of the sheet which is not yet in the vortex remains horizontal as shown. The error which is a consequence of this assumption is discussed below.

The time rate of change of circulation in the vortex is given by

$$\frac{d\Gamma'}{dt} = \left[v - \frac{d\bar{y}_v}{dt} \right] \gamma(\bar{y}_v, t) \tag{A.1}$$

where v is the horizontal velocity at station A induced by the vorticity and γ is the vortex sheet strength at station A. The term $d\bar{y}_v/dt$ accounts for the inward motion of the vortex as roll-up proceeds.

In the evaluation of the sheet strength, it is necessary to account for sheet stretching which is the result of nonuniform convection along the sheet. To obtain an expression governing the stretching, the two-dimensional inviscid vorticity equation

$$\frac{\partial \omega}{\partial t} + v \frac{\partial \omega}{\partial y} + w \frac{\partial \omega}{\partial z} = 0 \tag{A.2}$$

is integrated through the sheet from $z = -\infty$ to $z = \infty$. After integrating by parts and using the continuity equation, we obtain

$$\frac{\partial \gamma}{\partial t} + \frac{\partial}{\partial y} \int_{-\infty}^{\infty} v\omega \, dz = 0 \tag{A.3}$$

where $\gamma = \int_{-\infty}^{\infty} \omega \, dz$.

The horizontal velocity v may be thought of as the sum of two terms v_c and v_s; v_c is the velocity due to the rolled-up portion of the sheet and is given by

$$v_c = \frac{z\Gamma'}{2\pi} \left\{ -\left[(y - \bar{y}_v)^2 + z^2 \right]^{-1} + \left[(y + \bar{y}_v)^2 + z^2 \right]^{-1} \right\} \tag{A.4}$$
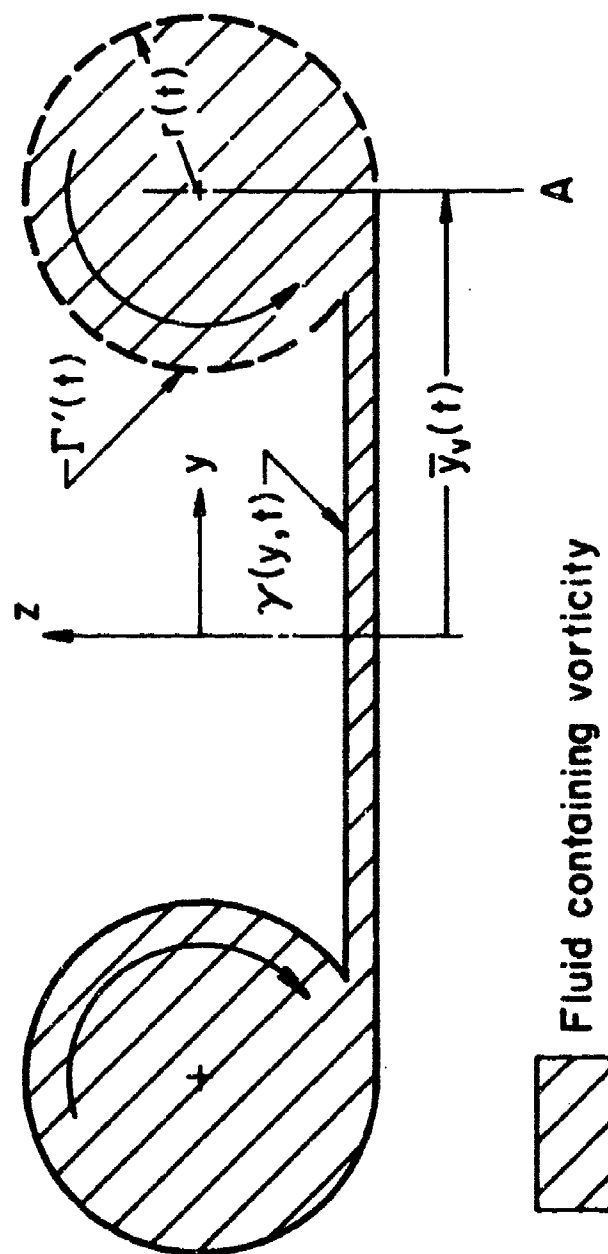
Figure A-1. A simple two-dimensional roll-up model

Since the sheet is of negligible thickness, Eq. (A.3) may be written

$$\frac{\partial \gamma}{\partial t} + \frac{\partial}{\partial t}(v_c \gamma) = -\frac{\partial}{\partial y}\int_{-\infty}^{\infty} v_s \omega \, dz \qquad (A.5)$$

When a vortex sheet is planar, v_s is identically zero which motivated the assumption regarding the geometry of the sheet. The error introduced is not too severe, however, since had the sheet been allowed to deform having a characteristic radius R, the horizontal induced velocities would be of order Γ_s/R where Γ_s is the circulation of the sheet. Initially, R is infinite. When roll-up has proceeded for some time, R is finite; however, Γ_s is small since most of the circulation has already been rolled up into the vortex. We therefore neglect the right-hand side of (A.5). This approximation implies that the roll-up phenomenon is strongly dominated by the developing vortex. The approximations introduced thus far will underestimate the time to roll-up, since sheet stretching is also underestimated.

Unfortunately, even with the above-noted simplifications, the solution of (A.5) with v_c given by (A.4) is quite difficult. Therefore, the functional form of the convecting velocity is chosen so that it is possible to find an analytic solution to (A.5) and yet retain the physics of the stretching phenomenon. One such velocity is

$$v_c = g(t)y \qquad (A.6)$$

where

$$g(t) = \frac{\Gamma'}{2\pi r(t)\bar{y}_v} \qquad (A.7)$$

The general solution of (A.5) can now be found by the method of characteristics and is

$$\gamma(y,t) = \frac{\Gamma_o f(\delta)}{y} \qquad (A.8)$$

where

$$\delta = \frac{y}{s} \exp\left(-\int_o^t g(t)dt\right) \qquad (A.9)$$

f is an arbitrary function of δ and is determined from the initial sheet strength distribution.

We will present results for the linear, parabolic, and elliptical wing loading. The initial sheet strengths are calculated from $\gamma = -d\Gamma/dy$ and are

$$\frac{\gamma s}{\Gamma_o} = \begin{cases} 1 & \text{Linear} \\ \dfrac{2y}{s} & \text{Parabolic} \\ \dfrac{y}{s}\left[1 - \left(\dfrac{y}{s}\right)^2\right]^{-1/2} & \text{Elliptic} \end{cases} \qquad (A.10)$$

The vortex sheet strength at station A as a function of time is

$$\frac{\gamma s}{\Gamma_o} = \begin{cases} B(t) \\ \dfrac{2B(t)^2 \bar{y}_v}{s} \\ \dfrac{1}{s}\left\{1 - \left[\dfrac{B(t)\bar{y}_v}{s}\right]^2\right\}^{-1/2} B(t)^2 \bar{y}_v \end{cases} \qquad (A.11)$$

where

$$B(t) = \frac{\delta s}{y} \qquad (A.12)$$

The location of the developing vortex $\bar{y}_v(t)$ is not known and is determined from the conservation of impulse. The calculation appears tractable for only the linear load case where

$$\frac{\bar{y}_v(t)}{s} = \left(1 + \frac{\Gamma'}{\Gamma_o}\right)^{-1} \qquad (A.13)$$

However, a good approximation to $\bar{y}_v$ is to use $\bar{y}$ as defined in Eq. (2) or rewritten as an explicit function of Γ as

$$\bar{y}(\Gamma) = y(\Gamma) - \frac{1}{\Gamma}\int_o^\Gamma \Gamma\left(\frac{d\Gamma}{dy}\right)^{-1} d\Gamma \qquad (A.14)$$

For the linear load, $\bar{y}/s = 1 - \Gamma/2\Gamma_o$ $\qquad (A.15)$

When (A.15) is used to approximate $\bar{y}_v$, an error of 6.25% in the impulse for the linear load occurs during the roll-up. The error is less than this value for lift distributions more highly loaded at the tip and is, therefore, not serious.

For wings having a linear load distribution, an ordinary non-linear integrodifferential equation describing the time rate of growth of the vortex is

$$\frac{d\Gamma'}{dt} = -\frac{1}{\pi}\left(\frac{\Gamma_o}{s}\right)^2 \left\{\frac{1}{2} - \exp\left[\int_o^t \frac{2}{\pi}\frac{\Gamma_o}{s^2}\left(2 - \frac{\Gamma'}{\Gamma_o}\right)^{-1} dt\right]\right\}^{-1} \qquad (A.16)$$

106

The solution is

$$\frac{\Gamma'}{\Gamma_0} = 1 - \exp\left[- \frac{2\Gamma_0 t}{\pi s^2} \right] \qquad (A.17)$$

The equations governing the roll-up for the parabolic and elliptic-ally loaded wing are considerably more complicated and are not given here. The solutions for these cases must be determined numerically and are shown along with the linear case in Figure A-2.

Spreiter and Sacks (Ref. 7) have also made estimates of the downstream distance at which the vortex can be considered to be essentially rolled up by applying the results obtained by Kaden (Ref. 6) for a semi-infinite wing. For elliptic wing loading, they obtained the nondimensional downstream distance of $xC_L/4\bar{y}AR = 0.18$ which corresponds to having approximately 55% of the wing root circulation in the vortex (as calculated here). The discrepancy is believed to arise as a consequence of using Kaden's solution where it is not strictly valid.

For small times, the solutions can be shown to behave as

$$\frac{\Gamma'}{\Gamma_0} \approx \begin{cases} \dfrac{2t\Gamma_0}{\pi s^2} & \text{Linear} \\[3ex] \dfrac{8t\Gamma_0}{\pi s^2} & \text{Parabolic} \\[3ex] 3\left(\dfrac{t\Gamma_0}{4\pi s^2}\right)^{1/3} & \text{Elliptic} \end{cases} \qquad (A.18)$$

The $t^{1/3}$ behavior for the elliptic load agrees with the similarity solution obtained by Kaden.

In Figure A-3 our results are compared with those recently obtained by Moore (Ref. 5). Part of the discrepancy has already been explained by the approximations which have been made. However, an additional point is that Moore has chosen the station past which the sheet is to be considered rolled up at a location 90° in the counterclockwise sense from station A in Figure A-1. His results are, therefore, biased to be lower than those obtained here. The amount is difficult to calculate, but the difference is expected to be most significant for small times. The result, neglecting sheet stretching, is obtained by taking v_c constant in Eq. (A.5) equal to the horizontal velocity at station A in Figure A-1. In this case, complete roll-up occurs in finite time.
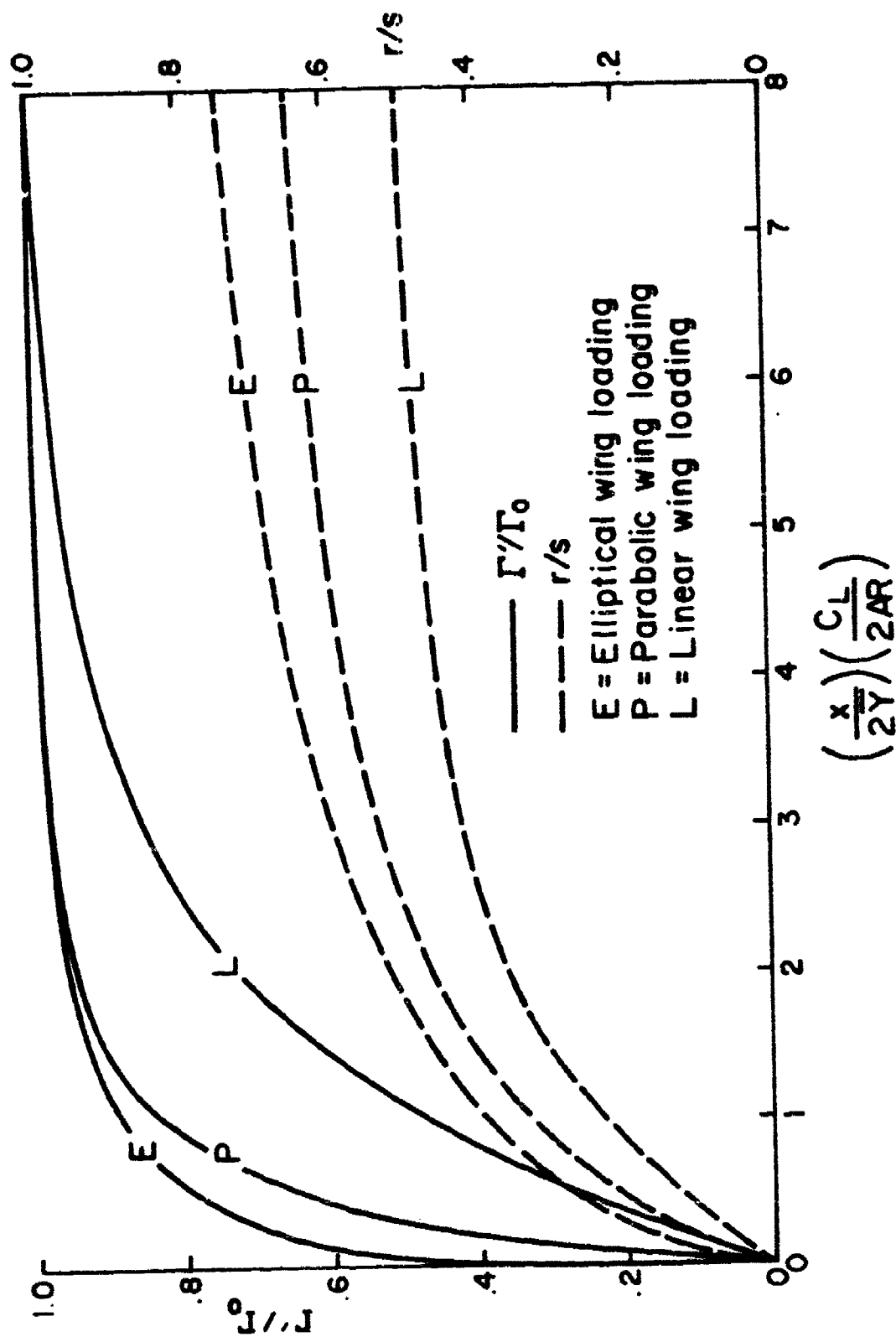
Figure A-2. Vortex circulation and radius as a function of downstream distance (time has been replaced by x/U_∞)
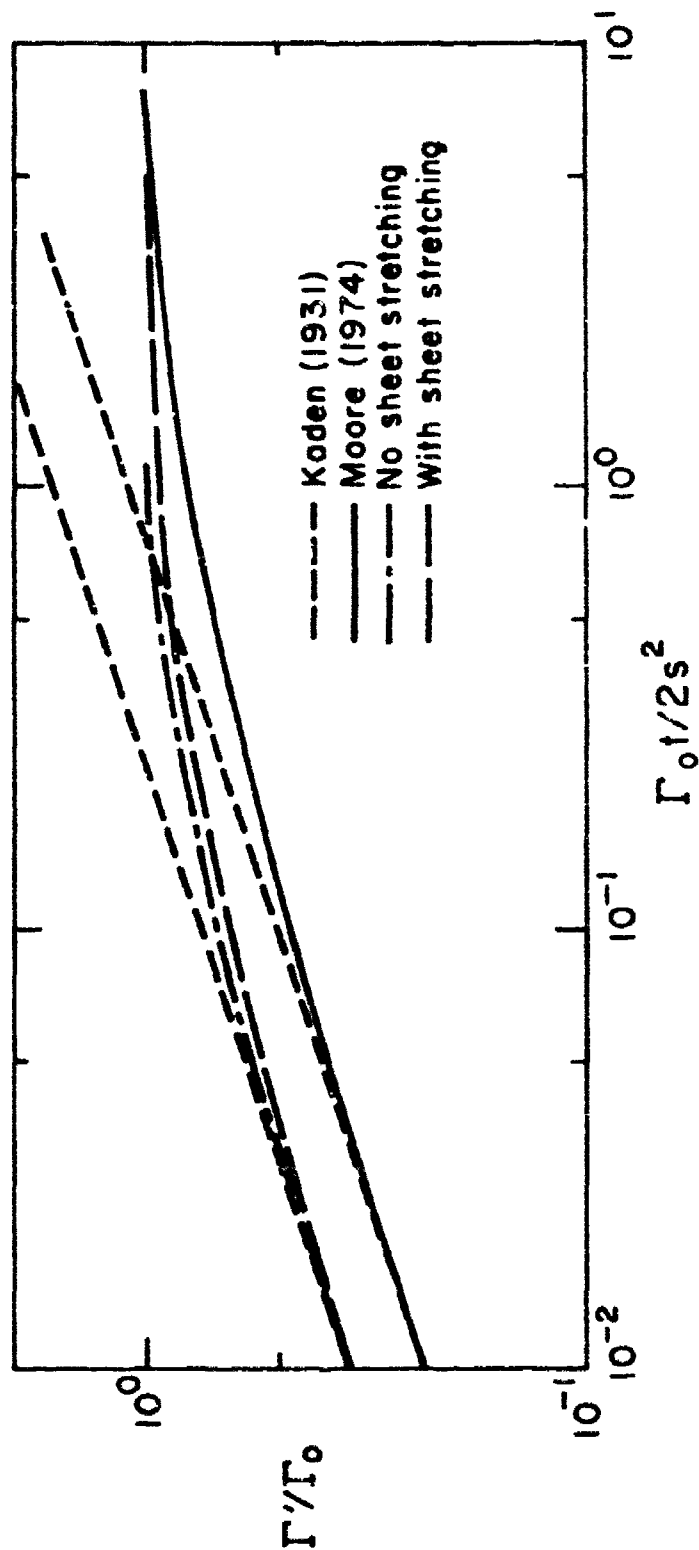
Figure A-3. Comparison of the simple roll-up model with the detailed calculations of Moore (Ref. 5). The constant in Kaden's solution (Ref. 6) has been adjusted to give agreement at $2\Gamma_o t/b^2 = 10^{-2}$.

APPENDIX B

ADDITIONAL EXPERIMENTAL WAKE VELOCITY DISTRIBUTIONS

Appendix B contains measured wake vortex velocity distributions for configurations 3 and 4. Swirl velocity distributions are computed and compared for tip vortices only. Flap vortices have not rolled up sufficiently at the five-chord downstream measuring station to discern a distinct axisymmetric structure.
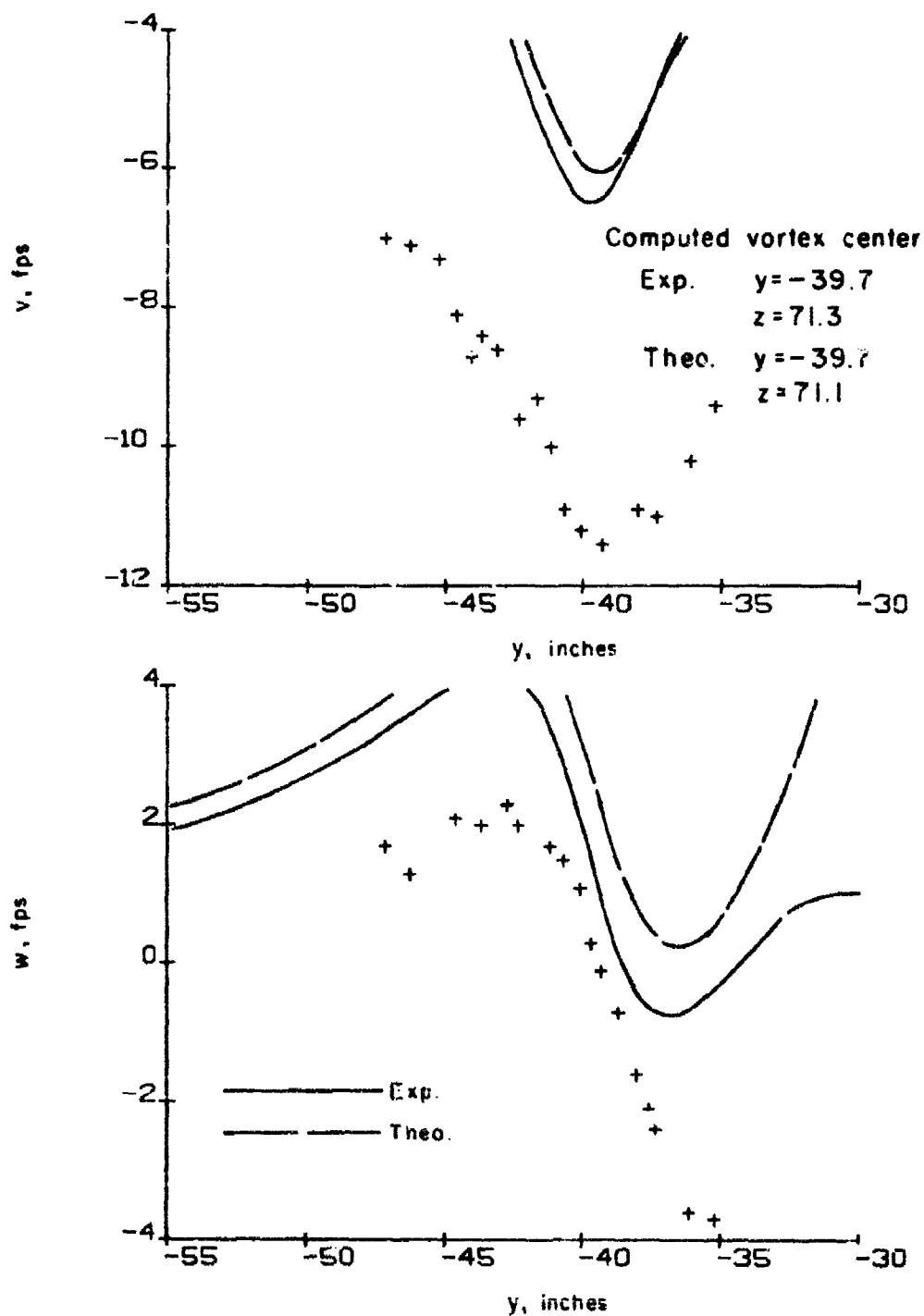
Figure B-1a.   Configuration 3; tip vortex.   Comparison of measured
and computed horizontal and vertical velocities
(x = 50 in., z = 67.4 in.)

112
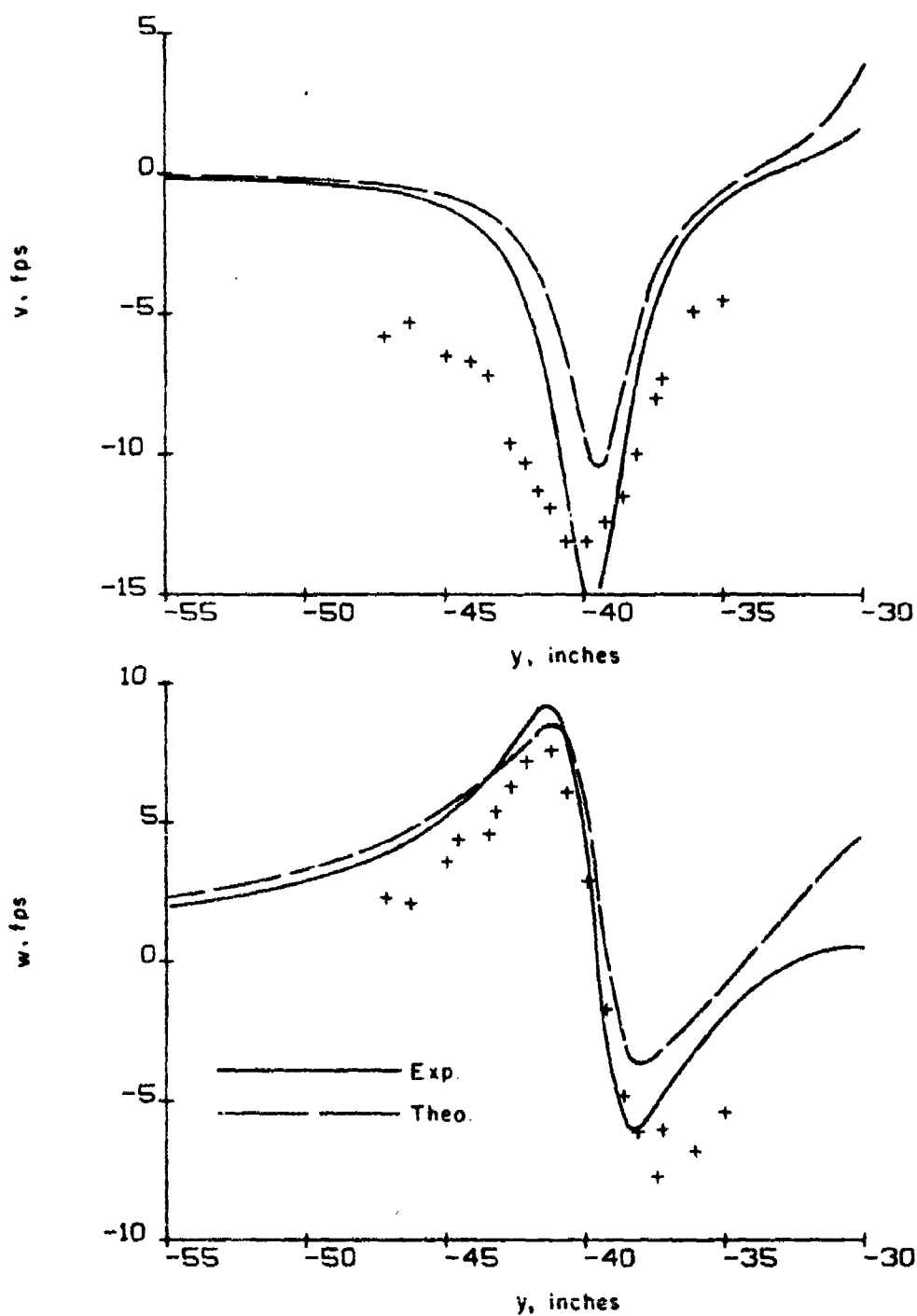
Figure B-1b. Configuration 3; tip vortex. Comparison of measured and computed horizontal and vertical velocities (x = 50 in., z = 69.7 in.)

113
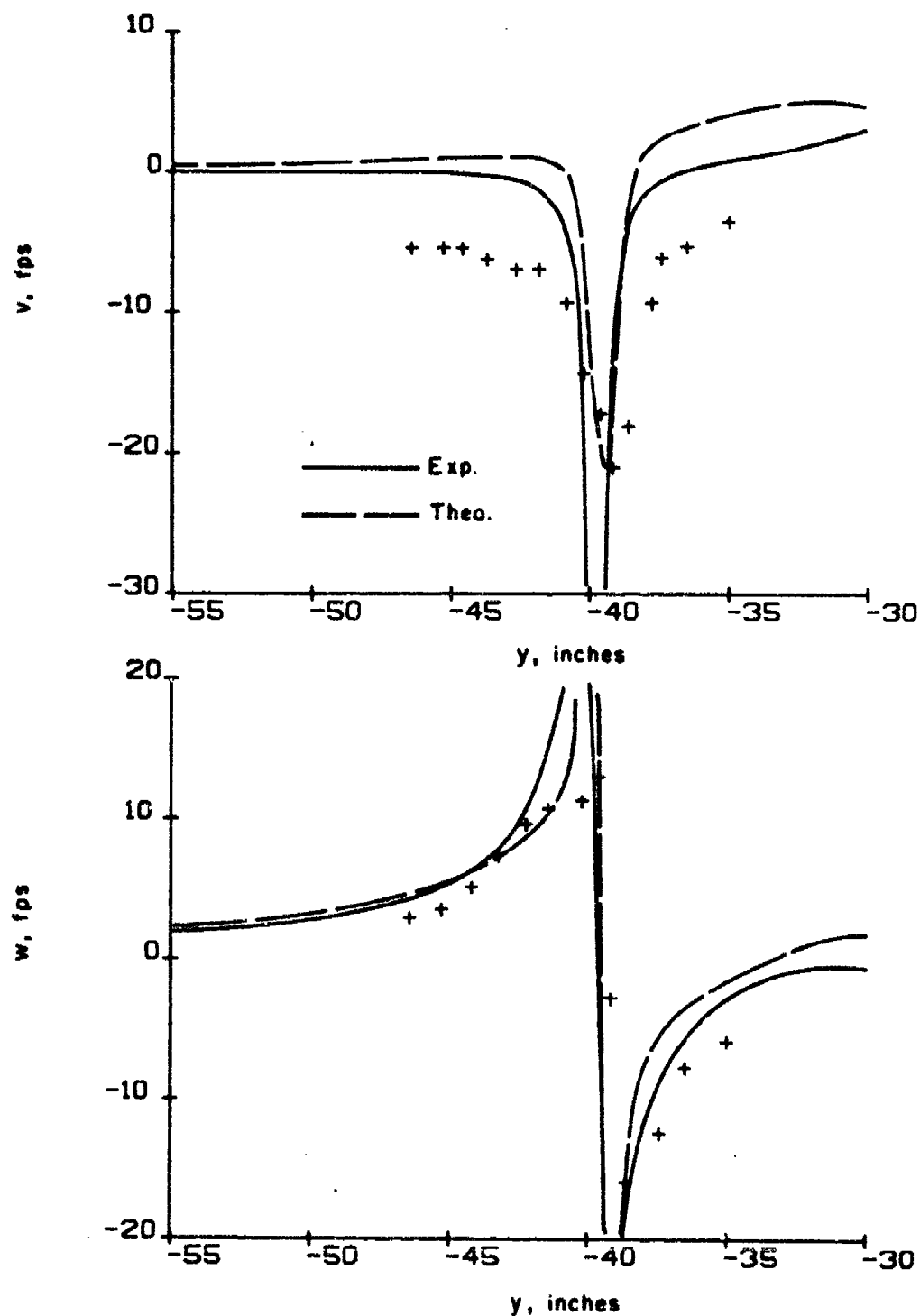
Figure B-1c. Configuration 3; tip vortex. Comparison of measured
and computed horizontal and vertical velocities
(x = 50 in., z = 71 in.)

114
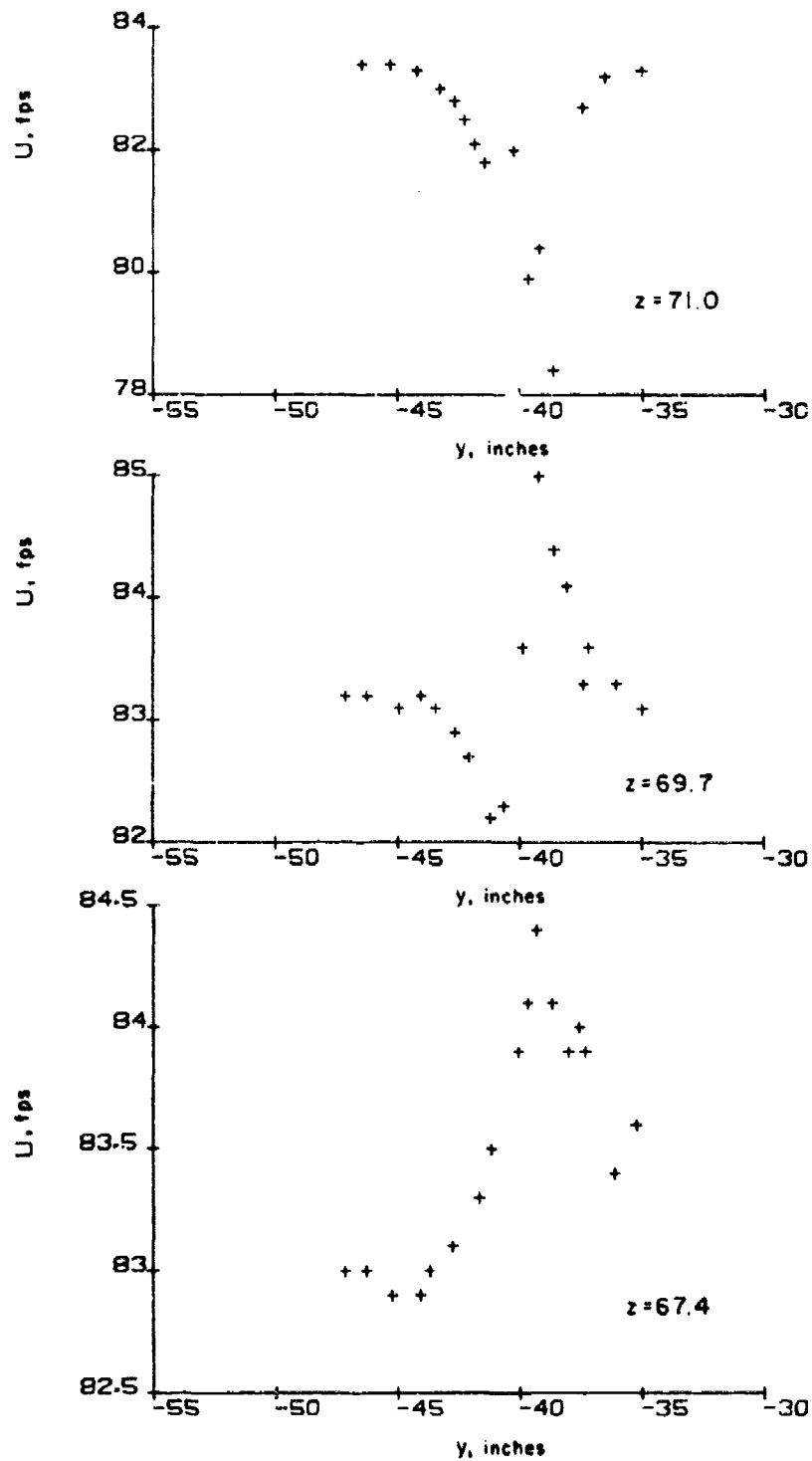
Figure B-1d.   Configuration 3; measured axial velocities (x = 50 in.)
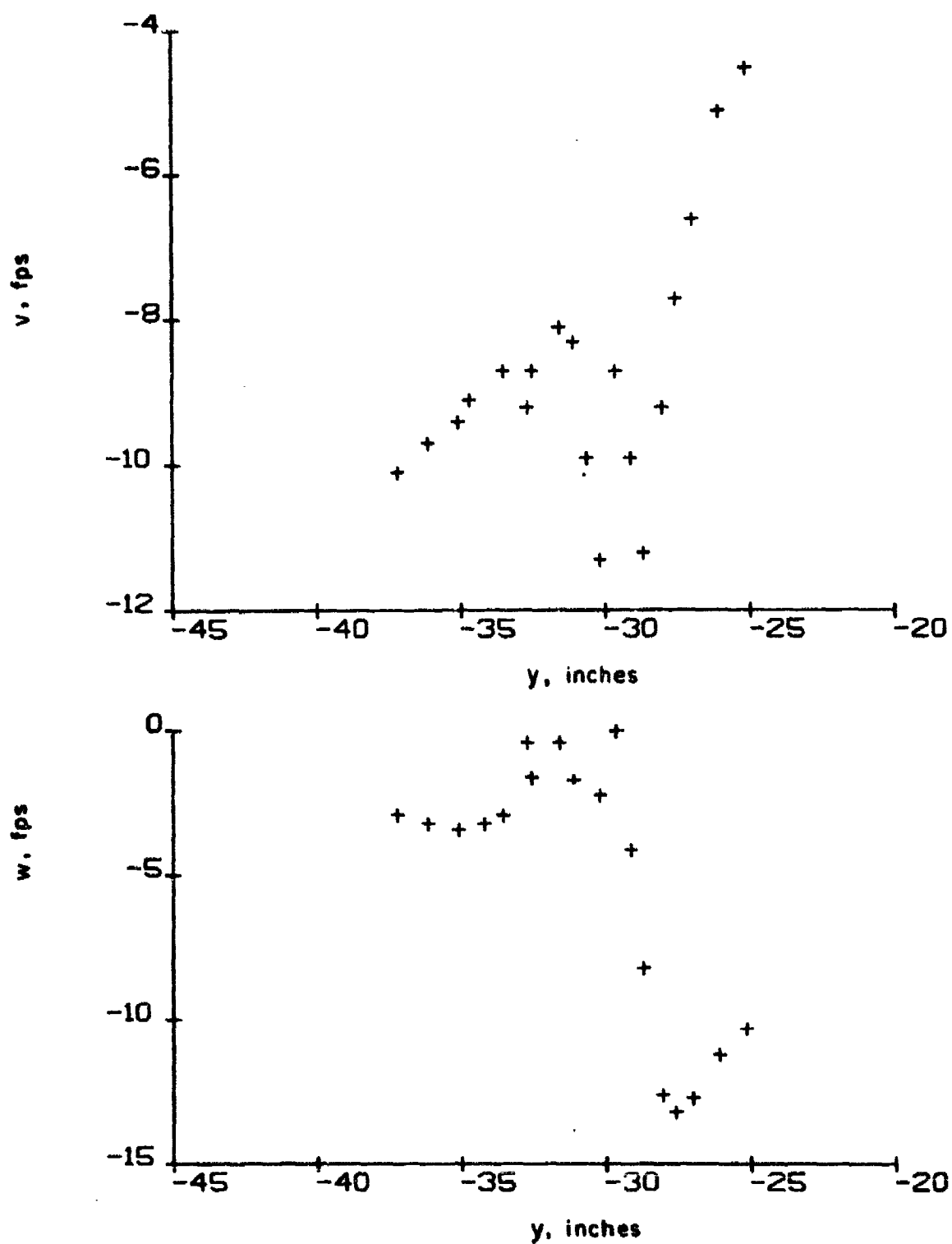
Figure B-2a.   Configuration 3; flap vortex.   Measured horizontal and vertical velocities (x = 50 in., z = 66.5 in.)
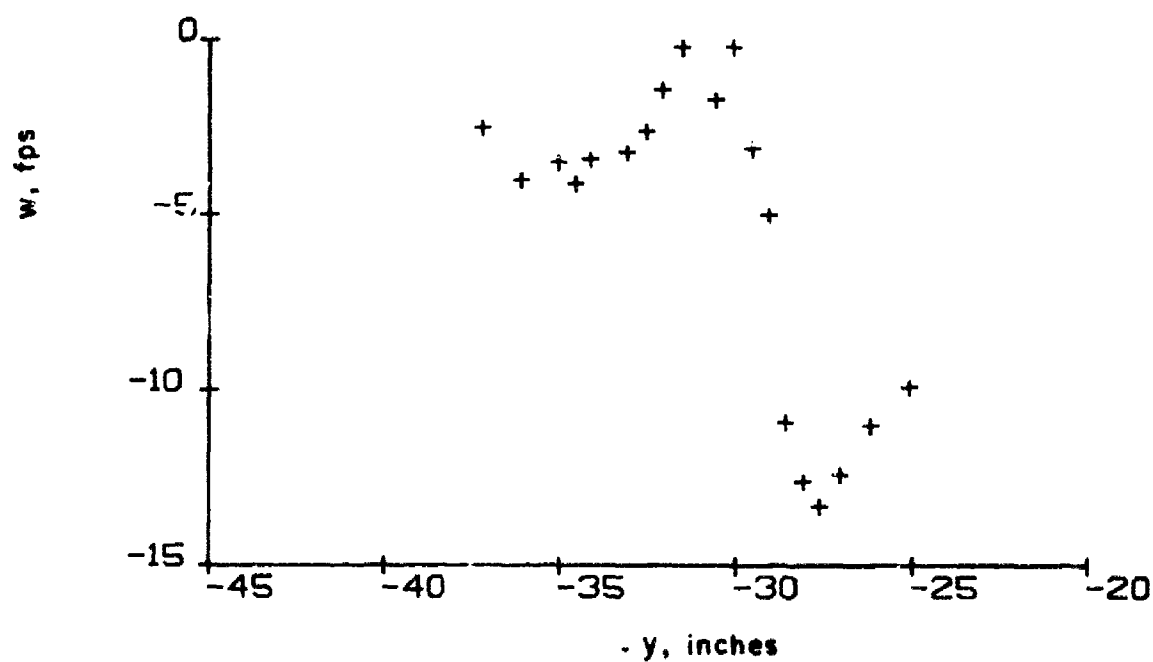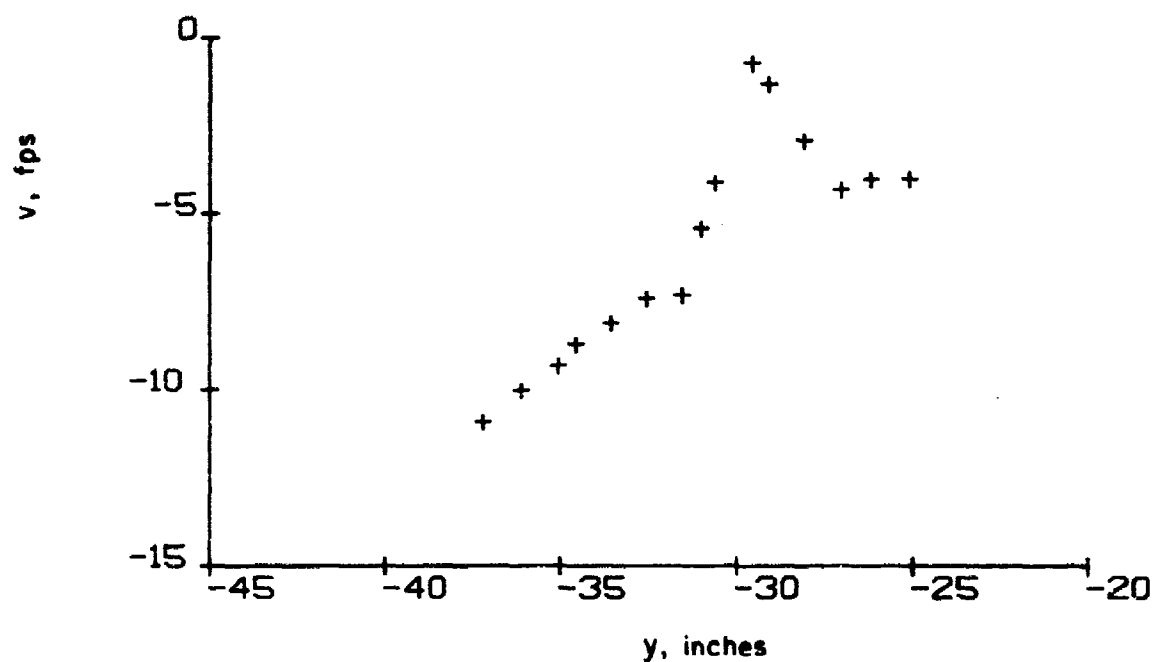
Figure B-2b.   Configuration 3; flap vortex.   Measured horizontal
and vertical velocities (x = 50 in., z = 67.4 in.)
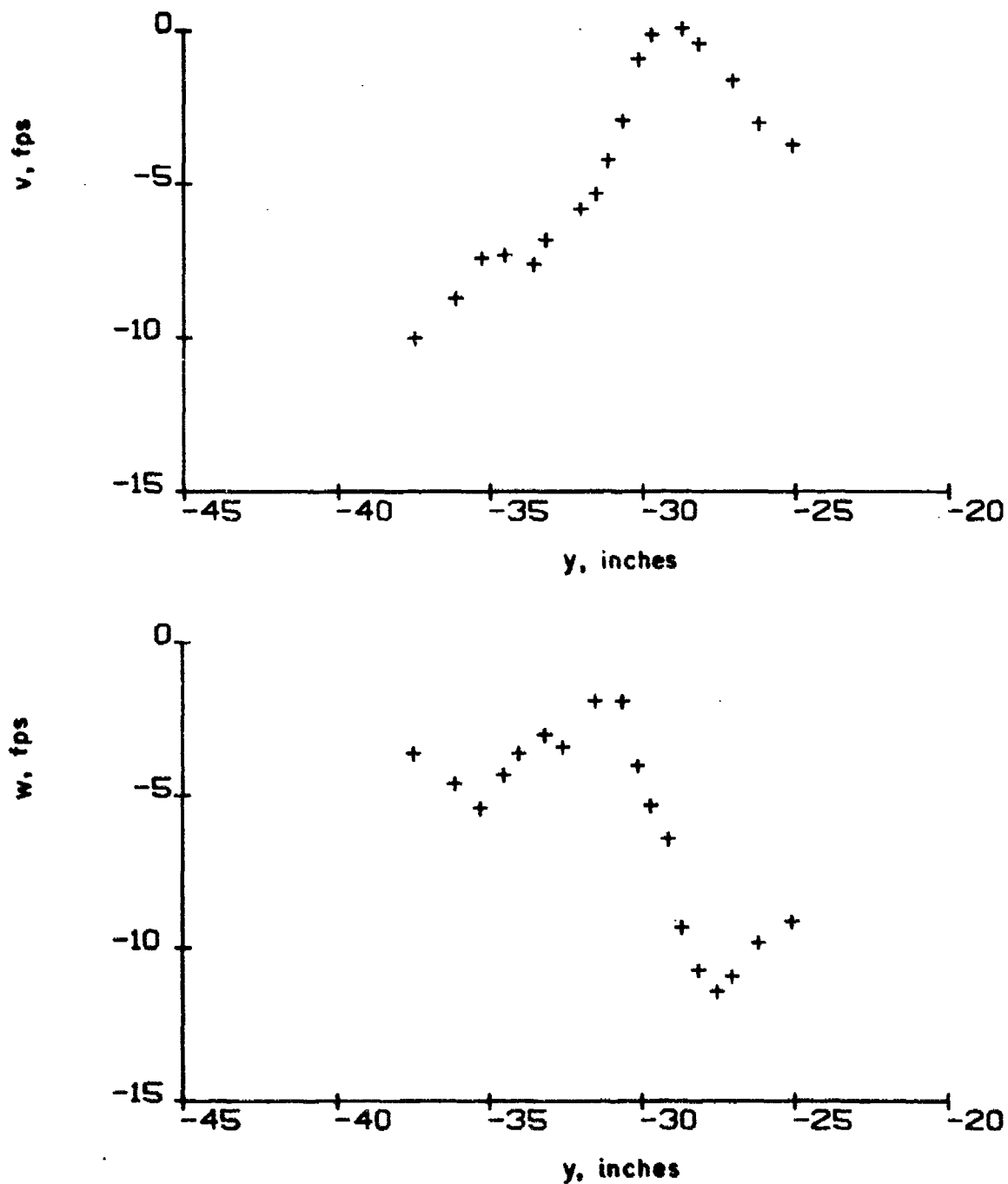
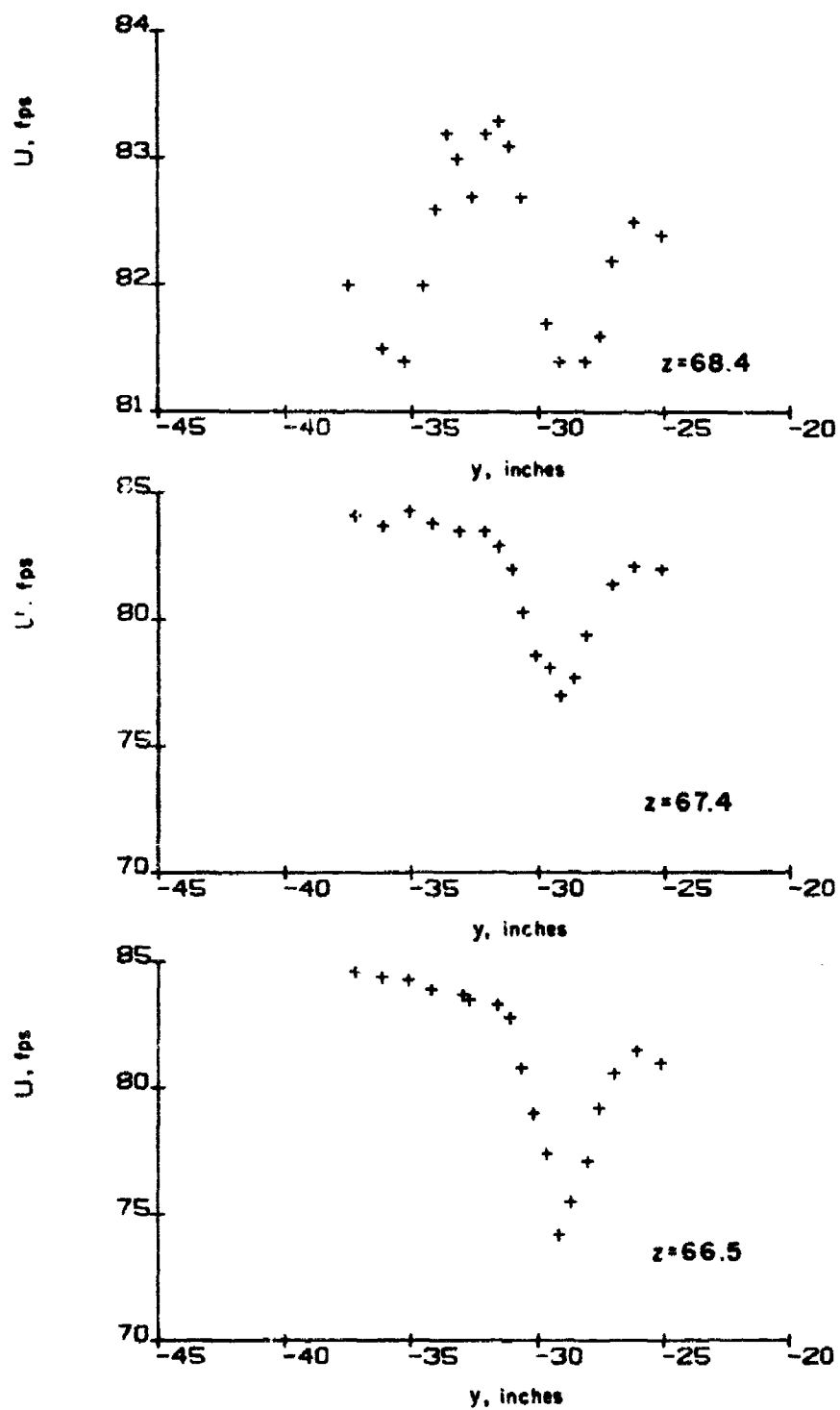Figure B-2c. Configuration 3; flap vortex. Measured horizontal and vertical velocities (x = 50 in., z = 68.4 in.)

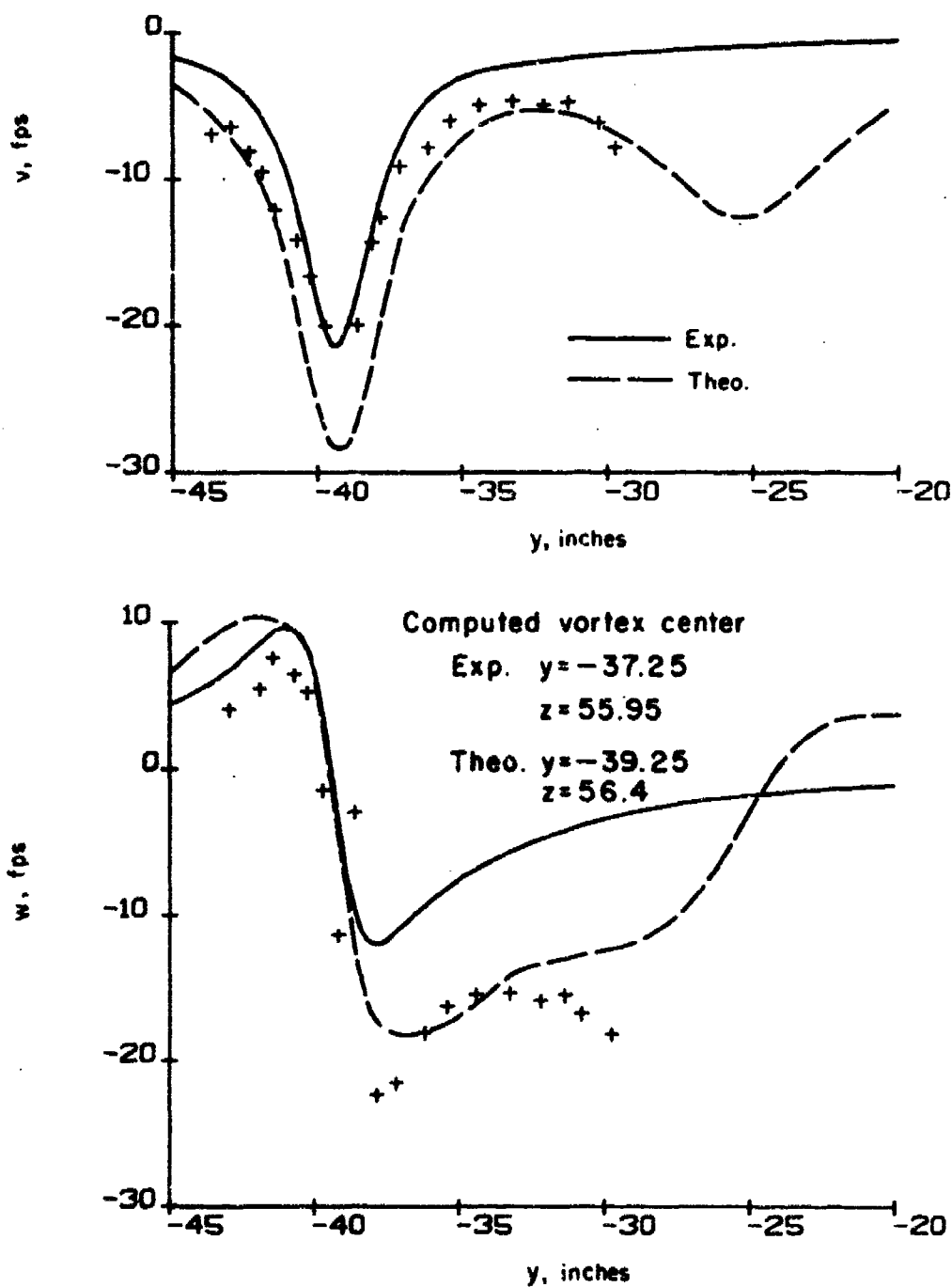Figure B-2d.   Configuration 3; measured axial velocities (x = 50 in.)

Figure B-3a. Configuration 4; tip vortex. Comparison of measured and computed horizontal and vertical velocities (x = 50 in., z = 54.5 in.)
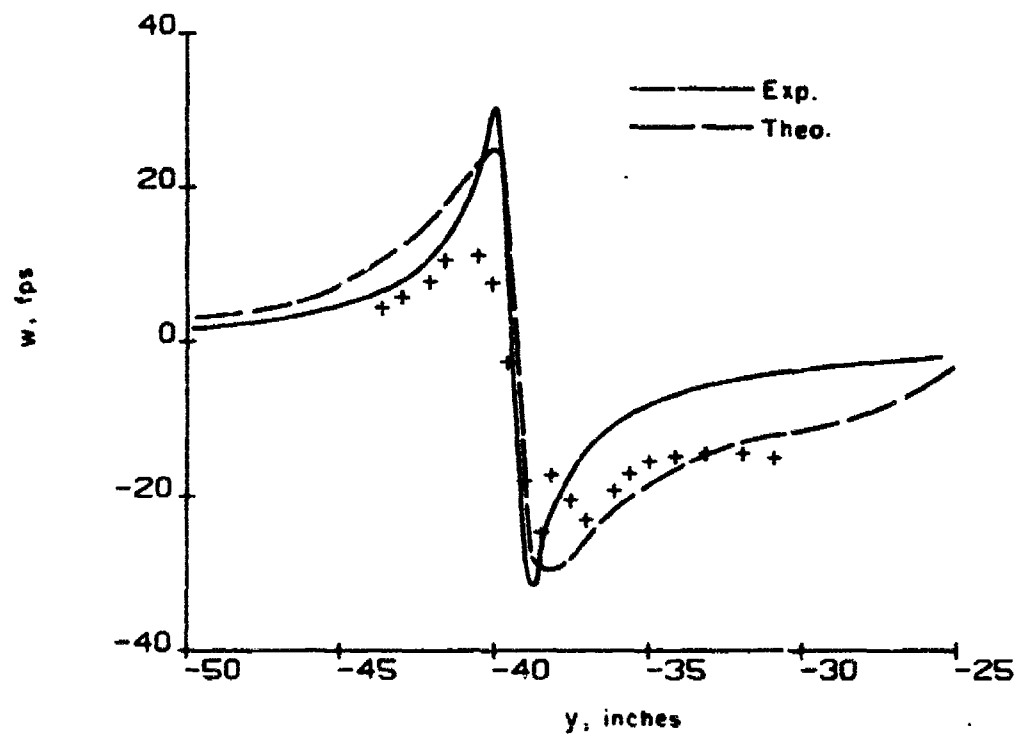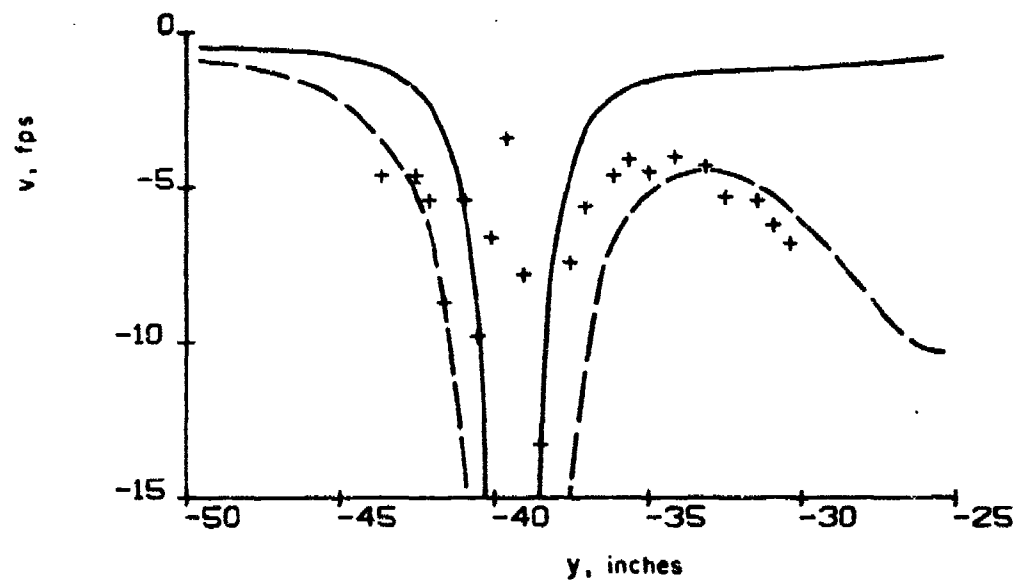
Figure B-3b. Configuration 4; tip vortex. Comparison of measured and computed horizontal and vertical velocities (x = 50 in., z = 55.4 in.)
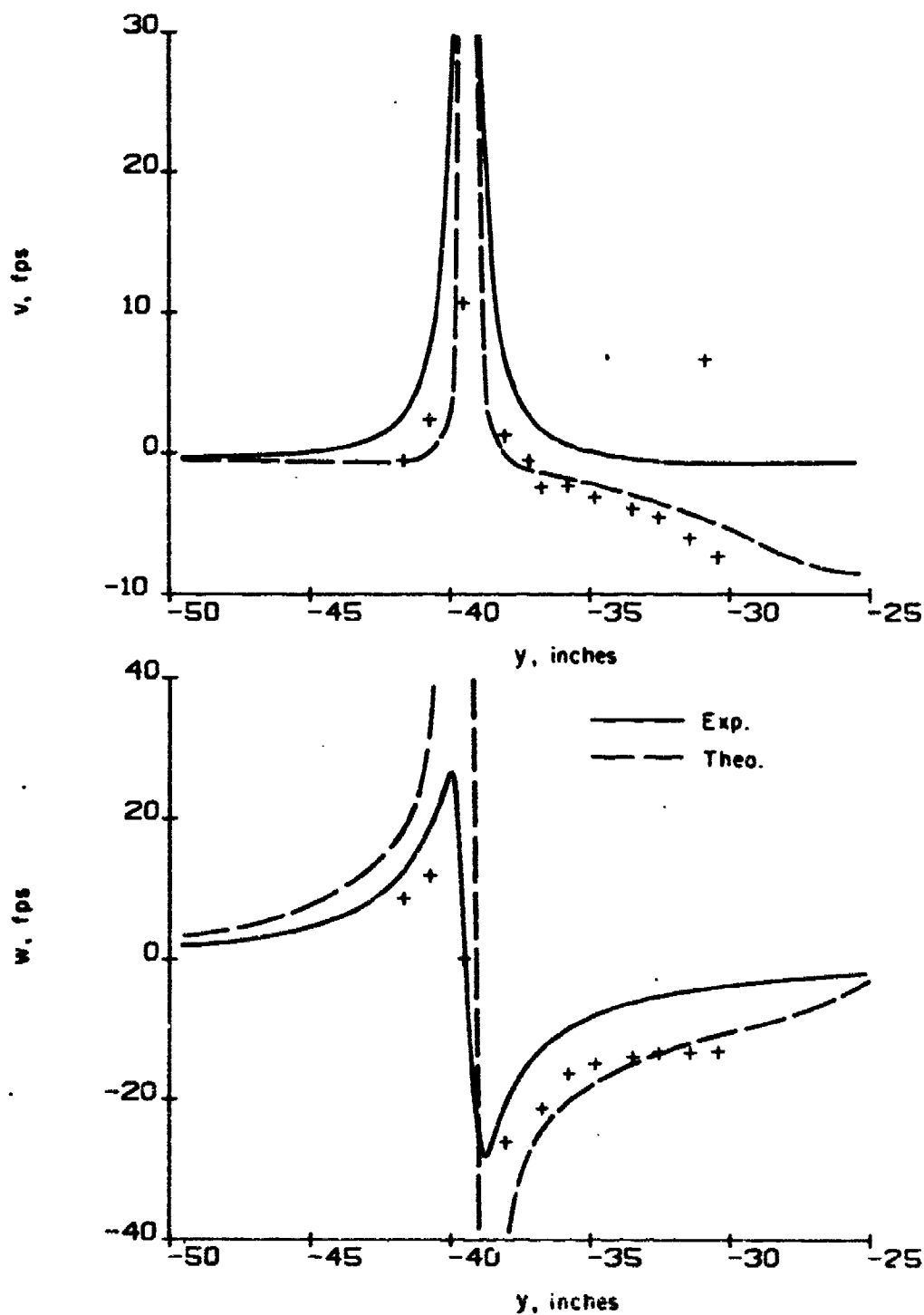
Figure B-3c. Configuration 4; tip vortex. Comparison of measured and computed horizontal and vertical velocities (x = 50 in., z = 56.5 in.)

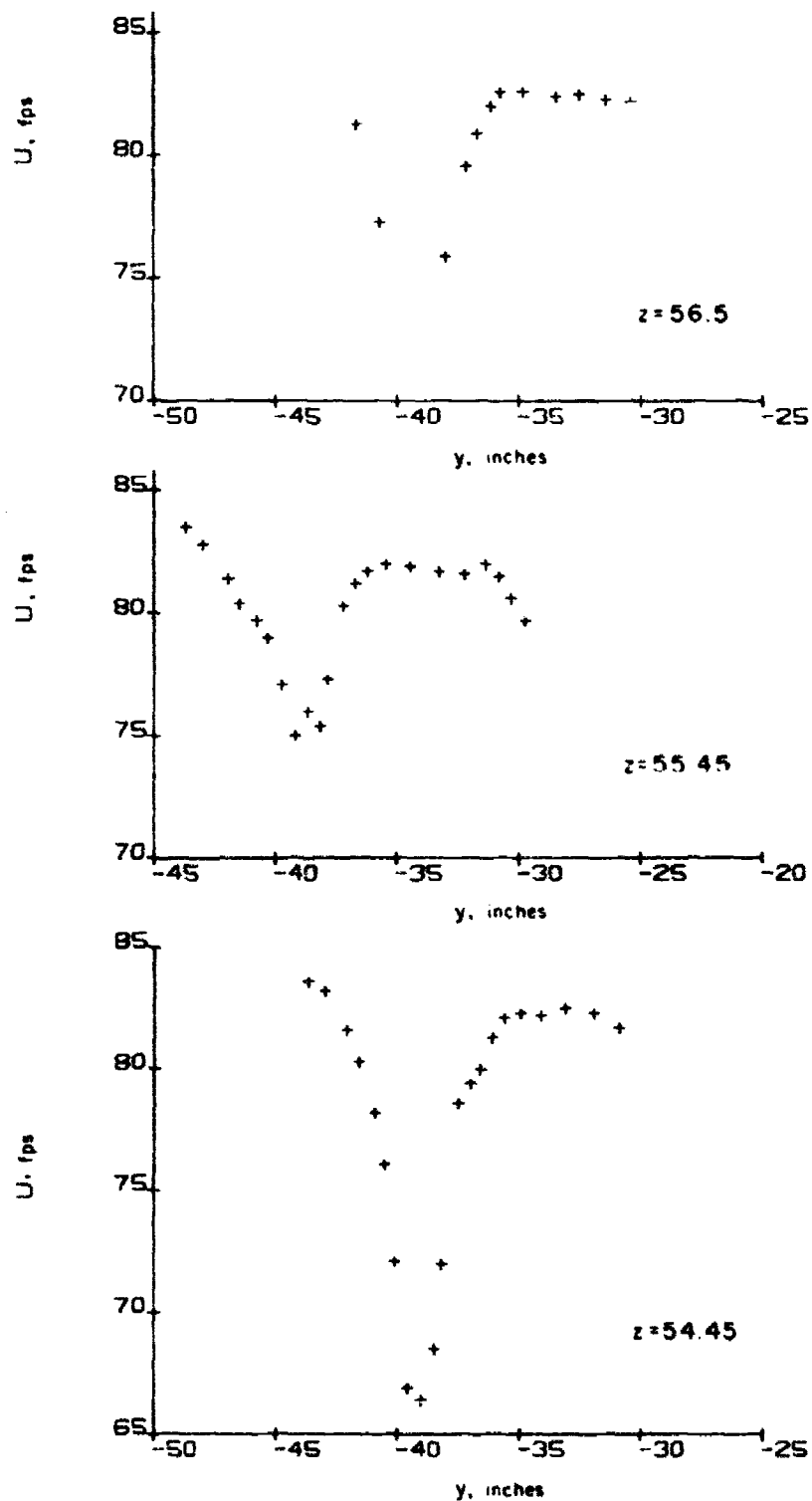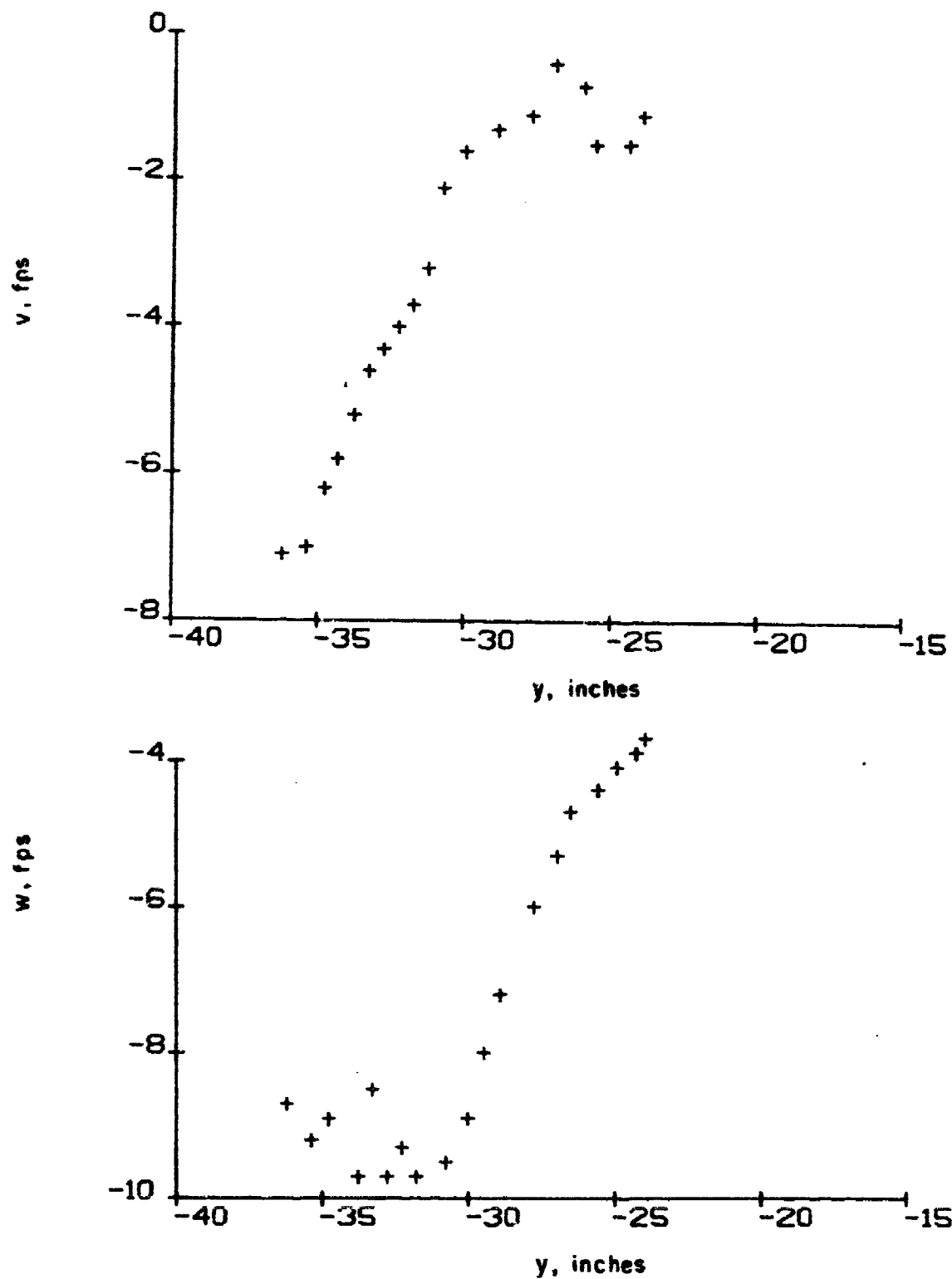Figure B-3d.   Configuration 4; measured axial velocities (x = 50 in.)

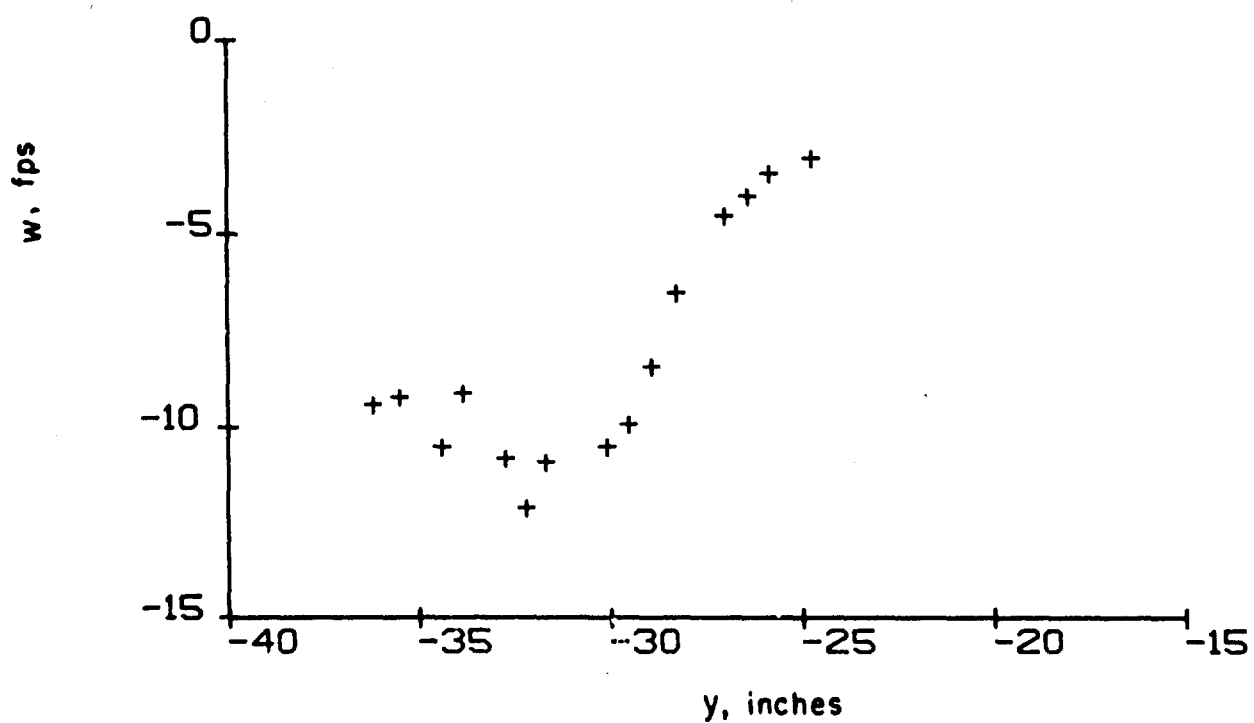Figure B-4a.   Configuration 4; flap vortex. Measured horizontal and vertical velocities (x = 50 in., z = 48.8 in.)
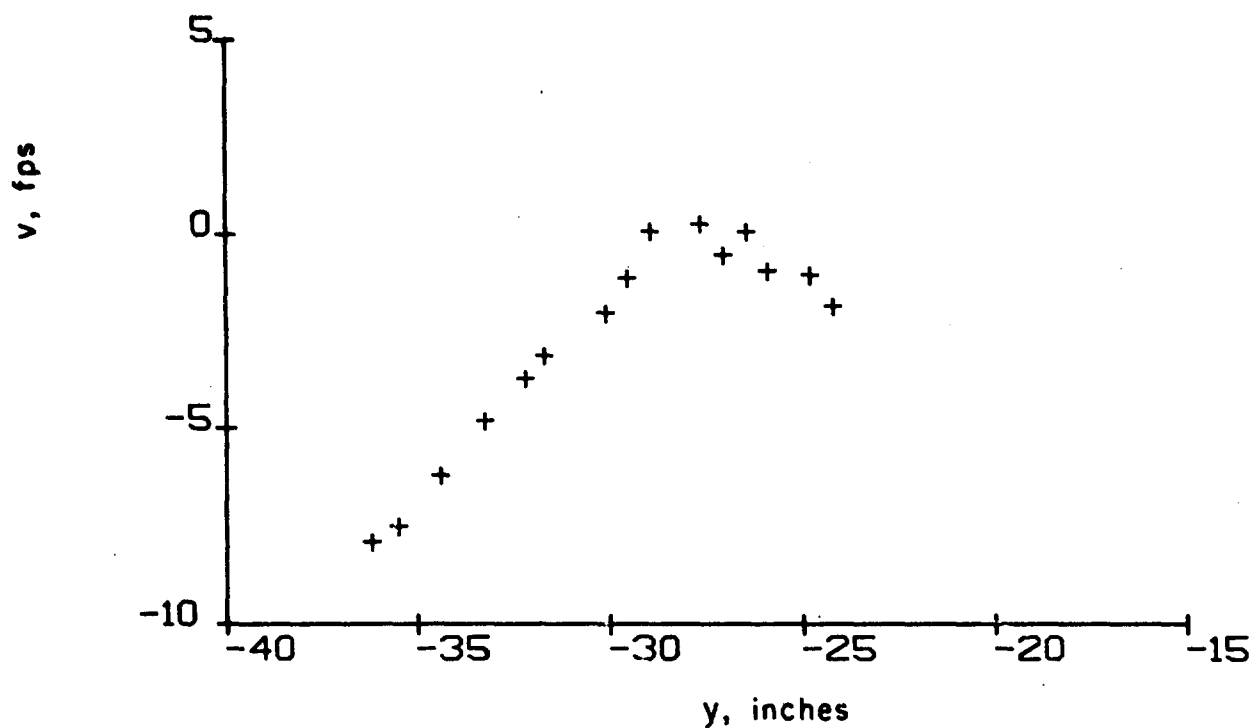
Figure B-4b. Configuration 4; flap vortex. Measured horizontal and vertical velocities (x = 50 in., z = 49.9 in.)
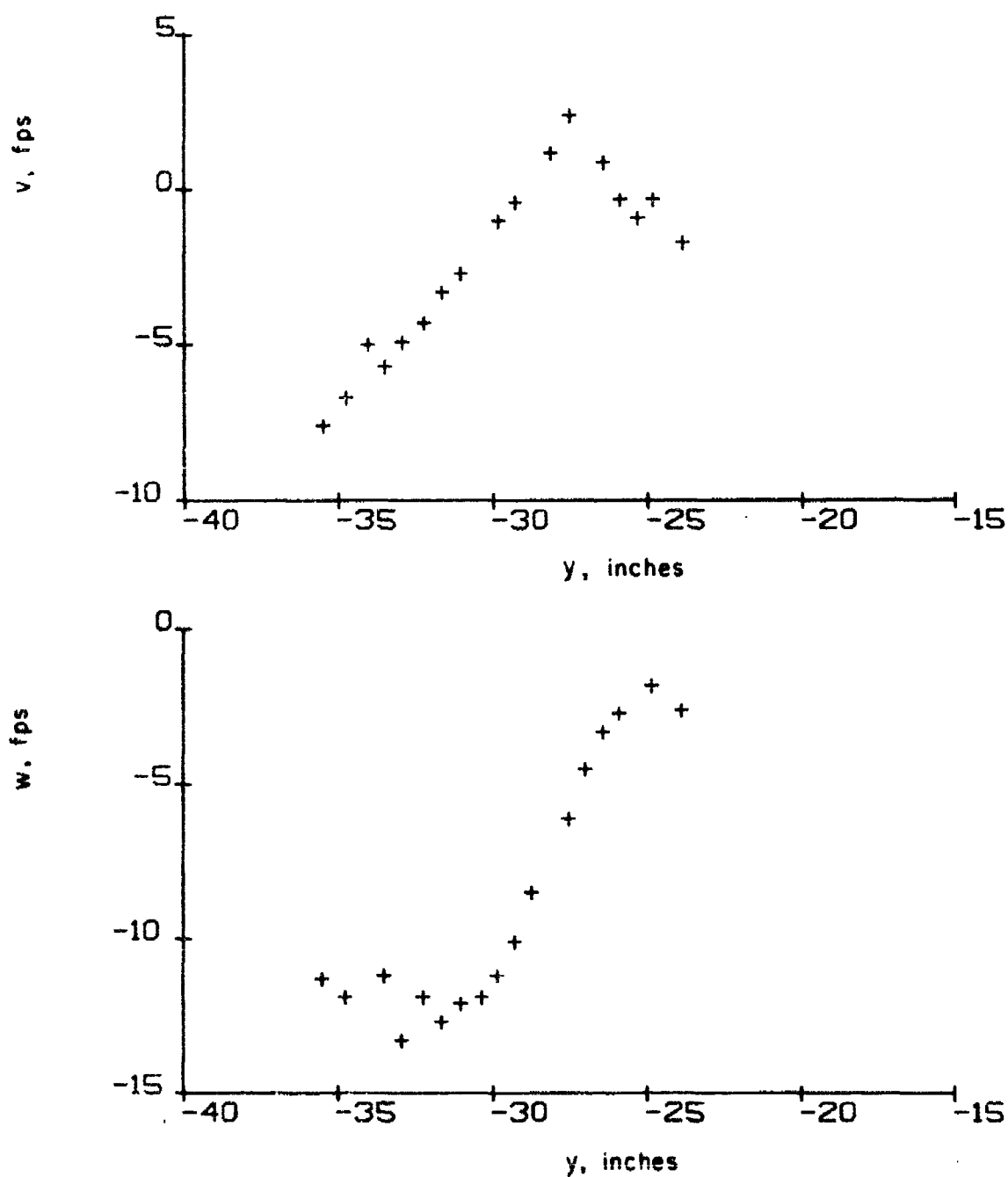
125

Figure B-4c. Configuration 4; flap vortex. Measured horizontal and vertical velocities (x = 50 in., z = 50.9 in.)
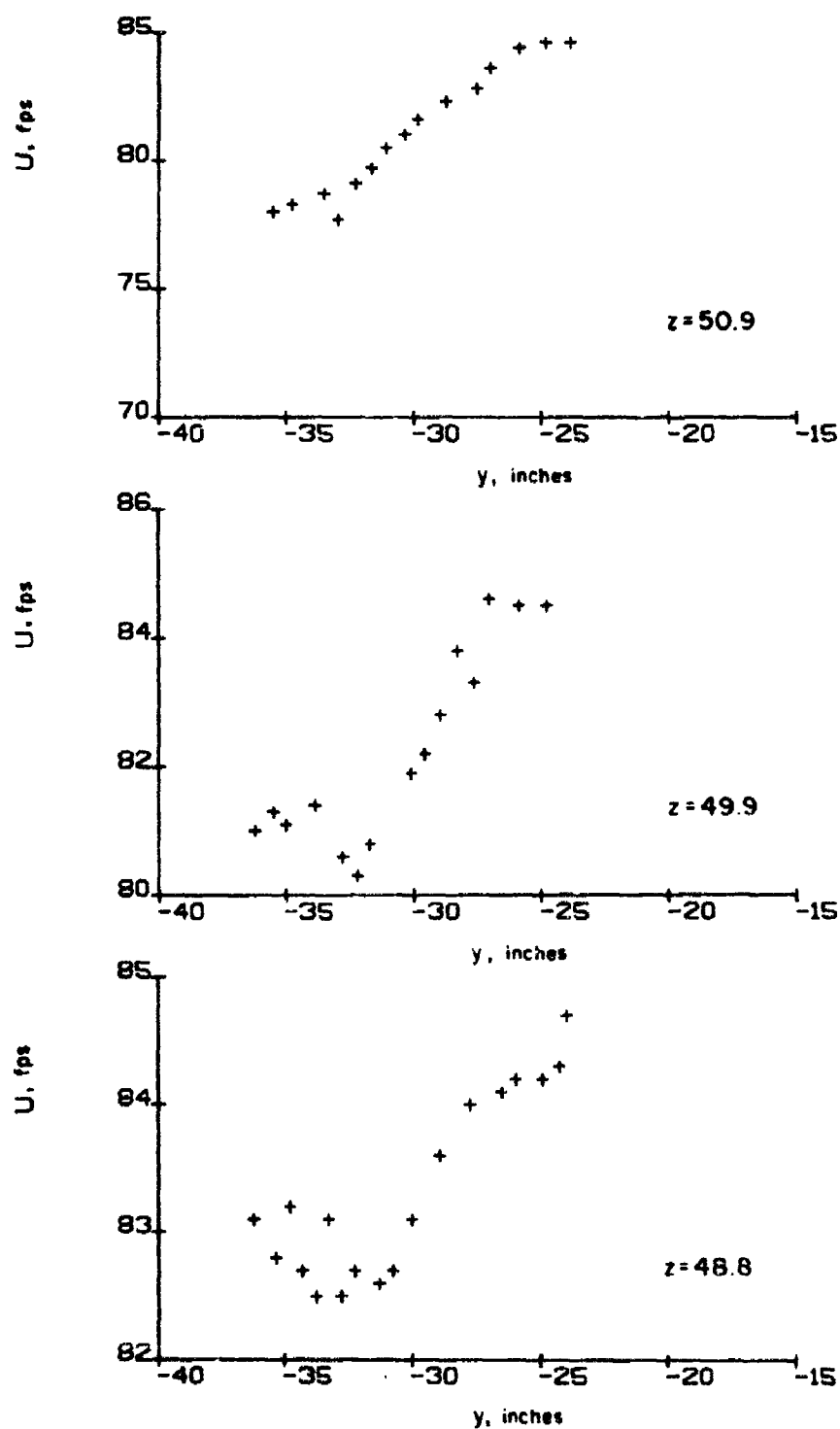
126

Figure B-4d. Configuration 4; measured axial velocities (x = 50 in.)

REFERENCES

1. Westwater, F. L., "Rolling Up of the Surface of Discontinuity Behind an Aerofoil of Finite Span," Aero. Res. Council of Great Britain, Report No. R&M 1962, 1935.

2. Hackett, J.E. and Evans, M.R., "Vortex Wakes Behind High-Lift Wings," J. Aircraft, Vol. 8, No. 5, 1971, p. 334.

3. Bloom, A.M. and Jen, H., "On the Roll-up of Aircraft Trailing Vortices Using Artificial Viscosity," NASA Langley Research Center, 1974.

4. Kurwahara, K. and Takami, H., "Numerical Studies of Two-Dimensional Vortex Motion by a System of Point Vortices," J. Phys. Soc. Japan, Vol. 34, 1973, p. 247.

5. Moore, D.W., "A Numerical Study of the Roll-up of a Finite Vortex Sheet," J. Fluid Mechanics, Vol. 63, Part 2, 1974, p. 225.

6. Kaden, H., "Aufwicklung einer Unstabilen Unstetigkeitsfläche," Ing. Archiv., Vol. 2, 1931, p. 140.

7. Spreiter, J.R. and Sacks, A.H., "The Rolling Up of the Trailing Vortex Sheet and its Effect on the Downwash Behind Wings," J. Aero. Sci., Vol. 18, No. 1, 1951, p. 21.

8. Donaldson, Coleman duP., "A Brief Review of the Aircraft Trailing Vortex Problem," AFOSR-TR-71-1910, presented at National Aerospace Electronics Conf., May 1971, Dayton, Ohio.

9. Mason, W.H. and Marchman, J.F., III, "Farfield Structure of an Aircraft Trailing Vortex," J. Aircraft, Vol. 10, No. 2, 1973, p. 86.

10. Brown, Clinton E., "Aerodynamics of Wake Vortices," AIAA Journal, Vol. 11, No. 4, 1973, p. 531.

11. Jordan, Peter F., "Structure of Betz Cores," J. Aircraft, Vol. 10, No. 11, 1973, p. 691.

12. Rossow, V., "On the Inviscid Rolled-Up Structure of Lift Generated Vortices," J. Aircraft, Vol. 10, No. 11, 1973, p.647.

13. Donaldson, Coleman duP., Snedeker, Richard S., and Sullivan, Roger D., "A Method of Calculating Aircraft Wake Velocity Profiles and Comparison with Full-Scale Experimental Measurements," AIAA Paper No. 74-39, 1974.

14. Yates, John E., "Calculation of Initial Vortex Roll-up in Aircraft Wakes," J. Aircraft, Vol. 11, No. 7, 1974, p. 397.

Preceding page blank

15. Sullivan, Roger D., "A Program to Compute the Behavior of a Three-Dimensional Turbulent Vortex," ARL-TR-74-0009, January 1974.

16. Crow, Steven C., "Stability Theory for a Pair of Trailing Vortices," AIAA Journal, Vol. 8, No. 12, 1970, p. 2172.

17. Batchelor, G.K., *An Introduction to Fluid Mechanics*, Cambridge University Press, London, 1967, p. 527.

18. Parlett, L.P. and Shivers, J.P., "Wind Tunnel Investigation of an STOL Aircraft Configuration Equipped with an External Flow Jet Flap," NASA TN-D 5364, 1969.

19. Donaldson, Coleman duP. and Sullivan, Roger D., "An Invariant Second-Order Closure Model of the Compressible Turbulent Boundary Layer on a Flat Plate," Aeronautical Research Associates of Princeton, Inc., Report No. 178, 1972.